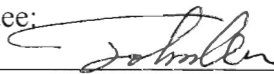
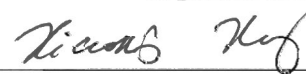



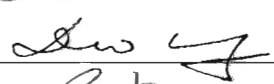
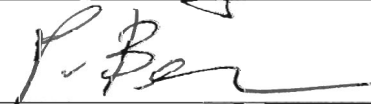
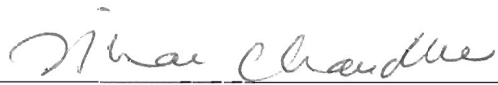


REMOTE SENSING TECHNIQUES FOR SOIL MOISTURE AND AGRICULTURAL
DROUGHT MONITORING

by

Lingli Wang
A Dissertation
Submitted to the
Graduate Faculty
of
George Mason University
in Partial Fulfillment of
The Requirements for the Degree
of
Doctor of Philosophy
Earth Systems and GeoInformation Sciences

Committee:

	Dr. John J. Qu, Dissertation Director
	Dr. Xiaoxiong Xiong, Committee Member
	Dr. Richard B. Gomez, Committee Member
	Dr. Ruixin Yang, Committee Member
	Dr. Xianjun Hao, Committee Member
	Dr. David Wong, Department Chairperson
	Dr. Peter Becker, Associate Dean for Graduate Studies, College of Science
	Dr. Vikas Chandhoke, Dean, College of Science

Date:

02/08/2008

Spring Semester 2008
George Mason University
Fairfax, VA

Remote Sensing Techniques for Soil Moisture and Agricultural Drought Monitoring

A dissertation submitted in partial fulfillment of the requirements for the degree of
Doctor of Philosophy at George Mason University

By

Lingli Wang
Master of Science
Hohai University, P. R. China, 2000

Director: John J. Qu, Associate Professor
Department of Earth Systems and GeoInformation Sciences

Spring Semester 2008
George Mason University
Fairfax, VA

Copyright 2008 Lingli Wang
All Rights Reserved

ACKNOWLEDGEMENTS

My dissertation committee deserves a special thanks for their guidance in this research endeavor. I must first thank my Ph.D. advisor, Dr. John J. Qu, who has always encouraged me to pursue my ideas, offered innumerable creative insights and guided me with unmatched wisdom. He has walked me through all the stages of the writing of this thesis. Without his consistent and illuminating instruction, this thesis could not have reached its present form. I equally thank Dr. Xiaoxiong Xiong, for his support and encouragement of excellence in all phases of my research. A very special thanks is given to Dr. Xianjun Hao, who has instructed and helped me a lot in the past three years. I thank Dr. Ruixin Yang for his expertise in data analysis that he most gratefully shared. Thanks are also due to Dr. Richard B. Gomez, for his thoughtful insight and knowledge on material spectral characteristics in remote sensing technology.

I would also like to thank all those in EastFIRE Lab who have contributed time and effort to make this research effort a reality. Special recognition is given to Emmanuel A. Smith, for editing my research papers and this dissertation. The valuable suggestions offered by Swarvanu Dasgupta throughout my research were gratefully appreciated. Thanks are also given to Dr. William Sommers, Wanting Wang, Yong Xie, Min Li, and Sanjeev Bhoi, who have helped in my dissertation in many ways.

I also owe my sincere gratitude to my friends who gave me their unwavering support and help. Special appreciation is given to Mrs. Xiaofeng Ren, Juan Luo and Ms. Xin Zhang, for always being around me whenever I need the help.

I wish to extend a special thanks to my beloved family for their loving considerations and great confidence in me all through these years. I thank my parents, Songbo Wang and Jiulan Xu, for instilling a sense of wonder and exploration in me, and my brother, Jianxin Wang, for his support and encouragement.

Thanks also go out to the NASA EOS Gateway for providing data which this dissertation relies on.

Finally, my most sincere thanks go out to The One for having come into my life and always standing by me.

TABLE OF CONTENTS

	Page
LIST OF TABLES	vi
LIST OF FIGURES	vii
LIST OF ABBREVIATIONS	ix
ABSTRACT.....	x
1. INTRODUCTION	1
1.1 Importance of soil moisture.....	1
1.2 Statement of problem	3
1.3 Objectives and scopes	4
1.4 Organization of Dissertation	5
1.5 Major data sources	7
1.6 Principal results	9
2. LITERATURE REVIEW: DROUGHT AND DROUGHT INDICES.....	10
2.1 Drought definition.....	10
2.2 Drought indices	12
2.2.1 Palmer Drought Severity Index (PDSI).....	12
2.2.2 Standardized Precipitation Index (SPI)	14
2.3 Chapter summary	15
3. LITERATURE REVIEW: SOIL MOISTURE ESTIMATION.....	16
3.1 Remote sensing of near-surface soil moisture.....	17
3.1.1 Passive microwave remote sensing	19
3.1.2 Optical/IR remote sensing.....	22
3.1.3 Combining microwave and optical/IR remote sensing.....	24
3.2 Soil moisture profile estimation	25
3.2.1 Regression approach.....	26
3.2.2 Hydrological models	26
3.2.3 Data assimilation.....	27
3.2.4 Water transport model	28
3.3 Chapter summary	30
4. SOIL MOISTURE ESTIMATION USING MULTI-SENSOR AND GROUND MEASUREMENTS	32
4.1 Soil moisture estimation using MODIS and ground measurements.....	32
4.1.1 Algorithm theory	33
4.1.2 Study area and data sources.....	36
4.1.3 Algorithm construction and validation	38
4.1.4 Discussion and conclusion	42
4.2 Soil moisture estimation using AMSR-E products.....	42
4.2.1 AMSR-E soil moisture products.....	42
4.2.2 Relationship between AMSR-E and ground measurements.....	45
4.3 Chapter summary	47
5. SOIL MOISTURE ESTIMATION USING MULTIPLE MODIS SRB	

MEASUREMENTS	48
5.1 Sensitivity studies of moisture effects	49
5.1.1 Model	50
5.1.2 Simulation setup	52
5.1.3 Model simulation	54
5.1.4 Conclusion	68
5.2 Soil moisture estimation using MODIS SRB measurements	70
5.2.1 MODIS SRB measurements	70
5.2.2 Formation of NMDI	71
5.2.3 Validation of NMDI	76
5.2.4 Uncertainty analysis	81
5.2.5 Conclusion	86
5.3 Application of NMDI in fire detection	87
5.3.1 Study area and data	88
5.3.2 Methodology for fire detection	90
5.3.3 Indices testing and discussion	93
5.3.4 Conclusion	104
5.4 Chapter summary	105
6. SOIL MOISTURE PROFILE ESTIMATION	107
6.1 Richards Equation	108
6.2 Numerical solution to Richards Equation	110
6.2.1 Introduction	111
6.2.2 Discretization of kinematic wave equation	112
6.2.3 Conditions for simulating the physical diffusion	115
6.2.4 Stability considerations	117
6.2.5 Application example	120
6.3 Chapter summary	123
7. CONCLUSIONS AND FUTURE DIRECTION	125
7.1 Conclusions	125
7.1.1 Soil moisture estimation using multi-sensor and ground measurements	126
7.1.2 Soil moisture estimation using multiple MODIS SRB measurements	127
7.1.3 Soil moisture profile estimation	128
7.2 Applications of this research	129
7.3 Limitations of this work	131
7.4 Future works	132
7.4.1 Extensive applications of NMDI	132
7.4.2 Improvements of soil moisture profile estimation	132
7.4.3 Development of an operational system for drought monitoring	133
REFERENCES	134

LIST OF TABLES

Table	Page
1. Table 1.1 Data and sources	8
2. Table 3.1 Summary of remote sensing techniques for measurement of near-surface soil moisture content.....	18
3. Table 4.1 Statistics for algorithm derived soil moisture	39
4. Table 4.2 Regression coefficients for main land cover and soil types	40
5. Table 4.3 Statistics for land cover and soil type oriented algorithms	40
6. Table 4.4 Statistics for validation.....	41
7. Table 4.5 Coefficients of determination between AMSR-E and ground measurements.....	45
8. Table 5.1 Input parameters to soil reflectance model for MODIS bands	52
9. Table 5.2 Input parameters to PROSPECT and SAIL models.....	53
10. Table 5.3 MODIS 250 m and 500 m SRB specifications	71
11. Table 5.4 Results of NMDI soil uncertainties	83
12. Table 5.5 Results of NMDI veg uncertainties.....	85
13. Table 5.6 Confusion matrices for fire detection by NMDI against MODIS products.....	98
14. Table 5.7 Comparison of active fire detection results by MODIS products and NMDI (Georgia fire).....	99
15. Table 5.8 Comparison of active fire detection results by MODIS products and NMDI (Greek fire).....	103
16. Table 6.1 Values for numerical solutions	122

LIST OF FIGURES

Figure	Page
1. Figure 4.1 ‘Universal Triangle’ Relation between soil moisture, temperature and NDVI.....	34
2. Figure 4.2 Schematic flow diagram for the soil moisture estimation algorithm.....	36
3. Figure 4.3 Map of the study area and the distribution of ground stations.....	37
4. Figure 4.4 Soil moisture map at 1 km resolution over the study area on November 26 th , 2005.....	41
5. Figure 4.5 AMSR-E soil moisture map over the study area on Nov. 16 th , 2005.....	44
6. Figure 4.6 Scatter plots of ground measurements and AMSR-E data.....	46
7. Figure 5.1 Effects of leaf biochemical constituents such as chlorophyll C _{ab} , dry matter C _m , leaf water content C _w , and leaf structural parameter N on canopy reflectance.....	54
8. Figure 5.2 Simulated canopy spectra with LAI of 0.01 and 2 and varying soil moisture.....	56
9. Figure 5.3 Difference of simulated spectra by using low and high values of each parameter separately with LAI of 1 and 2.....	58
10. Figure 5.4 Sensitivity of MODIS SWIR reflectance to soil moisture.....	60
11. Figure 5.5 Sensitivity of MODIS SWIR reflectance to leaf water content.....	62
12. Figure 5.6 Sensitivity of NDWI and NDII to soil moisture.....	65
13. Figure 5.7 Sensitivity of NDWI and NDII to leaf water content.....	66
14. Figure 5.8 Sensitivity of $[(R_{860nm}-R_{2130nm})/(R_{860nm} + R_{2130nm})]$ to soil moisture and leaf water content.....	68
15. Figure 5.9 Simulated soil spectra at various soil moisture (upper) and canopy spectra at different leaf water content (lower).....	73
16. Figure 5.10 Sensitivity of NMDI to soil moisture (upper) and leaf water content (lower)	75
17. Figure 5.11 (a) Spectral reflectance curves for Newtonia silt loam at various moisture contents. (b) GeoSAIL model simulated spectra of bare soil with varying soil moisture.....	77
18. Figure 5.12 Sensitivity of NMDI to soil moisture values corresponding to Figures 5.11 (a) and 5.11 (b).....	78
19. Figure 5.13 True color image of the study area on September 6, 2004.....	79
20. Figure 5.14 Spatial distribution of NMDI over the Flint Hills.....	80
21. Figure 5.15 Uncertainties of NMDI _{soil} due to a 2% reflectance calibration uncertainty.....	84
22. Figure 5.16 Uncertainties of NMDI _{veg} due to a 2% reflectance calibration uncertainty.....	86

23. Figure 5.17 Flowchart of the multi-threshold method for fire detection.....	92
24. Figure 5.18 Images of active fire, NMDI, NDWI and NBR on 17 April, 2007	94
25. Figure 5.19 Images of active fire, NMDI, NDWI and NBR on 25 April, 2007	95
26. Figure 5.20 Images of active fire, NMDI, NDWI and NBR on 29 April, 2007	97
27. Figure 5.21 Images of active fire, NMDI, NDWI and NBR on 23 August, 2007	100
28. Figure 5.22 Images of active fire, NMDI, NDWI and NBR on 24 August, 2007	101
29. Figure 5.23 Images of active fire, NMDI, NDWI and NBR on 25 August, 2007	102
30. Figure 6.1 Space-time discretization of kinematic wave equation.....	112
31. Figure 6.2 Evolution of the daily vertical profile of the soil water content from 19 to 27 July 1999.....	123

LIST OF ABBREVIATIONS

AMSR-E	Advanced Microwave Scanning Radiometer –EOS
AVHRR	Advanced Very High Resolution Radiometer
EKF	Extended Kalman Filter
EOS	Earth Observing System
FD	Finite Difference
FE	Finite Element
IR	Infrared
LAD	Leaf Angle Distribution
LAI	Leaf Area Index
LST	Land Surface Temperature
MMS	Moving Mean Slope
MODIS	MODerate resolution Imaging Spectroradiometer
NBR	Normalized Burn Ratio
NDII	Normalized Difference Infrared Index
NDVI	Normalized Difference Vegetation Index
NDWI	Normalized Difference Water Index
NIR	Near Infrared
NMDI	Normalized Multi-band Drought Index
PDSI	Palmer Drought Severity Index
RG	Relative Greenness
SAIL	Scattering by Arbitrarily Inclined Leaves
SPI	Standardized Precipitation Index
SRB	Solar Reflectance Band
SVAT	Soil-Vegetation-Atmosphere Transfer
SWIR	Shortwave Infrared
USGS	U.S. Geological Survey
VIIRS	Visible/Infrared Imager/Radiometer Suite
VIS	Visible
VNIR	Visible-Near Infrared

ABSTRACT

REMOTE SENSING TECHNIQUES FOR SOIL MOISTURE AND AGRICULTURAL DROUGHT MONITORING

Lingli Wang, Ph.D.

George Mason University, 2008

Dissertation Director: Dr. John J. Qu

Drought is the most complex and least understood of all natural hazards, affecting more people than any other hazard. Soil moisture is a primary indicator for agricultural drought. This dissertation is aimed at evaluating and investigating soil moisture and drought monitoring using remote sensing techniques.

Recent technological advances in remote sensing have shown that soil moisture can be measured by a variety of remote sensing techniques, each with its own strengths and weaknesses. This research is designed to combine the strengths of optical/infrared as well as microwave remote sensing approaches for soil moisture estimation. A soil moisture estimation algorithm at moderate resolution was developed based on the well known 'Universal Triangle' relation by using MODIS land parameters as well as ground measured soil moisture. Though lower in spatial resolution, AMSR-E microwave measurements provides daily global soil moisture of the top soil layer, which are typically less affected by clouds, making them complementary to MODIS measurements over

regions of clouds.

Considering that the 'Universal Triangle' approach for soil moisture estimation is based on empirical relations which lack solid physical basis, a new physics based drought index, the Normalized Multi-band Drought Index (NMDI) was proposed for monitoring soil and vegetation moisture from space by using one near-infrared (NIR) and two shortwave infrared (SWIR) channels. Typical soil reflectance spectra and satellite acquired canopy reflectances are used to validate the usefulness of NMDI. Its ability for active fire detection has also been investigated using forest fires burning in southern Georgia, USA and southern Greece in 2007. Combining information from multiple NIR and SWIR channels makes NMDI a most promising indicator for drought monitoring and active fire detecting.

Given the current technology, satellite remote sensing can only provide soil moisture measurements for the top soil profile, and these near-surface soil moisture must be related to the complete soil moisture profile in the unsaturated zone in order to be useful for hydrologic, climatic and agricultural studies. A new numerical method was presented to solve the governing equation for water transport in unsaturated soil by matching physical and numerical diffusion. By applying a new numerical scheme with which to discretize the kinematic wave equation on the space-time plane, this method shows the capability to simulate the physical diffusion of the diffusive wave with the numerical diffusion generated in the difference solution under certain conditions. Compared with other numerical methods with the first-order finite differences scheme, this method has enhanced the solution precision to the second order. An example application shows a

good agreement with the observed data and suggests this new approach can be appropriate for soil moisture profile estimation.

By combining the proposed soil moisture and drought estimation techniques, the daily soil moisture profile at high resolution can be gained, and is thus expected to be helpful not only in drought monitoring and active fire detecting, but also in agricultural applications and climate studies.

CHAPTER ONE

1. INTRODUCTION

This dissertation develops soil moisture estimation algorithms, which can be used to estimate the spatial distribution and temporal variation of soil moisture content and drought with satellite remote sensing. The methodology is developed mainly for application to the optical/infrared (IR) measurements provided by current remote sensing platforms.

By taking the advantage of the strengths of optical/IR, microwave and ground measurements, a new approach is suggested for estimating soil moisture to achieve higher accuracy and spatial resolution. A new index, the Normalized Multi-band Drought Index (NMDI), which combines information from multiple near infrared (NIR), and short wave infrared (SWIR) channels, is proposed for monitoring soil and vegetation moisture from space based on the sensitivity analyses of the impact of soil and leaf water content on the surface reflectance. Finally, the near-surface soil moisture is related to the complete soil moisture profile in the unsaturated zone by using numerical soil moisture models.

1.1 Importance of soil moisture

Drought is the most complex and least understood of all natural hazards, affecting

more people than any other hazard (Wilhite Ed., 2000a). Bryant (1991) ranked natural hazards based on various criteria, such as severity, duration, spatial extent, loss of life, economic loss, social effect, and long-term impact and found that drought ranks first among all natural hazards (Narasimhan, 2004). In spite of the economic and the social impact caused by drought, it is the least understood of all natural hazards due to the complex nature and varying effects of droughts on different economic and social sectors (Wilhite, 2000). The wide variety of sectors affected by drought, its diverse geographical and temporal distribution, and the demand placed on water supply by human-use systems make it difficult to develop a single definition of drought (Richard and Heim, 2002). After analyzing more than 150 definitions of drought, Wilhite and Glantz (1985) broadly grouped those definitions into four categories: meteorological, agricultural, hydrological and socio-economic drought.

A number of different indices have been developed to quantify drought. Palmer Drought Severity Index (PDSI) (Palmer, 1965) and Standardized Precipitation Index (SPI) (McKee et al., 1993) are most widely used to assess and respond to drought. Most of the existing drought indices were based on precipitation and/or temperature, however, the amount of available soil moisture at the root zone is more critical for agricultural drought than the actual amount of precipitation deficit or excess (Narasimhan, 2004).

Soil moisture in the top one to two meters of the Earth's surface is one of the key variables in controlling the exchange of water and heat energy between land surface and atmosphere through evaporation and plant transpiration (Betts et al., 1996; Clark and Arritt, 1995). Compared to the total amount of water on the global scale, the volume of

soil moisture is small; nonetheless, it is of fundamental importance to many hydrological, biological and biogeochemical processes (http://www.ghcc.msfc.nasa.gov/landprocess/lp_home.html). As a result, soil moisture plays an important role in the development of weather patterns and the production of precipitation (Fennessey and Shukla, 1999). Accurate and reliable soil moisture estimates have important implications for drought monitoring.

As a result of the heterogeneity of soil properties, topography, land cover, evapotranspiration and precipitation, soil moisture, however, is highly variable both spatially and temporally (Engman, 1991; Wood et al., 1992; Walker, 1999). Hence, the development of a reliable drought index for agriculture requires proper consideration of the spatial and temporal variability of soil and land use properties, as well as of root soil moisture development, which will certainly improve the ability to monitor drought on a much more precise scale (Narasimhan, 2004).

1.2 Statement of problem

In spite of its importance, widespread and/or continuous measurement of soil moisture is all but nonexistent (http://www.ghcc.msfc.nasa.gov/landprocess/lp_home.html). Direct observations of soil moisture are currently restricted to discrete measurements at specific locations, and such point-based measurements do not reveal large-scale soil moisture and are therefore inadequate to carry out regional and global studies (<http://www.geotimes.org/may02/WebExtra0503.html>). Satellite remote sensing offers a

means of measuring soil moisture across a wide area continuously over time (Engman, 1990), while techniques in the microwave and optical/IR frequency regimes have attracted more attention (Chauhan, 2003). Microwave remote sensing technology has demonstrated a quantitative ability to retrieve soil moisture physically for most ranges of vegetation cover (Njoku et al., 2002). However, current microwave technology limits the spatial resolution of soil moisture data. Optical/IR techniques can provide fine spatial resolution for soil moisture estimation (Idso et al., 1975), but it is difficult to decouple signals from vegetation and soil. In addition, satellite remote sensing can only provide soil moisture measurements for the top few centimeters of the soil profile (Engman et al., 1995), while the complete soil moisture profile in the unsaturated zone is more useful for hydrologic, climatic and agricultural studies (Jackson, 1980; Mancini et al., 1995; Newton et al., 1983).

Therefore, to establish robust algorithms for soil moisture estimation, further efforts are needed to study the physical principles so as to identify the quantitative relationships between soil moisture content and remote sensing variables. The feasibility and capability of soil moisture retrieval from space need to be assessed in more details (Hao, 2006).

1.3 Objectives and scopes

The general objectives of this research are to present the potential of satellite optical/IR measurements as a diagnostic tool to assess soil moisture and drought status. Subsequently, we wish to develop new algorithms for making improved estimates of the spatial distribution and temporal variation of soil moisture and drought, by using satellite

optical and IR measurements. The specific objectives are proposed as follows:

- i) To estimate soil moisture by combining the strengths of multi-sensor and ground measurements to achieve higher accuracy and spatial resolution.
- ii) To investigate the potentials of using a combination of multiple NIR-SWIR spectral signatures to estimate soil moisture and vegetation moisture from space and to find the algorithm that will be best-suited for monitoring soil and vegetation moistures.
- iii) To retrieve soil moisture profile in the unsaturated zone by using numerical soil moisture models.

1.4 Organization of Dissertation

The dissertation consists of seven chapters. In order to better understand the study, the background and literature review are presented in the first three parts of the thesis. The next three parts give various works related to the objectives of the study and the last part concludes with summary and discussion of future directions.

Chapter 1 gives the general introduction, including the background for understanding the importance of soil moisture for drought monitoring, limitations of current methods for estimating soil moisture, research objectives, major data sources and principal results of the study.

Chapter 2 gives the literature review of drought definition and drought indices. The widely used Palmer Drought Severity Index and Standardized Precipitation Index will be explained in detail, as well as their limitations for drought monitoring.

Chapter 3 introduces the physical principles of soil moisture estimation from space,

with focuses on optical/IR and microwave remote sensing. Soil moisture profile estimation techniques such as regression approach, hydrological models, data assimilation, and water transport model are discussed in Chapter 3 as well.

A soil moisture estimation algorithm by linking MODIS land parameters with ground measured soil moisture is proposed in Chapter 4. The well known ‘Universal Triangle’ relation among vegetation, land surface temperature and soil moisture is presented in detail and two years of satellite measurements and ground observed data are employed to determine this relation. The relation, in conjunction with satellite measurements, is then regressed backward to obtain soil moisture at moderate resolution.

Chapter 5 develops a drought index by using measurements from multiple Solar Reflectance Bands (SRB). By combining information from multiple NIR, and SWIR channels, this newly designed drought index has enhanced the sensitivity to drought severity, and is well suited to estimate both soil and vegetation moisture from space.

A new numerical method for solving the one-dimensional soil moisture profile model is presented in Chapter 6, which investigates the feasibility of soil moisture profile estimation from near-surface soil moisture observations. Instead of directly solving the governing diffusion wave equation, the equation is approximated by applying a new numerical scheme with which to discrete the kinematic wave equation on the space-time plane. This method not only shows the capability to simulate the physical diffusion of the diffusive wave, but also enhances the solution precision to the second order.

Chapter 7 summarizes the results from the previous chapters and gives limitations, originalities, and discussions of future directions.

1.5 Major data sources

The major datasets used in this thesis include MODIS L1A Geolocation and MODIS L1B Calibrated Radiance, MODIS daily surface reflectance, MODIS daily surface temperature, MODIS 8-day surface reflectance, MODIS active fire map, MODIS thermal anomalies, fires, and biomass burning product, soil moisture observations from Shandong province, P. R. China, land cover type and soil type data collected from the Chinese Academy of Science. Table 1.1 lists the primary datasets and sources. The usages of these data sets in the study are described in details as follows:

1) MODIS Daily Surface Reflectance

Terra MODIS daily surface reflectance datasets for three years (2003-2005) over Shandong province, P. R. China are used in chapter 4 for soil moisture estimation.

2) Soil Moisture

Soil moisture measurements at 137 stations over Shandong province, P. R. China are used in chapter 4 for soil moisture estimation.

3) Land Cover Type

Land cover type data collected from the Chinese Academy of Science are used in chapter 4 to investigate the relationships among vegetation index, land surface temperature, and soil moisture for various surface types.

4) Soil Type

Soil type data collected from the Chinese Academy of Science are used in chapter 4 to investigate the relationships among vegetation index, land surface temperature, and soil moisture for various soil types.

5) MODIS 8-day surface reflectance

MODIS 8-day 500 m surface reflectance data (MOD09A1) are used to validate the usefulness of the newly designed drought index for remote sensing of vegetation drought in Chapter 5.

6) MODIS L1A Geolocation and MODIS L1B Calibrated Radiance

Terra MODIS L1A geolocation and L1B calibrated radiance data are used in chapter 5 for the estimation of water related indices.

7) MODIS active fire map

MODIS 250 m active fire data provided by the MODIS Rapid Response Team are used to evaluate the ability of the newly designed drought index for active fire detection in Chapter 5.

8) MODIS thermal anomalies, fires, and biomass burning product

MODIS 1 km fire products are used to evaluate the ability of the new drought index for active fire detection in Chapter 5.

Table 1.1 Data and sources

Data	Data Source
MODIS L1A Geolocation	USGS EOS Data Gateway
MODIS L1B Calibrated Radiance	USGS EOS Data Gateway
MODIS Daily Surface Reflectance	USGS EOS Data Gateway
MODIS 8-day surface reflectance	USGS EOS Data Gateway
MODIS active fire map	MODIS Rapid Response Team
MODIS fire product	USGS EOS Data Gateway
Land Cover Type	Chinese Academy of Science
Soil Type	Chinese Academy of Science
Soil Moisture	Shandong Province, P. R. China

1.6 Principal results

The principal results of this thesis include a semi-physical algorithm for estimating soil moisture by using MODIS optical/IR measurements and ground observations, a new drought index for monitoring both soil moisture and vegetation moisture from space, and a numerical method to relate the surface moisture to the layered soil profile.

The feasibility of estimating soil moisture with optical/IR remote sensing is investigated based on the ‘Universal Triangle’ method, a semi-physical approach derived from the Soil-Vegetation-Atmosphere-Transfer (SVAT) model. Results show good agreement between algorithm derived soil moisture and ground measurements, suggesting good potential of using MODIS optical/IR measurements and ground observations for soil moisture estimation.

A new index, the Normalized Multi-band Drought Index (NMDI), is proposed for monitoring soil and vegetation moisture from space based on the sensitivity analyses of the impact of soil and leaf water content on the surface reflectance. Typical soil reflectance spectra and satellite acquired canopy reflectances are used to validate the usefulness of NMDI for remotely sensing soil and vegetation moisture. Analysis revealed that by combining information from multiple NIR and SWIR channels, NMDI has enhanced the sensitivity to drought severity, and therefore, is a good indicator to estimate water content for both soil and vegetations. NMDI also demonstrates high performance in wildfires detection.

Finally, the satellite based near-surface soil moisture is related to the complete soil moisture profile in the unsaturated zone by using a new numerical soil moisture model.

CHAPTER TWO

2. LITERATURE REVIEW: DROUGHT AND DROUGHT INDICES

2.1 Drought definition

Drought is a recurring phenomenon that has plagued civilization throughout history. It affects natural habitats, ecosystems, and many economic and social sectors, from the foundation of civilization—agriculture—to transportation, urban water supply, and the modern complex industries (Richard and Heim, 2002). Drought is the most complex and least understood of all natural hazards, affecting more people than any other hazard (Wilhite, 2000). Bryant (1991) ranked natural hazards based on various criteria, such as severity, duration, spatial extent, loss of life, economic loss, social effect, and long-term impact and found that drought ranks first among all natural hazards (Narasimhan, 2004). Compared to other natural hazards like flood and hurricanes that develop quickly and last for a short time, drought is a creeping phenomenon that accumulates over a period of time across a vast area, and the effect lingers for years even after the end of drought (Tannehill, 1947). Hence, the loss of life, economic impact, and effects on society are spread over a long period of time, which makes drought the worst among all natural hazards.

In spite of the economic and the social impact caused by drought, it is the least understood of all natural hazards due to the complex nature and varying effects of

droughts on different economic and social sectors (Wilhite, 2000). The wide variety of sectors affected by drought, its diverse geographical and temporal distribution, and the demand placed on water supply by human-use systems make it difficult to develop a single definition of drought (Richard and Heim, 2002). In *Drought and Its Causes and Effects*, Tannehill (1947) wrote: "We have no good definition of drought. We may say truthfully that we scarcely know a drought when we see one...The first rainless day in a spell of fine weather contributes as much to the drought as the last, but no one knows how serious it will be until the last dry day is gone and the rains have come again... we are not sure about it until the crops have withered and died."

The difficulty of recognizing the onset or end of a drought is compounded by the lack of any clear definition of drought. Drought can be defined by various factors, such as rainfall amounts, vegetation conditions, agricultural productivity, soil moisture, levels in reservoirs and stream flow, or economic impacts. In the most basic terms, a drought is simply a significant deficit in moisture availability due to lower than normal rainfall (http://www.ncdc.noaa.gov/paleo/drought/drght_what.html).

After analyzing more than 150 definitions of drought, Wilhite and Glantz (1985) broadly grouped those definitions under four categories: meteorological, agricultural, hydrological and socio-economic drought.

- Meteorological drought: A period of prolonged dry weather condition due to precipitation departure.
- Agricultural drought: Agricultural impacts caused due to short-term precipitation shortages, temperature anomaly that causes increased evapotranspiration and soil water

deficits that could adversely affect crop production.

- Hydrological drought: Effect of precipitation shortfall on surface or subsurface water sources like rivers, reservoirs and groundwater.

- Socioeconomic drought: The socio economic effect of meteorological, agricultural and hydrologic drought associated with supply and demand of the society.

2.2 Drought indices

Based on the defined drought criteria, the intensity and duration of drought, a number of different indices have been developed to quantify drought, each with its own strengths and weaknesses. Drought indices integrate various hydrological and meteorological parameters like rainfall, temperature, evapotranspiration, runoff and other water supply indicators into a single number and gives a comprehensive picture for decision-making (Narasimhan and Srinivasan, 2005). Drought conditions are monitored constantly using these indices to provide current information on drought-impacted regions (http://www.ncdc.noaa.gov/paleo/drought/drght_what.html). Among various drought indices, Palmer Drought Severity Index (PDSI) (Palmer, 1965) and the Standardized Precipitation Index (SPI) (McKee et al., 1993) have been most commonly used for agricultural drought monitoring and forecasting.

2.2.1 Palmer Drought Severity Index (PDSI)

The Palmer Drought Severity Index (PDSI) was developed by Palmer in 1965 to measure the departure of the moisture supply (Palmer, 1965). Palmer based his index on

the supply-and-demand concept of the water balance equation, incorporated antecedent precipitation, moisture supply, and moisture demand.

PDSI is a meteorological drought index formulated to monitor both abnormally dry and abnormally wet weather conditions. PDSI has gained the widest acceptance because the index is based on a simple lumped parameter water balance model. The PDSI is calculated based on precipitation and temperature data, as well as the local available water content of the soil. From the inputs, all the basic terms of the water balance equation can be determined, including evapotranspiration, soil recharge, runoff, and moisture loss from the surface layer.

Despite the widespread acceptance of PDSI, various limitations have been observed by different studies (Akinremi and McGinn, 1996; Alley, 1984; Guttman, 1998; Narasimhan, 2004) including:

- Large spatial resolution of model parameters. The model doesn't consider the spatial variability of parameters like land use/land cover, and soil properties and assumes that they are uniform over the entire climatic zone encompassing several thousand squares. However, land use/land cover and soil properties are spatially highly variable in reality.
- Poorest performing of potential evapotranspiration calculation. In PDSI, potential evapotranspiration is calculated using Thornthwaite's method, which estimates evapotranspiration based on an empirical relationship between evapotranspiration and temperature (Thornthwaite, 1948). However, studies by Jensen et al. (1990) concluded that the poorest performing method overall was the Thornthwaite equation after they

evaluated and ranked different methods of estimating evapotranspiration under various climatic conditions.

- Moreover, the water balance model used by Palmer (1965) is a two-layer lumped parameter model. The two soil layers within the water balance computations are simplified and may not be accurately representative of a location.

2.2.2 Standardized Precipitation Index (SPI)

Similar to PDSI, SPI (McKee et al., 1993) is primarily a meteorological drought index. McKee et al. developed the SPI in 1993 based on the understanding that a deficit of precipitation has different impacts on groundwater, reservoir storage, soil moisture, snowpack, and stream flow. A key feature of the SPI is the flexibility to measure drought at different time scales. These time scales reflect the impact of drought on the availability of the different water resources. McKee et al. (1993) originally calculated the SPI for 3-, 6-, 12-, 24-, and 48-month time scales. The SPI calculation for any location is based on the long-term precipitation record for a desired period. This long-term record is first fitted to a probability distribution, which is then transformed into a normal distribution (Edwards and McKee, 1997) and gives the value of the SPI for the time scale used.

Unlike PDSI, SPI takes into account the stochastic nature of the drought and is therefore a good measure of short- and long-term meteorological drought. However, SPI does not account for the effect of soil, land use characteristic, crop growth, and temperature anomalies that are critical for agricultural drought monitoring as well. Moreover, the useable precipitation ultimately available for crop growth depends on the available soil moisture at the root zone rather than total rainfall itself. Hence, a drought

index based on soil moisture conditions would be a better indicator of agricultural drought (Narasimhan, 2004).

2.3 Chapter summary

This chapter has reviewed the drought definition and drought indices along with the limitations of the two mostly used indices PDSI and SPI. It has been found that most of the existing drought indices were solely based on precipitation and/or temperature which are useful for monitoring meteorological drought. The amount of available soil moisture at the root zone, however, is a more critical factor for agricultural drought than the actual amount of precipitation deficit or excess. Further the indices, such as PDSI and SPI, are based on a lumped parameter model that assumes a uniform soil property, precipitation and temperature for the entire climatic division.

Hence, the development of a reliable index for agriculture drought requires accurate and reliable estimates of soil moisture with proper consideration of the spatial and temporal variability of soil and land use properties, as well as of soil moisture condition and root development, which will certainly improve the ability to monitor agriculture drought on a much more precise scale. Recent technological advances in satellite remote sensing offer a means of a more effective drought monitoring system at a higher spatial and temporal resolution.

CHAPTER THREE

3. LITERATURE REVIEW: SOIL MOISTURE ESTIMATION

Soil moisture is the water that is held in the spaces between soil particles. Surface soil moisture is the water that is in the upper 10 cm of soil, whereas root zone soil moisture is the water that is available to plants, which is generally considered to be in the upper 200 cm of soil (http://www.ghcc.msfc.nasa.gov/landprocess/lp_home.html). Soil moisture content can be expressed gravimetrically or volumetrically, i.e.,

$$\theta_g = \frac{M_{water}}{M_{solid}} * 100\%, \quad (3.1)$$

$$\theta_v = \frac{V_{water}}{V_{solid}} * 100\%, \quad (3.2)$$

where θ_g and θ_v are the gravimetric and volumetric soil moisture content respectively, M_{water} and M_{solid} are mass of water and solid materials in soil respectively, and V_{water} and V_{solid} are volume of water and solid materials in soil respectively.

Soil moisture in the top one to two meters of the Earth's surface is one of the key variables in controlling the exchange of water and heat energy between land surface and atmosphere through evaporation and plant transpiration (Betts et al., 1996; Clark and Arritt, 1995). Compared to the total amount of water on the global scale, the volume of soil moisture is small; nonetheless, it is of fundamental importance to many hydrological, biological and biogeochemical processes

(http://www.ghcc.msfc.nasa.gov/landprocess/lp_home.html). As a result, soil moisture plays an important role in the development of weather patterns and the production of precipitation (Fennessey and Shukla, 1999).

In spite of its importance, widespread and/or continuous measurement of soil moisture is all but nonexistent (http://www.ghcc.msfc.nasa.gov/landprocess/lp_home.html). The lack of a convincing approach of global measurement of soil moisture is a serious problem (National Research Council, 1992). Direct observations of soil moisture are currently restricted to discrete measurements at specific locations, such as those made with the U.S. Department of Agriculture Soil Climate Analysis Network. But such point-based measurements do not reveal large-scale soil moisture and are therefore inadequate to carry out regional and global studies (<http://www.geotimes.org/may02/WebExtra0503.html>). Clearly, a need exists for continuous measurements of soil moisture with global coverage.

Satellite remote sensing offers a means of measuring soil moisture across wide areas continuously over time instead of at discrete point locations that are inherent with ground measurements. The moisture content change in soil and vegetation can leave significant signatures in remote sensing measurements. Thus, inversion of remote sensing measurements can retrieve the moisture content parameters of soil and vegetation.

3.1 Remote sensing of near-surface soil moisture

Research in soil moisture remote sensing began in the mid 1970's shortly after the surge in satellite development (Barton, 1978; Eagleman and Lin, 1976; Idso et al., 1975;

Njoku and Kong, 1977; Schmugge, et al., 1977). A number of techniques that span the whole electromagnetic spectrum have been used to sense soil moisture. Numerous researches have shown that near-surface soil moisture content can be measured by visible and thermal infra-red remote sensing, as well as active and passive microwave remote sensing techniques. The main difference between these four techniques is the wavelength region of the electromagnetic spectrum that is used by the sensor, and the source of the electromagnetic energy (Walker, 1999). Table 3.1 summarizes the relative merits of the different remote sensing techniques.

Table 3.1 Summary of remote sensing techniques for measurement of near-surface soil moisture content
(Engman, 1991; Walker, 1999).

	Property Observed	Advantage	Limitations	Noise Sources
Visible	Soil albedo Index of refraction	Lots of data	Many noise sources	Numerous
Thermal Infrared	Surface temperature	High resolution Large swath coverage frequency Physical well understood	Cloud cover limits frequency of coverage	Meteorological conditions Topography Vegetation cover
Active Microwave	Backscatter coefficient Dielectric properties	Low atmospheric noise High resolution	Limited swath width Calibration of SAR	Roughness Surface slope Vegetation cover
Passive Microwave	Brightness temperature Dielectric properties Soil temperature	Low atmospheric noise Moderate vegetation penetration	Low resolution Man made radiation limits operating range	Roughness Surface slope Vegetation cover

Among abovementioned four techniques, estimating soil moisture by passive microwave and optical/IR remote sensing have attracted more attention (Chauhan, 2003). Following sections present overviews of the current state of near-surface soil moisture

measurement from passive microwave and optical/IR remote sensing observations.

3.1.1 Passive microwave remote sensing

Microwave remote sensing measures the electromagnetic radiation in the microwave region of the electromagnetic spectrum, with wavelengths greater than about 5 cm being particularly effective, as they have fewer problems with the atmosphere and vegetation, sense a deeper soil layer, and maximize soil moisture sensitivity (Schmugge, 1985; Jackson et al., 1996).

The fundamental basis of microwave remote sensing of soil moisture is the large contrast between the dielectric properties of liquid water (~ 80) and dry soil (< 4). As the moisture increases, the dielectric constant of the soil-water mixture increases and this change is detectable by microwave sensors (Njoku and Kong, 1977; Dobson et al., 1985). Current algorithms of soil moisture estimation using microwave measurements are primarily based on the emissivity of land surface (Hao, 2006). The emission of microwave energy is proportional to the product of the surface temperature and the emissivity, which is commonly referred to as the microwave brightness temperature (http://weather.msfc.nasa.gov/surface_hydrology/surface_hydrology_inverse_model.html). According to the two-layer model proposed by Peake (1959), the surface scattering albedo W_q is composed of the diffused component W_q^{diff} and the specular component W_q^{spec} (Chauhan et al., 1999). Microwave brightness temperature T_q can be computed in the form

$$T_q = T[1 - (W_q^{diff} + W_q^{spec})], \quad (3.3)$$

where T is physical temperature of the surface, q represents the polarization direction, either vertical polarization or horizontal polarization.

The specular albedo for a vegetated rough surface is expressed as

$$W_q^{spec} = |R_q|^2 e^{-2\tau_q} e^{-4k_0^2 s^2 \cos^2 \theta}, \quad (3.4)$$

where τ_q , k_0 , s , θ are vegetation optical depth, free-space vegetation constant, surface root mean square (RMS) height, and view angle, respectively, and $|R_q|^2$ is the Fresnel reflectivity of flat surface.

The diffused albedo from a vegetated rough surface is contributed both by the vegetation and the rough surface. It can be expressed as sum of the vegetation and rough surface albedos. For a vegetated surface, the model is simplified by assuming that the vegetation scattering is weak, mathematically, this assumption means the diffused scattering albedo of the vegetation canopy to be zero. For a non-vegetated surface, it is assumed that the diffused albedo from a rough surface is negligibly small. Therefore, the brightness temperature of a vegetated and/or a rough surface is written as

$$T_q = T[1 - W_q^{spec}] = T[1 - |R_q|^2 e^{-2\tau_q} e^{-4k_0^2 s^2 \cos^2 \theta}] \quad (3.5).$$

For soil moisture estimation using both horizontal and vertical polarizations, equation (3.5) can be rewritten as

$$\frac{T - T_h}{T - T_v} = \left| \frac{R_h}{R_v} \right|^2 e^{2(\tau_v - \tau_h)} \quad (3.6)$$

The subscripts h and v refer to horizontal and vertical polarization, respectively.

When the viewing angle is less than 35° , it is reasonable to assume that $\tau_h - \tau_v \approx 0$

. Under this assumption, equation (3.6) can be further simplified to

$$\frac{T - T_h}{T - T_v} = \left| \frac{R_h}{R_v} \right|^2 \quad (3.7).$$

For dual polarization approaches, once the surface temperature T and the brightness temperatures for vertical and horizontal polarization are known, $|R_h / R_v|^2$ can be determined. Physically, the reflection coefficients R_h and R_v are expressed as (Chauhan et al., 1999).

$$R_h = \frac{\cos \theta - \sqrt{\epsilon_g - \sin^2 \theta}}{\cos \theta + \sqrt{\epsilon_g - \sin^2 \theta}} \quad (3.8)$$

and

$$R_v = \frac{\epsilon_g \cos \theta - \sqrt{\epsilon_g - \sin^2 \theta}}{\epsilon_g \cos \theta + \sqrt{\epsilon_g - \sin^2 \theta}}, \quad (3.9)$$

where ϵ_g is the real part of soil dielectric constant. ϵ_g can be determined from equations (3.8) and (3.9). By applying the empirical relation between dielectric constant ϵ_g and volumetric soil moisture content θ_v , the volumetric soil moisture content θ_v can be estimated quantitatively (Hallikainen et al., 1985; Hao, 2006).

Microwave retrieval of soil moisture has solid physical basis, and it has the potential to provide a direct measure of soil moisture. It also has the advantage of all-weather observations and better vegetation especially at the lower frequencies such as L bands (Njoku, 1999; Njoku et al., 2002). However, there are some reasons why microwave techniques have not been applied for the global estimation of soil moisture.

First, the spatial resolution of passive microwave sensors from space is poor, which

is usually in decades of kilometers. Present microwave sensor technology is not able to provide high-resolution data. In fact, the resolution available for passive microwave remote sensing from space has improved very little from its beginnings with the launch of the Electronically Scanned Microwave Radiometer in 1972.

Further, the available wavelengths from satellites do not provide adequate soil moisture sensitivity for all types and levels of vegetation cover. Current algorithms are mainly valid for weakly vegetated regions and relatively flat surface. Lower frequencies in the 1 to 10 GHz range (L- to X-Band) are recognized to be of the greatest utility in measuring soil moisture content since they provide adequate sensitivity to soil moisture for most ranges of vegetation cover (Njoku et al., 2002). However, long wavelengths require large antennas in orbit, which amounts to a challenge for engineering within operational cost constraints (Zhan et al., 2002; Crosson et al., 2005).

In addition, operational microwave technologies from remote platforms have wavelengths in the range of a few centimeters to a few decimeters. Due to these limited wavelengths, microwave techniques can only provide estimates of the near-surface soil moisture content, i.e., the upper few centimeters of the soil profile (Engman and Chauhan, 1995; Njoku and Entekhabi, 1996; Jackson, 1997).

In general, the limitation of microwave methods is that they cannot be used to estimate soil moisture at fine resolution in the root zone under lush green vegetation, such as in agriculture or in wetlands and other environmentally sensitive zones.

3.1.2 Optical/IR remote sensing

Remote sensing of soil moisture content using the optical/IR spectrum with

wavelengths between 0.4 and 2.5 μm measures the reflected radiation of the sun from the Earth's surface, known as albedo (Sadeghi et al., 1984). Soil albedo is defined as the ratio of reflected to incoming radiation (Idso et al., 1975), and has long been recognized as being influenced by soil moisture along with numerous other factors (Ångström, 1925).

There are some physical models to link soil biophysical and geophysical parameters with sensor measurements in optical/IR region. Inversion and sensitivity analysis of these models provide physical basis for soil moisture estimation (Hao, 2006). The SVAT model and the 'Universal Triangle' method have been most widely used.

Vegetation and land surface temperature have a complicated dependence on soil moisture. Careful analyses of data by Carlson et al. (1994) and Gillies et al. (1997) showed that there is a unique relationship sometimes referred to as the 'Universal Triangle' among soil moisture θ , the Normalized Difference Vegetation Index (NDVI), and the Land Surface Temperature (LST) for a given region. The results were later confirmed by theoretical studies using the SVAT model, which was first named by Gillies and Carlson (1995) and designed to describe the basic evaporation processes at the surface, together with the water partitioning between vegetation transpiration, drainage, surface runoff and soil moisture variations. More details of the 'Universal Triangle' method will be given in Chapter 4.

Carlson et al. analyzed NDVI and fractional vegetation cover in details and claimed the triangle relation is valid for a wide range of surface types (Carlson and Ripley, 1997). The relation between fractional vegetation cover and scaled NDVI, however, is very complicated. The triangle approach is a simplification based on empirical relations

between NDVI and fractional vegetation cover, and therefore it is a semi-physical method (Hao, 2006).

In addition, the relation between soil moisture content and optical/IR measurements is quite complex since soil reflectance is also influenced by organic matter, soil texture, surface roughness, angle of incidence, and plant cover and color (Engman, 1991; de Troch et al., 1996), causing a wide variation in albedo of different soil types even when dry (Sadeghi et al., 1984). These complicating factors, as well as the fact that the reflected solar energy responds to only the top few millimeters of the soil profile (Idso et al., 1975), limit the usefulness of solar reflectance measurements for soil moisture content determination (Walker, 1999).

Since radiative transfer model is all but nonexistent to simulate reflectance with soil parameters so far, ‘Universal Triangle’ method is still the primary approach for soil moisture estimation with optical/IR measurements.

3.1.3 Combining microwave and optical/IR remote sensing

Microwave measurement is the current primary approach for soil moisture measurement estimation from space, due to the limited penetration depth of waves in optical/IR region. Chauhan (2003) proposed a synergistic approach to estimate soil moisture content at higher spatial resolution by combining microwave and optical/IR measurements. The soil moisture estimation algorithm consists of two steps. Step one involves soil moisture estimation at microwave resolution using microwave brightness temperature and aggregated LST. The theoretical basis for measuring soil moisture in step one is based on the large contrast between the dielectric properties of water and dry

soil, which has been described in section 3.1.1. Step two deals with improving the resolution of soil moisture estimated in the first step by incorporating non-aggregated km-scale LST, NDVI, and albedo measurements. The second step is based on the ‘Universal Triangle’ relationship among soil moisture, NDVI, temperature, and albedo. Using the microwave derived soil moisture and optical/IR derived NDVI, temperature and albedo, a soil moisture product at high resolution can be produced. Both steps are based on well known physics.

However, the low spatial resolution of microwave measurements, as well as surface heterogeneity makes it difficult to derive robust relationships between optical/IR measurements and soil moisture estimated from microwave remote sensing (Hao, 2006).

3.2 Soil moisture profile estimation

Given the current technology, satellite remote sensing can only provide soil moisture measurements for the top few centimeters of the soil profile. Since these upper few centimeters of the soil are the most exposed to the atmosphere, their moisture varies rapidly in response to rainfall and evaporation (Jackson, 1993). These observations of near-surface soil moisture must be related to the complete soil moisture profile in the unsaturated zone (Walker, 1999), in order to be more useful for agricultural, hydrologic and climatic studies. Lots of attempts have been made to extrapolate these near-surface soil moisture observations to estimate the soil moisture content over the entire soil profile (top one to two meters of the Earth’s surface). This section reviews the approaches that have been made for estimation of the soil moisture profile from observations of

near-surface soil moisture content, including regression approach, hydrological models, data assimilation by combining remotely sensed data with hydrologic models (Kostov and Jackson, 1993), and water transport model in unsaturated soil.

3.2.1 Regression approach

Developing a regression equation is the simplest approach to estimate the soil moisture profile from near-surface measurements. The basis for using simple regression relationships to predict the soil moisture profile from near-surface measurements under some conditions, is that the laws of physics link all layers of the soil together (Kostov and Jackson, 1993).

However, most of the studies have demonstrated that for a given thickness of near-surface layer, the correlation of soil moisture contents between two soil layers decreased as the profile depth increased, and that for a given profile depth the correlation increased as the near-surface layer thickness increased, suggesting that the profile depth over which useful soil moisture information can be determined from near-surface soil moisture measurements using linear regression is shallow. In addition, such an approach is usually based on data for typical soil and land use conditions, and generally cannot be extrapolated from one location to another (Ragab, 1995).

3.2.2 Hydrological models

Recent developments in using hydrologic models to estimate soil moisture profiles provide an alternative to soil moisture observations in the field (Schmugge et al., 1980). The principal advantage of hydrologic models is that they can provide timely information

on the spatial soil moisture distribution without the necessity of field visits (Walker, 1999).

A limitation of many existing hydrologic models is their emphasis on runoff estimation (Wood et al., 1992; Otle' and Vidal-Madjar 1994) at the expense of a realistic representation of the soil moisture profile. For example, the NOAH model used in Land Data Assimilation Scheme, includes two soil layers: a 10 cm thick surface layer and a 190 cm thick root zone layer (Ek et al., 2003). These two soil layers are conceptual based and may not well represent the real water transportation in the soil. Another general disadvantage of hydrologic models is that even though they have been verified on basin scales with discharge data at various time scales, the estimated soil moisture in the various layers has not been verified against measured soil moisture data (Georgakakos and Baumer, 1996).

3.2.3 Data assimilation

As one of the key advances in recent years, data assimilation has received increasing attention given its ability to retrieve the soil moisture profile by assimilating near-surface soil moisture measurements in a soil model. The soil model expresses how the surface moisture and the deeper layer moisture are related (<http://cee.mit.edu/index.pl?id=3333&isa=Category&op=show>). Remote sensing observations can provide spatial and temporal information on soil moisture content, which can be used as input for the model, as independent feedback, or to keep the simulation on track (Kostov and Jackson, 1993; Walker, 1999). The surface measurement will allow the model to better predict the soil moisture down through the root zone, which

is where plants draw up moisture and transpire (<http://cee.mit.edu/index.pl?id=3333&isa=Category&op=show>). The statistical assimilation techniques such as the Extended Kalman Filter (EKF), through their ability to modify directly the soil moisture estimates of deeper soil layers, show the most promise in this application. EKF updates the soil moisture profile based on the relative magnitudes of the co-variances of the observations and the model profile estimates.

Despite the advantages of data assimilation, the incomplete knowledge of soil model physics and the limitation of assimilation technique itself restrict the use of data assimilation approach. Most of the hydrological models developed and evaluated for modeling soil moisture content have been for bare soils. Furthermore, in most hydrologic models, the soil moisture component is an intermediary component within the water balance equation, and has not been verified against measured soil moisture data (Kite and Pietroniro, 1996). Recent studies by Walker et al. (2001) indicated that soil moisture profile estimation with the EKF assimilation scheme is only as good as the model representation of the dominant soil physical processes and its calibration. In addition, the assimilation is only useful for correcting error as a result of errors in initial conditions and/or atmospheric forcing data and not as a result of error in the physics of the soil moisture model.

3.2.4 Water transport model

Vertical water infiltration in layered soil profiles is usually modelled using the nonlinear partial differential Richards Equation (Parlange et al., 1972, 1980; Sanders et al., 1988), which was derived by linking the continuity equation and Darcy's Law.

Richards Equation describes the changes of moisture content in space and time due to vertical flows. Procedures for solving unsaturated flow problems very often require the use of either analytical or numerical techniques.

Analytical solutions have received considerable attention because they are very useful for assessing the accuracy of numerical models and provide insight into the physics of flow phenomena (Si and Kachanoski, 2000). Despite the success of analytical solutions, they usually provide answers for a simplified class of problems, while problems of a more general type are handled with numerical solutions through attendant discretization of the solution domain.

Numerical simulation of the Richards Equation has been the focus of considerable research (Hills et al., 1989; Celia et al., 1990; Pan and Wierenga, 1995). The solutions to the governing differential equations for water transport in unsaturated soil are normally obtained by using finite difference (FD) or finite element (FE) calculation schemes (Van Genuchten, 1982). Often, explicit FD models become numerically unstable and give large numerical errors because of the strong nonlinearity inherent in the equation. The numerically more involved FE and implicit FD models are numerically stable and accurate if appropriate values of the time and depth increments are chosen. However, criteria for selecting the correct values of the time and depth increments, are poorly understood and often not available. In addition, the FE and implicit FD models are relatively complicated to program and to solve (Moldrup et al., 1992).

3.3 Chapter summary

This chapter has reviewed the commonly used methods for measuring the near-surface soil moisture content from satellite remote sensing techniques, along with approaches to estimate the entire soil profile from near-surface soil moisture observations.

There are a fairly wide variety of approaches, which have been used to retrieve soil moisture from satellite remote sensing. Most of the studies have demonstrated the considerable potential of microwave and optical/IR frequency regimes for soil moisture retrievals. Monitoring soil moisture from space, however, remains challenge. Microwave remote sensing has advantages for all-weather observations and solid physics, with the limitation of poor spatial resolution. Optical/IR remote sensing can provide measurements at relatively higher spatial resolution, while the physical relationships between optical/IR measurements and soil moisture have not been established. Moreover, only the moisture in the top few centimeters of soil can be detected by current satellite remote sensing techniques.

The review of soil moisture profile estimation from near-surface soil moisture has shown that most previous studies have assimilated the near-surface soil moisture observations into a hydrologic model. As near-surface soil moisture observations become available, they are assimilated into the system to yield an updated estimate of the system states. Data assimilation has received increasing attention due to its ability to retrieve the soil moisture profiles. However, the incomplete knowledge of soil model physics and the limitation of assimilation technique itself restrict the use of data assimilation approach.

Therefore, to establish robust algorithms for estimating soil moisture at higher spatial and temporal resolution, further efforts are needed to study the physical principles so as to identify the quantitative relationships between soil moisture content and remote sensing variables. The feasibility and capability of soil moisture profile estimation from near-surface soil moisture also need to be assessed in more details (Hao, 2006).

CHAPTER FOUR

4. SOIL MOISTURE ESTIMATION USING MULTI-SENSOR AND GROUND MEASUREMENTS

Most of the studies have demonstrated the considerable potential of microwave and optical/IR frequency regimes for soil moisture retrievals, each with its own strengths and weaknesses. Chauhan (2003) proposed a synergistic approach to estimate soil moisture by combining the strengths of microwave and optical/IR measurements. However, the poor spatial resolution of microwave sensors, as well as the surface heterogeneity makes it difficult to establish robust relationships between optical/IR measurements and soil moisture estimated from microwave remote sensing (Hao, 2006).

The present study is designed to produce a soil moisture estimation algorithm at moderate resolution by linking soil moisture measurements from multiple space-borne sensors (optical/IR and microwave), and ground stations based on the ‘Universal Triangle’ relation among soil moisture, vegetation cover and land surface temperature.

4.1 Soil moisture estimation using MODIS and ground measurements

The MODerate resolution Imaging Spectroradiometer (MODIS) is a key research instrument for the NASA Earth Observing System (EOS) mission (Barnes and Salomonson, 1993). The first MODIS instrument was launched onboard the EOS Terra

satellite in December 1999 and the second onboard the EOS Aqua satellite in May 2002 (Barnes et al., 2002, 2003; <http://modis.gsfc.nasa.gov>). Because MODIS senses all the Earth's surface in 36 spectral bands spanning the visible (VIS, 0.415 μm) to IR (14.235 μm) spectrum at nadir spatial resolutions of 1 km, 500 m and 250 m, the MODIS remote sensing applications are of interest not only to land, ocean, and atmosphere researchers but to application, interdisciplinary and environmental scientists (Justice et al., 1998; Qu et al., 2001; Salomonson et al., 2002).

In this section, MODIS 1 km NDVI and LST products will be combined with ground measurements to investigate the potential of soil moisture estimation at higher spatial and temporal resolution.

4.1.1 Algorithm theory

Vegetation and land surface temperature have a complicated dependence on soil moisture. An earlier description of the vegetation and atmosphere relationship is from the vegetation index/temperature trapezoid (Moran et al., 1994). Careful analyses of data by Carlson et al. (1994) and Gillies et al. (1997) showed that there is a unique relationship among soil moisture, vegetation cover, and surface temperature for a given region. The results were later confirmed by theoretical studies using the SVAT model, which was first named by Gillies and Carlson (1995).

Figure 4.1 represents a schematic description of the relationship sometimes referred to as the 'Universal Triangle' (Zhan et al., 2002). The abscissa and the ordinate are scaled temperature and NDVI respectively such that:

$$T^* = \frac{T - T_0}{T_s - T_0} \quad (4.1)$$

$$NDVI^* = \frac{NDVI - NDVI_0}{NDVI_s - NDVI_0} \quad (4.2)$$

where, T and $NDVI$ are observed land surface temperature and $NDVI$, respectively, and the subscripts o and s stand for minimum and maximum values.

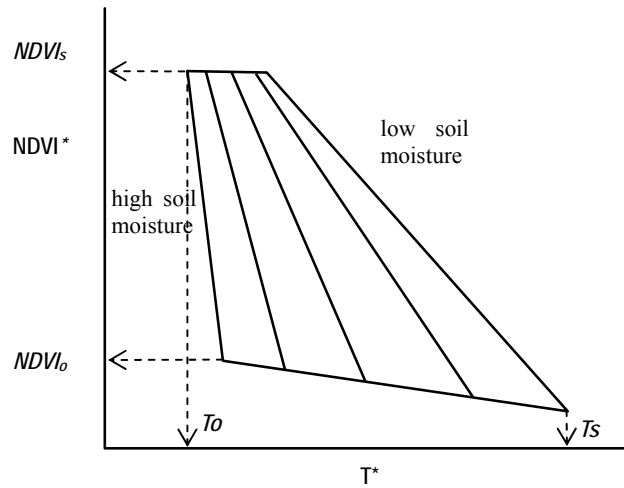


Figure 4.1. 'Universal Triangle' Relation between soil moisture, temperature and NDVI

The idea behind the triangle is that the vegetation radiometric temperature is always close to air temperature, but that the surface radiant temperature over bare soil can vary depending on the soil water content. This implies that the spatial variation in surface radiant temperature will be small (except for emission from underlying bare soil) over a full vegetation but will vary from warm to cold surface moisture availability goes from zero to one for bare soil (<http://www.essc.psu.edu/~tnc/howto.html>).

That the triangle does not exhibit a sharp vertex is due to the fact some emission of long wave radiation at full vegetation cover is able to penetrate the canopy and reach the radiometer. Thus, even when $NDVI^* = 1$, the underlying dryness of the soil produces a spatial variation in surface radiant temperature which is manifested in the above figure as a lateral variation in the soil moisture isopleths. Because the lateral variation at $NDVI^* = 1$ is so much less than that at $NDVI^* = 0$, the figure resembles a triangle, though perhaps it is more appropriately called a trapezoid. Eliminating the variation of soil thermal inertia (or conductivity and diffusivity) with soil water content will considerably sharpen the upper vertex of the triangle (<http://www.essc.psu.edu/~tnc/howto.html>).

Carlson et al. (1994) found that the relationship between soil moisture θ , $NDVI^*$, and T^* can be expressed through a regression formula such as:

$$\theta = \sum_{i=0}^{i=n} \sum_{j=0}^{j=n} a_{ij} NDVI^{*(i)} T^{*(j)} \quad (4.3)$$

In terms of a second order polynomial, the above equation can be expanded as (Chauhan, 2003)

$$\begin{aligned} \theta = & a_{00} + a_{10} NDVI^* + a_{20} NDVI^{*2} \\ & + a_{01} T^* + a_{02} T^{*2} \\ & + a_{11} NDVI^* T^* + a_{22} NDVI^{*2} T^{*2} \\ & + a_{12} NDVI^* T^{*2} + a_{21} NDVI^{*2} T^* \end{aligned} \quad (4.4).$$

Equations (4.1), (4.2) and (4.4) have been employed for the study presented in this section.

The flowchart of the soil moisture estimation algorithm is given in Figure 4.2. The

regression relationships are identified by combining the ground measurements of soil moisture and MODIS scaled NDVI and LST. By applying these regression relationships to MODIS measurements, daily soil moisture estimates at MODIS resolution can be obtained.

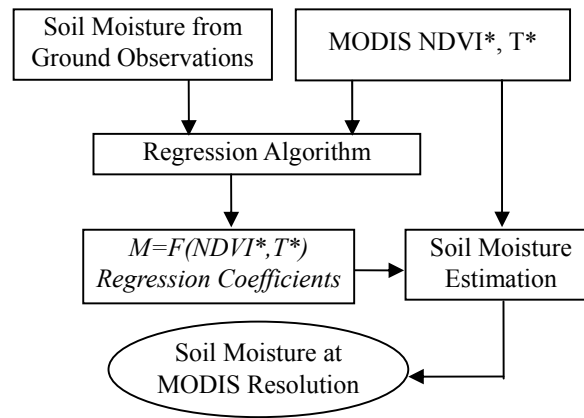


Figure 4.2. Schematic flow diagram for the soil moisture estimation algorithm

This soil moisture estimation technique is later applied to a new set of MODIS NDVI and LST products. In-situ soil moisture is compared against the predictions. A statistic analysis has also been performed on the estimation procedure. Finally, the advantages and limitations of this approach are discussed.

4.1.2 Study area and data sources

The current study is conducted over Shandong Province, situated in the eastern part of P. R. China bounded by 34.3°-38.2°N latitudes and 114.7°-122.7°E longitudes. It has a total area of 156,000 km², and 65% of its land is plains and low-lying land, while 35% is

mountainous or hilly land (<http://www.cpirc.org.cn/en/30Province1999-shandong.htm>). Shandong belongs to the warm temperate monsoon climate region with four distinct seasons, the mean annual temperature ranges from 11 to 14 degrees Celsius, and the mean annual precipitation ranges from 550 to 950 mm (<http://www.out369.com/2005/main/english.asp?id=4>). The bulk of this region is cropland along with other short vegetation in the agriculture fields.

There are 137 reasonably distributed ground stations over Shandong Province (Figure 4.3), which collect soil samples to measure the soil water content gravimetrically at the top 10 cm, 20 cm, and 40 cm soil layers at 8 AM on the 6th, 16th, and 26th of each month since the year 2003.



Figure 4.3. Map of the study area and the distribution of ground stations

The local overpass time of the satellite Terra almost matches the observation time of ground measurements, so we used Terra MODIS data in this study. Three years (2003~2005) of Terra MODIS data and ground observed soil moisture over the study area

were acquired. MODIS data are daily surface reflectance (MOD09) to derive NDVI, and daily surface temperature (MOD11) at 1 km resolution. In order to investigate the dependency of the regression relations on land cover and soil types, data on land surface and soil types at 1 km resolution of the study area have been collected from the Chinese Academy of Science. The land cover includes 13 types and 110 subordinate types, and the soil data includes 57 types and 178 subordinate types.

4.1.3 Algorithm construction and validation

Two years of data (2003 and 2004) were used for algorithm calibration and one year of data (2005) for validation. A system of equations (4.4) was set up using ground observed soil moisture and MODIS scaled NDVI and LST for all the pixels matching the site of each ground station. The regression coefficients a_{ij} for each station were determined using the least square method. To check the accuracy of the regression coefficients, the MODIS scaled NDVI and LST were used in conjunction with calculated a_{ij} in equation (4.4) to compute soil moisture. The coefficients of determination, relative errors and standard deviation between the algorithm derived and the ground observed soil moisture were calculated (Table 4.1).

For a total of 93 ground stations with valid data, the relative errors approach 0, and the standard errors are less than 0.05; the coefficients of determination for 55 stations are greater than 0.8, 71 stations greater than 0.7 and 82 stations greater than 0.6. The results demonstrated the feasibility of soil moisture estimation using equation (4.4).

Table 4.1 Statistics for algorithm derived soil moisture

	R ²				Relative Error (%)	Standard Error
	>0.8	>0.7	>0.6	>0.5	<1*10 ⁻¹⁰	<0.05
Number of Stations	55	71	82	90	93	93

For practical use, we investigated the dependency of the regression relationships on land cover and soil types, and calibrated equation (4.4) for the major land cover and soil types in the study area. Grassland, Cropland, Wooded Grassland, Closed Shrub-Land and Urban and Built-up are the five main land covers, and Loam, Clay Loam and Sandy Clay Loam are the three main soil types for the study area. Table 4.2 lists the regression coefficients for two dominant land cover types: Grassland and Cropland. These land cover and soil types based regression relations, in conjunction with MODIS scaled NDVI and LST, were then regressed backward to obtain soil moisture. Coefficients of determination and *p*-values between the regression derived and the ground measured soil moisture show that regression relations are land cover and soil type dependent (Table 4.3). Considering the Cropland and Grassland, which account for more than 85% of the study area (1165 pixels against a total of 1360 pixels), the overall coefficients of determination are greater than 0.4, and the *p*-values are less than 0.02. The same results can be seen for the most dominant soil type, Loam, which accounts for a total of 767 pixels. In this sense, these regression relations can be applied to estimate the soil moisture over non-ground measurement areas based on land cover and soil type information. Thus the moderate resolution soil moisture maps can be generated over the study area. Figure 4.4 is the soil moisture map at 1 km resolution on 26 November, 2005. The white regions in the map are the areas where soil moisture is not computed because of corrupted data due to clouds.

Clearly, the 1 km image shows more detail in the soil moisture quantitative estimates and spatial pattern than the sparse ground measurements.

Table 4.2 Regression coefficients for main land cover and soil types

Land Cover Soil Type	Grassland			Cropland		
	Loam	Sandy Clay Loam	Clay Loam	Loam	Sandy Clay Loam	Clay Loam
a_{00}	0.3019	-2.868	0.2821	0.3513	0.3612	0.2133
a_{10}	-0.7071	7.639	-0.7888	-0.8727	-1.199	-0.4935
a_{20}	0.6581	-4.792	0.7275	0.7577	1.478	0.5112
a_{01}	0.0922	10.95	-0.4151	0.0482	-0.5267	0.2665
a_{02}	0.0660	-9.543	0.356	-0.0128	0.4068	0.0432
a_{11}	0.7794	-29.08	3.046	1.283	3.926	0.7354
a_{22}	0.8246	-17.20	2.350	0.8761	6.685	1.330
a_{11}	-0.9992	25.68	-2.547	-0.9416	-3.547	-1.359
a_{12}	-0.8351	19.22	-2.772	-1.409	-5.551	-1.006

Table 4.3 Statistics for land cover and soil type oriented algorithms

Land Cover	Soil Type	P-Value	R ²	Pixels
Wooded Grassland	Loam	0.0526	0.5488	49
	Sandy Clay Loam	0.3047	0.9556	11
	Clay Loam	0.1651	0.6340	29
Closed Shrubland	Loam	0.0440	0.9242	15
Grassland	Loam	3.40E-14	0.4248	412
	Sandy Clay Loam	0.0256	0.6746	35
	Clay Loam	0.0003	0.5295	95
Cropland	Loam	1.50E-09	0.4481	262
	Sandy Clay Loam	0.0040	0.6464	48
	Clay Loam	3.40E-12	0.4540	313
Urban and Built-up	Loam	0.0497	0.7036	29
	Sandy Clay Loam	0.0031	0.7443	35
	Clay Loam	0.2738	0.6153	27

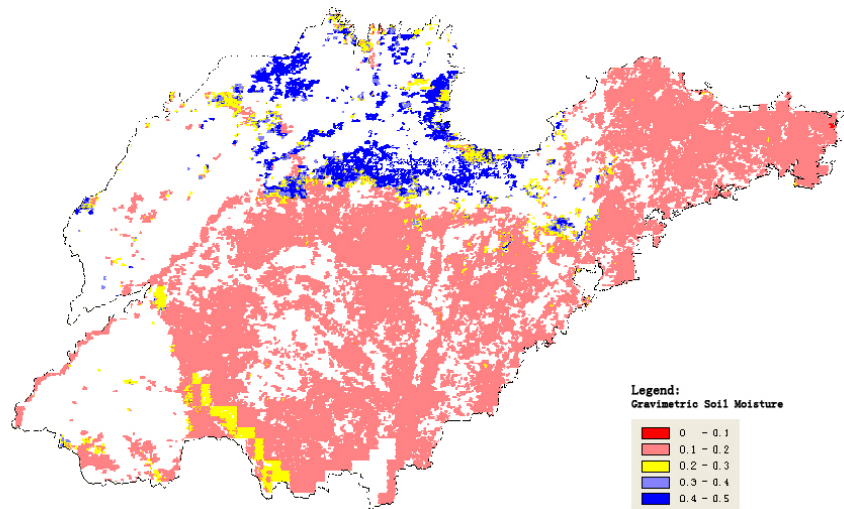


Figure 4.4. Soil moisture map at 1 km resolution over Shandong Province of 26 November, 2005

The ground observed soil moisture and MODIS scaled NDVI and LST for the year 2005 were used to validate the regression algorithms. Table 4.4 shows the validation results of surface type dependent soil moisture estimation algorithms. The maximum standard error is less than 0.07, and the relative errors are around 10%.

Table 4.4 Statistics for validation

Land Cover	Regression derived and measured soil moisture		
	Percentage Relative Error (%)	Standard Error	Pixels
Wooded Grassland	15.01	0.0585	43
Closed Shrubland	-9.83	0.1454	3
Grassland	-10.87	0.0497	230
Cropland	-8.74	0.0481	289
Urban and Built-up	11.41	0.0609	31

Above results indicate that the soil moisture estimation approach using MODIS and ground measurements is feasible.

4.1.4 Discussion and conclusion

There are still some limitations of this soil moisture estimation approach. The time difference between the ground measurements and the Terra overpass could impact on the results. In addition, the 10 cm depth layer observation does not actually correspond to the surface parameters. The estimation errors could also come from the fact that the point ground soil samples may not represent the 1 km footprints of MODIS observations. Moreover, for the cloudy worst case, it is difficult to derive soil moisture from MODIS land parameters, which operate in the Optical/IR bands. Fusion of soil moisture data from multiple sensors and ground stations may be a solution to this problem.

Notwithstanding the limitations just mentioned, the primary conclusions of the present research are clear: (1) the core process to link ground measured soil moisture and MODIS land parameters is ‘Universal Triangle’ relation, which is reinforced by the application in this study; (2) the results suggest that soil moisture estimation by combining ground measurements and MODIS land parameters is feasible; (3) compared with the ground measurements, the soil moisture map at 1 km resolution generated by the regression algorithm provides more regional soil moisture details and spatial patterns (Wang et al., 2007a).

4.2 Soil moisture estimation using AMSR-E products

4.2.1 AMSR-E soil moisture products

The Advanced Microwave Scanning Radiometer - Earth Observing System (AMSR-E) is a multichannel passive microwave radiometer launched aboard NASA's

Aqua Satellite on May 4, 2002. This conically scanning instrument measures brightness temperature at six frequencies, 6.925, 10.65, 18.7, 23.8, 36.5, and 89.0 GHz, with vertical and horizontal polarizations at each frequency for a total of twelve channels. It achieves global swath coverage every two days or less, separately for ascending and descending passes, except for a small region near the poles. The mean footprint diameter ranges from 60 km at 6.92 GHz to 5 km at 89 GHz. The AMSR-E land surface products of surface soil moisture, vegetation water content and surface temperature are available on a daily basis in 25 km Equal-Area-Scalable Earth grid with a global cylindrical, equal area projection true at 30⁰N and 30⁰S (<http://www.ghcc.msfc.nasa.gov/AMSR/>).

The AMSR-E land surface parameter algorithm uses a simplified physically-based radiative transfer model to retrieve surface soil moisture (g/cm³), vegetation water content (kg/m²) and surface temperature (K) (Njoku, 1999). The retrieval algorithm uses the two lowest frequencies (6.9 and 10.7 GHz) since modeling surface roughness and vegetation scattering effects above 10 GHz becomes more complex and uncertain. These two frequencies also have better vegetation penetration although at the cost of decreased spatial resolution. Microwave retrievals are more reliable in regions of low vegetation since sensitivities to moisture and vegetation decrease for high vegetation levels (Njoku, 1999).

AMSR-E soil moisture products include daily global soil moisture of the top 2 cm soil layer with spatial resolution of 25 km. Figure 4.5 is AMSR-E soil moisture map projected to the study area described in section 4.1.2 on 16 November, 2005.

Though lower in spatial resolution than MODIS optical bands, AMSR-E microwave

measurements are typically less affected by clouds, making them complementary to MODIS measurements over regions of clouds such as the white area in the Figure 4.4.

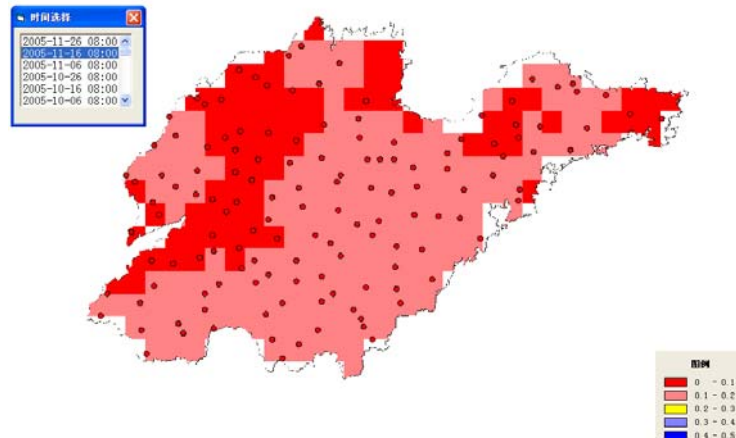


Figure 4.5. AMSR-E soil moisture map over the study area on 16 November, 2005

MODIS 1 km soil moisture products were aggregated to produce equivalent MODIS retrievals within the AMSR-E 25 km footprint. Since the AMSR-E observation has been shown to be area averaged measures over the sensor footprint, AMSR-E and aggregated MODIS soil moisture products are expected to be highly correlated (Dasgupta and Qu, 2006). This relationship was investigated using regression analysis. The relationship was reasonably assumed to be applicable at the MODIS resolution and was subsequently used to generate soil moisture data for the region of clouds where soil moisture is difficult to be derived from MODIS land parameters.

Combining AMSR-E and MODIS measurements thus has the potential for ensuring the data continuity of high spatial resolution soil moisture products and could be beneficial for drought monitoring.

4.2.2 Relationship between AMSR-E and ground measurements

To capture exactly the point observation of soil moisture at each ground station, an AMSR-E footprint covering the ground station was taken as the matching pixel. The ground measurements were compared with the corresponding AMSR-E data directly. Results show that these two datasets are poorly correlated (Table 4.5). For total 137 ground stations, only 8 stations have the coefficients of determination greater than 0.7, 22 stations greater than 0.6 and 42 stations greater than 0.5. Figure 4.6 are scatter plots of ground measurements and AMSR-E data for the best and worst case, respectively. Further work has been tried to improve the results, such as filtering out the data with heavy rainfall since rainfall is an important factor which affects the soil moisture value, and sorting the data by soil type or vegetation type. However, the improvement was not clearly visible.

Table 4.5 Coefficients of determination between AMSR-E and ground measurements

	R^2		
	>0.7	>0.6	>0.5
Number of stations	8	22	42

The poor correlation might be caused by different spatial scale between AMSR-E and ground measurements. Since soil moisture is highly variable spatially, high risk will be involved using the point soil samples to represent the 25 km footprints of AMSR-E observations. The difference of observation depth between the ground measurements and

the AMSR-E products could also impact the correlation. The soil moisture observations at the 10 cm depth layer do not correspond to AMSR-E top 2 to 3 cm soil layer products.

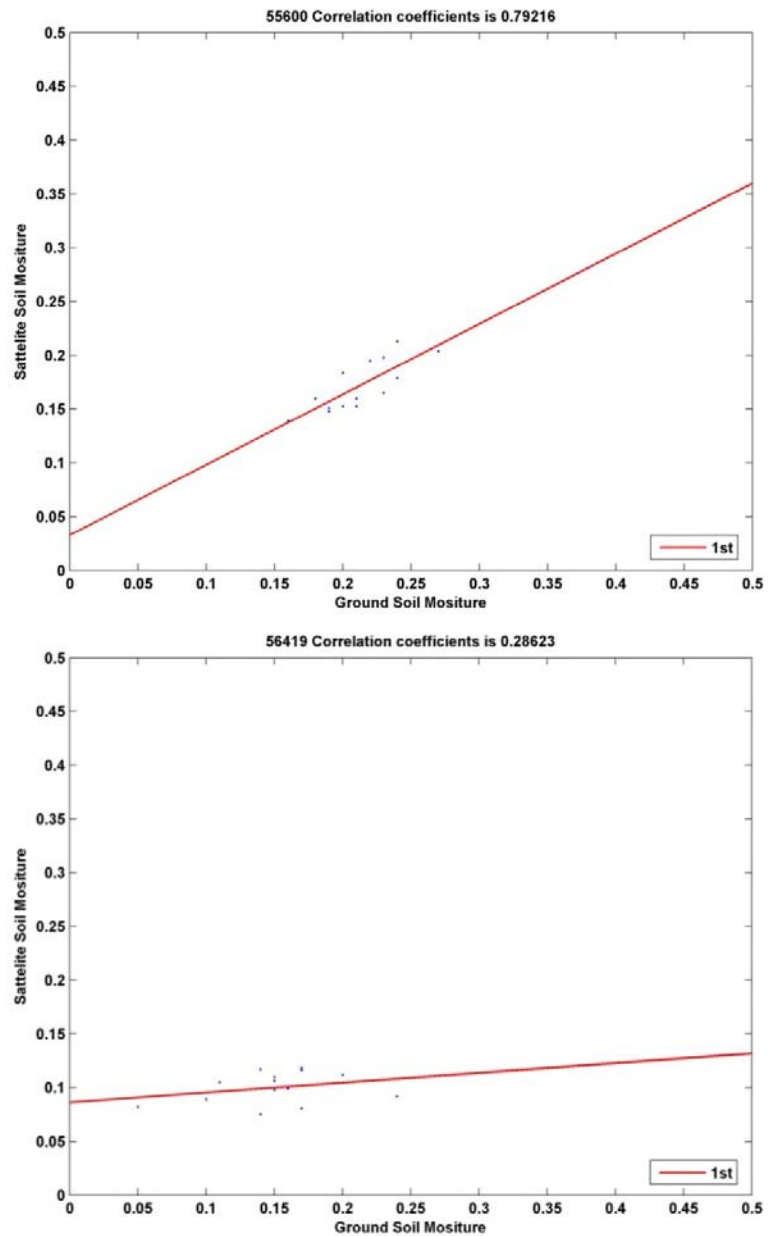


Figure 4.6. Scatter plots of ground measurements and AMSR-E data (best case and worst case)

4.3 Chapter summary

A soil moisture estimation algorithm by linking MODIS land parameters to ground measured soil moisture is developed in this Chapter. The algorithm is built on the basis of the well known ‘Universal Triangle’ relation among soil moisture, NDVI and LST. Good agreements between the algorithm derived and observed soil moisture suggested that soil moisture estimation by combining ground measurements and MODIS land parameters is feasible. Compared with the ground measurements, the soil moisture map at 1 km resolution generated by the algorithm provides more regional soil moisture details and spatial patterns (Wang et al., 2007a). AMSR-E soil moisture products were also described in this Chapter. Though lower in spatial resolution than MODIS optical bands, AMSR-E microwave measurements are typically less affected by clouds, making them complementary to MODIS measurements over regions of clouds.

Notice that the ‘Universal Triangle’ approach used in this Chapter to estimate soil moisture at MODIS resolution is based on empirical relations between NDVI and fractional vegetation cover, which lacks solid physical basis. Physical retrieval of soil moisture from space is still a challenge, and therefore, requires further efforts to study the physical principles so as to identify the quantitative relationships between soil moisture content and remote sensing variables.

CHAPTER FIVE

5. SOIL MOISTURE ESTIMATION USING MULTIPLE MODIS SRB MEASUREMENTS

Water stress causes physiologic changes in vegetation and soil, which in turn causes variations in vegetation and soil spectral signatures. Based on the spectral variations of water absorption characteristic, several indices using the reflectances from near infrared (NIR) and shortwave infrared (SWIR) channels have been proposed for remote sensing of vegetation water content from space (Dasgupta, 2007), such as NDII, the Normalized Difference Infrared Index (Hardisky et al., 1983); LWCI, the Leaf Water Content Index (Hunt et al., 1987); WI, the Water Index (Penuelas et al., 1993, 1996, 1997); NDWI, the Normalized Difference Water Index (Gao, 1996); SRWI, the Simple Ratio Water Index (Zarco-Tejada and Ustin 2001; Zarco-Tejada et al., 2003), and GVWI, the Global Vegetation water Moisture Index (Ceccato et al., 2002).

However, satellite-measured surface reflectances are mixed results of signals reflected from vegetation and bare soils. Reflectance of a canopy is strongly influenced by the soil reflectance especially when plant density is low or the canopy has not reached ground closure (Bach and Verhoef, 2003). Uncertainties arise in estimating vegetation water content using NIR-SWIR indices since they cannot completely remove the background soil effects (Gao, 1996). Soil reflectance in turn is influenced by soil

moisture along with numerous other factors such as mineral composition, organic matter, and soil texture (Asner, 1998; Ben-Dor et al., 1999). For a given location, the soil reflectance is primarily determined by the moisture of the soil surface since other factors change very slowly with time (Liu et al., 2002). Baret et al. (1993) found that mineral- and organic matter-related absorptions are stronger in the shorter visible wavelengths, while soil moisture significantly affects the NIR-SWIR spectral domain (Baret et al., 1993; Lobell and Asner 2002), where the vegetation water indices operate. Since soil moisture is not only spatially but also temporally highly variable, it has to be considered in realistic simulations of land surface reflectances and optical vegetation water indices.

In order to identify the quantitative relationships between soil moisture content and the canopy reflectance, and vegetation water indices, sensitivity analysis is performed using simulations with the coupled soil-leaf-canopy reflectance model. Based on the sensitivity analysis, a new index, the Normalized Multi-band Drought Index (NMDI), is proposed for monitoring soil and vegetation moisture from space. Typical soil reflectance spectra and satellite-acquired reflectances, are used to validate the usefulness of NMDI. Its ability for active forest fire detection has also been investigated.

5.1 Sensitivity studies of moisture effects

Radiative transfer models providing reflectance spectra of leaves and vegetation canopies are used for sensitivity analyses in direct mode. First the soil reflectance in NIR and SWIR range over a typical soil type in croplands is obtained using a moist soil reflectance model. The moist soil reflectance model is then linked with a leaf and canopy

reflectance model to simulate canopy reflectance. Vegetation water indices are derived from the simulated canopy reflectance. The MODIS bands centred at 858, 1240, 1640 and 2130 nm, and vegetation water indices NDWI and NDII are used in this study.

5.1.1 Model

5.1.1.1 Moist soil reflectance model

The moisture effects on soil reflectance have been studied by many authors. These studies have reported the familiar darkening of soils upon wetting (Baumgardner et al., 1985; Ishida et al., 1991; Twomey et al., 1986). Lobell and Asner (2002) analyzed shortwave reflectances (400-2500 nm) for four different soils at various moisture contents and found that soil reflectance changes due to moisture were well explained by the following exponential model:

$$R = f \times R_{dry} + (1 - f) \times R_{dry} \times \exp(-c \times \theta) \quad (5.1)$$

where R is the soil reflectance at a particular wavelength, f is the ratio of the saturated to dry reflectance, R_{dry} is the reflectance of dry soil (at $\theta=0.0$), c describes the rate of soil reflectance change with moisture, θ is the volumetric soil water content. All variables except θ are soil type and wavelength dependent.

Similar exponential models have been reported in the soil reflectance modelling by Liu et al. (2002). Such nonlinear equations are representative of the physical processes underlying the relationship, i.e., Beer's Law for absorption in random homogenous media (Liu et al., 2002). It is thus expected that such a model would be useful for estimating soil reflectance under different soil moisture contents (Dasgupta, 2007).

5.1.1.2 Leaf and canopy reflectance models

The leaf and canopy radiative transfer models used in this study are the widely used PROSPECT and SAIL (Scattering from Arbitrarily Inclined Leaves) respectively. Numerous studies have employed coupled PROSPECT-SAIL model to investigate remote sensing retrievals of vegetation moisture. The well known and validated leaf radiative transfer model PROSPECT (Jacquemund and Baret, 1990) described a leaf as consisting of N homogeneous layers having particular absorbing and scattering properties, and reflectance and transmittance are calculated from the absorption coefficient and refractive index at a given wavelength for each layer. Leaf reflectance was simulated with the PROSPECT model with four input parameters: the leaf structure parameter, N , representing the number of elementary layers; the chlorophyll a and b content (C_{ab} , $\mu\text{g}/\text{cm}^2$); the leaf water content (C_w , g/cm^2 or cm); and the dry matter content or specific leaf weight (C_m , g/cm^2) of the leaf.

The PROSPECT simulated leaf reflectance and the moist soil reflectance model simulated soil reflectance are then coupled as the inputs of a canopy reflectance model SAIL. SAIL (Verhoef et al., 1984) is a turbid medium model that approximates the canopy as an infinitely extended plane-parallel scattering medium, made up of randomly oriented scattering phytoelements. Canopy reflectance is calculated from inputs of the leaf area index (LAI), leaf angle distribution (LAD), leaf and soil optical properties, and the solar and sensor illumination and viewing angles.

5.1.2 Simulation setup

To generate the reflectance database, parameter ranges were defined for each model variable first. In the main simulation, the variables were carefully set to represent the ranges expected in the ‘real world’, based on data from the literature.

5.1.2.1 Parameter ranges for soil reflectance model

Four types of soil have been studied by Lobell and Asner (2002), including Argic Aridisol in New Mexico representative of arid shrubland, Xeric Andisol in Oregon representative of temperate coniferous forest, Ustic Mollisol in Texas representative of temperate savanna, and Aridic Entisol in Texas representative of temperate shrubland. Considering that vegetation moisture status is more critical for cropland where the main soil type is loam or clay loam, parameters of Ustic Mollisol were used in the moist soil reflectance model. Table 5.1 lists the value of each parameter obtained from experiments by Lobell and Asner for MODIS Visible-Near Infrared (VNIR) bands 1 (645 nm), 2 (858 nm) and 4 (555 nm), and SWIR bands 5 (1240 nm), 6 (1640 nm) and 7 (2130 nm). The volumetric soil moisture content is set to be 0.005, 0.1, 0.15, 0.2, 0.25, 0.3, 0.35, 0.4 and 0.45, representative of the natural soil conditions experienced in cropland.

Table 5.1 Input parameters to soil reflectance model for MODIS bands

Mollisol	Band 1	Band 2	Band 4	Band 5	Band 6	Band 7
R_{dry}	0.110	0.213	0.090	0.373	0.416	0.405
c	10.9	7.5	12.2	5.0	3.33	6.25
f	0.538	0.612	0.560	0.610	0.429	0.300

5.1.2.2 Parameter ranges for PROSPECT and SAIL

To account for effects due to leaf water content C_w , leaf dry matter C_m , chlorophyll a and b content C_{ab} , and leaf internal structure N , the PROSPECT model is running for a range of values of C_w (in cm) and C_m (in g/cm²) between 0.004 and 0.04, C_{ab} between 20 and 80, and N between 1 and 4.

At the canopy level, a set of SAIL simulations are employed to account for canopy structural characteristics such as LAI and the viewing geometry described by solar zenith angle, view angle, and fraction of direct sun light. Ten discrete values of LAI were used ($LAI = 0.01, 0.5, 1.0, 1.5, 2.0, 3.0, 4.0, 5.0, 6.0, 7.0$). The canopy is assumed to have an erectophile LAD, typical of wheat (Atzberger et al., 2003). The acquisitions are simulated for a solar zenith angle of 30°, a sun angle of 45° (0.8 fraction of direct sun light), and nadir view angles for all the cases.

Outputs of soil reflectance and leaf reflectance/transmission from the moist soil reflectance model and PROSPECT were tied to the inputs of SAIL. The parameters used in the leaf and canopy simulations are summarized in Table 5.2.

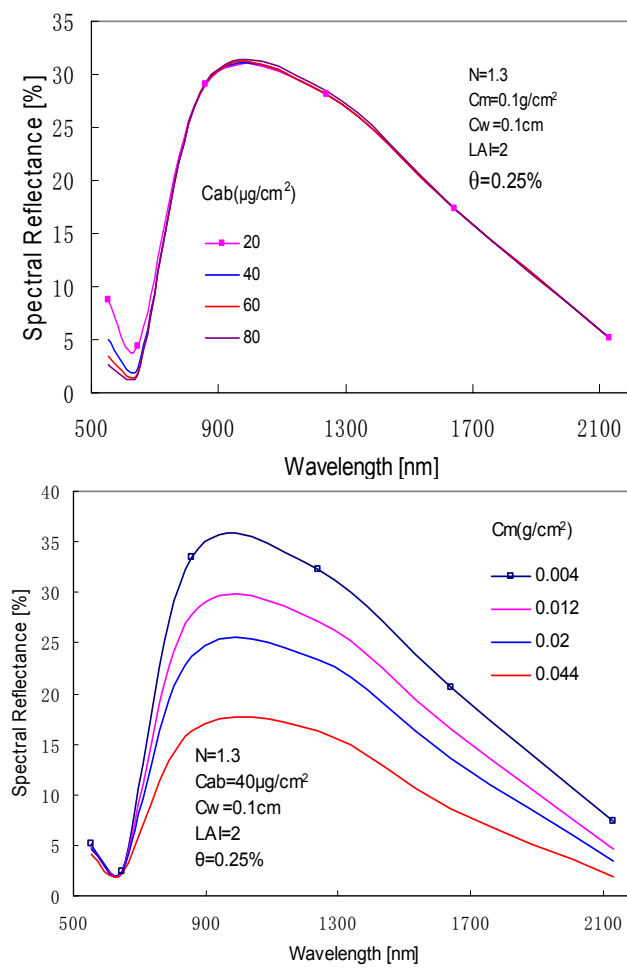
Table 5.2 Input parameters to PROSPECT and SAIL models

Parameters	Range
PROSPECT	
N	1-4
C_{ab} (μg/cm ²)	20-80
C_w (cm)	0.004-0.04
C_m (g/cm ²)	0.004-0.04
SAIL	
LAI (m ² /m ²)	0.01-7
LAD	erectophile
solar zenith angle	30°
Fraction Direct Solar	0.8
View angle	Nadir

5.1.3 Model simulation

5.1.3.1 Modeling the moisture effects on MODIS reflectance

As can be seen in Figure 5.1, the chlorophyll content C_{ab} only affect MODIS VIS bands 4 and 1, and has no effect on MODIS NIR and SWIR bands 2, 5, 6 and 7, while the change of leaf dry matter content C_m affects MODIS NIR and SWIR bands. The water content C_w affects MODIS SWIR bands 5, 6 and 7, while the effect of the leaf internal structure N on reflectance is distributed from VNIR to SWIR region.



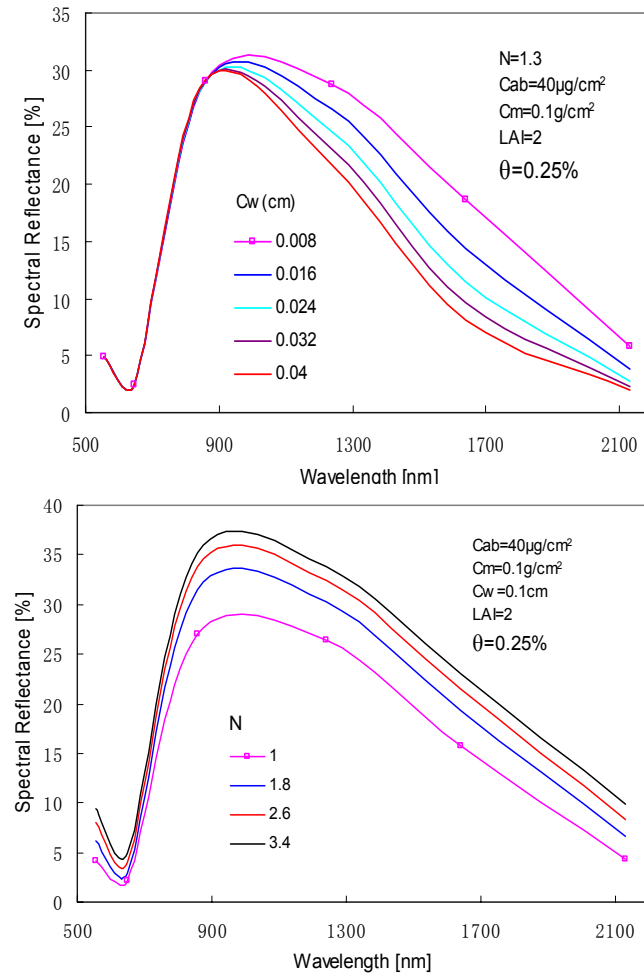


Figure 5.1. Effects of leaf biochemical constituents such as C_{ab} , C_m , C_w , and N on canopy reflectance

The soil background is known to disturb the canopy reflectance (Baret and Guyot, 1991; Clevers and Verhoef, 1991). The moist soil reflectance model is demonstrated with simulations obtained by varying soil moisture with a very small LAI value as 0.01 (upper plot of Figure 5.2). The modeling result shows that the SWIR region is better suited than VNIR to measure soil moisture changes. SWIR reflectance continues to respond to soil moisture in the entire range from 0.5% to 45%, representative of the most common

conditions found in agriculture fields, while VNIR saturates at intermediate soil moisture content near 20%. If the soil is covered by a vegetation canopy with a LAI of 2, the impact of soil moisture is still clearly visible over NIR and SWIR spectra range, although ground coverage of canopy was almost achieved (lower plot of Figure 5.2).

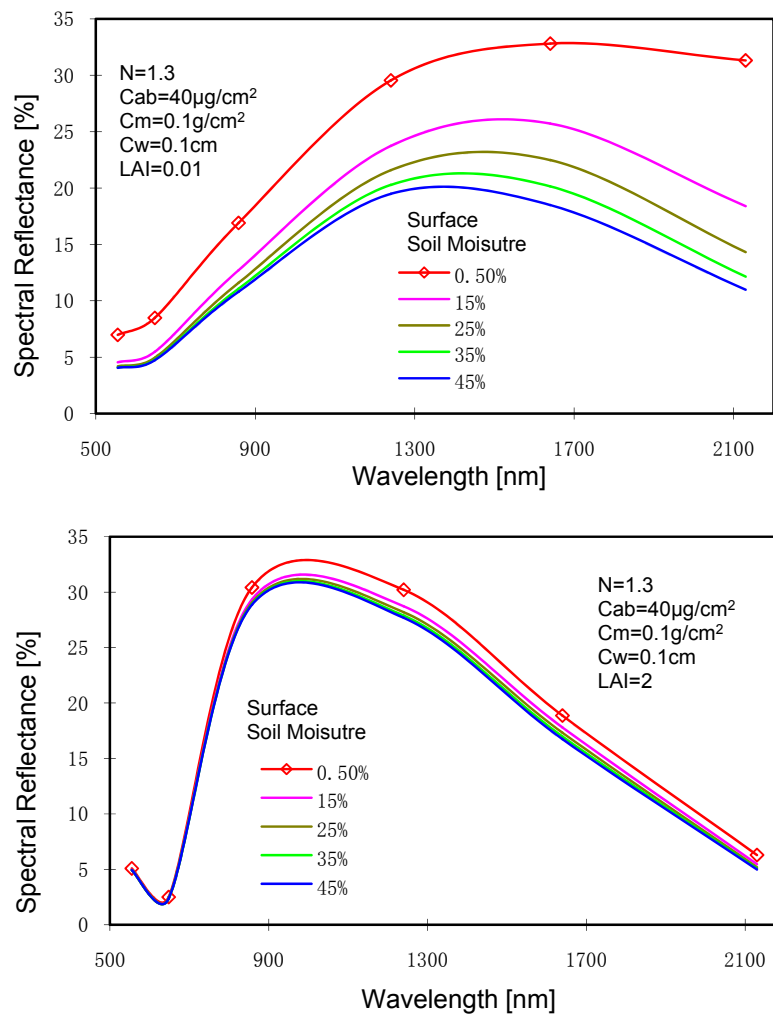


Figure 5.2. Simulated canopy spectra with LAI of 0.01 and 2 and varying soil moisture

The canopy biophysical variables are not totally independent, that is, a change in leaf water content may induce a change in chlorophyll concentration and leaf internal structure, as well as a change in the average leaf angle (Jacquemoud, 1993). In order to quantify the relative influence of each canopy parameter, the difference of spectral reflectance was obtained by varying each parameter separately from low to high values at a given time, while keeping other parameters fixed at medium values. The variables were changed over their normal range of variation: leaf dry matter and leaf water content from 0.004 to 0.04, leaf internal structure from 1 to 4, soil moisture content from 0.005 to 0.45, and leaf area index from 0.5 to 4. Medium values of $C_{ab}=40$, $C_m=0.01$, $C_w = 0.01$, $N=1.3$, $LAI=1, 2$, and soil moisture = 0.25 are used.

For a given set of input parameters, the results show that the primary affecting factors vary with specific wavelength (Figure 5.3). The NIR reflectance is highly sensitive to the canopy structural parameter LAI, obtaining an 18% variation when LAI changes from 0.5 to 4. The leaf internal structure and leaf dry matter have a major effect over the entire NIR and SWIR spectral region, generating 5-10% variations with larger effect at higher LAI values.

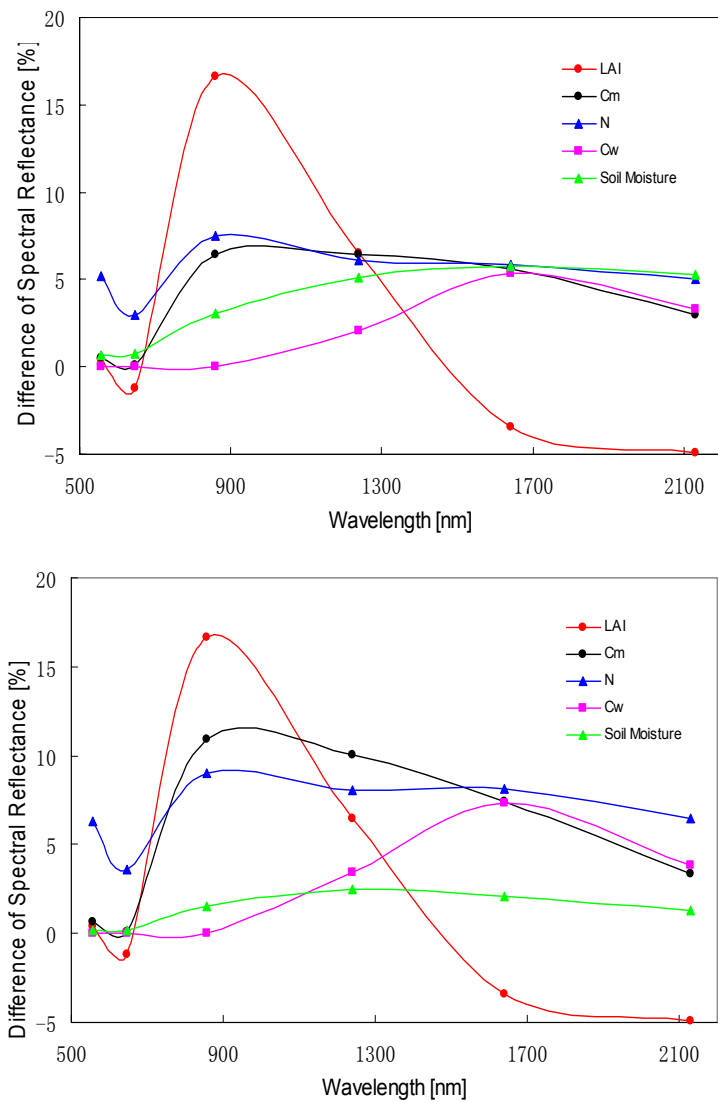


Figure 5.3. Difference of simulated spectra by using low and high values of each parameter separately with LAI of 1 and 2

Soil moisture effects are spectrally different from changes caused by variable leaf water contents. The impacts of soil moisture are clearly visible over the entire NIR and SWIR spectra range with MODIS SWIR bands 5, 6 and 7 located in the high value plateau, while the changes caused by leaf water contents are limited to the MODIS SWIR

bands and affect band 6 primarily. Further, at low LAI values less than 2, although changes of soil moisture and leaf water content both introduce around 5% variation to MODIS band 6, the soil moisture effects overshadow the latter on MODIS bands 5 and 7. However, when LAI values are higher than 2, the primary driver of SWIR reflectance variations is leaf water content, while the difference due to soil moisture change is reduced to 1%. Following sections will mainly focus on soil moisture and leaf water content effects on MODIS SWIR bands 5, 6 and 7.

The effects of soil moisture on the SWIR reflectance were illustrated for MODIS bands 5, 6 and 7 in Figure 5.4 with an LAI range of 0.01-4 assuming different soil moisture contents. In each case, an increase of soil moisture is connected with a reduction of the reflectance. The soil effects on the SWIR reflectance are stronger at low LAI values less than 2 when vegetation does not completely cover soil background, especially for MODIS band 5, which continues to respond to soil moisture up to an LAI of 3. MODIS band 7 is more sensitive to soil moisture at low moisture levels, obtaining more than 10% variation when soil moisture changes from 0.005 to 0.01. When LAI values are higher than 3, sensitivity to soil background is minimal and no background effects are found on SWIR reflectance for any soil moisture range.

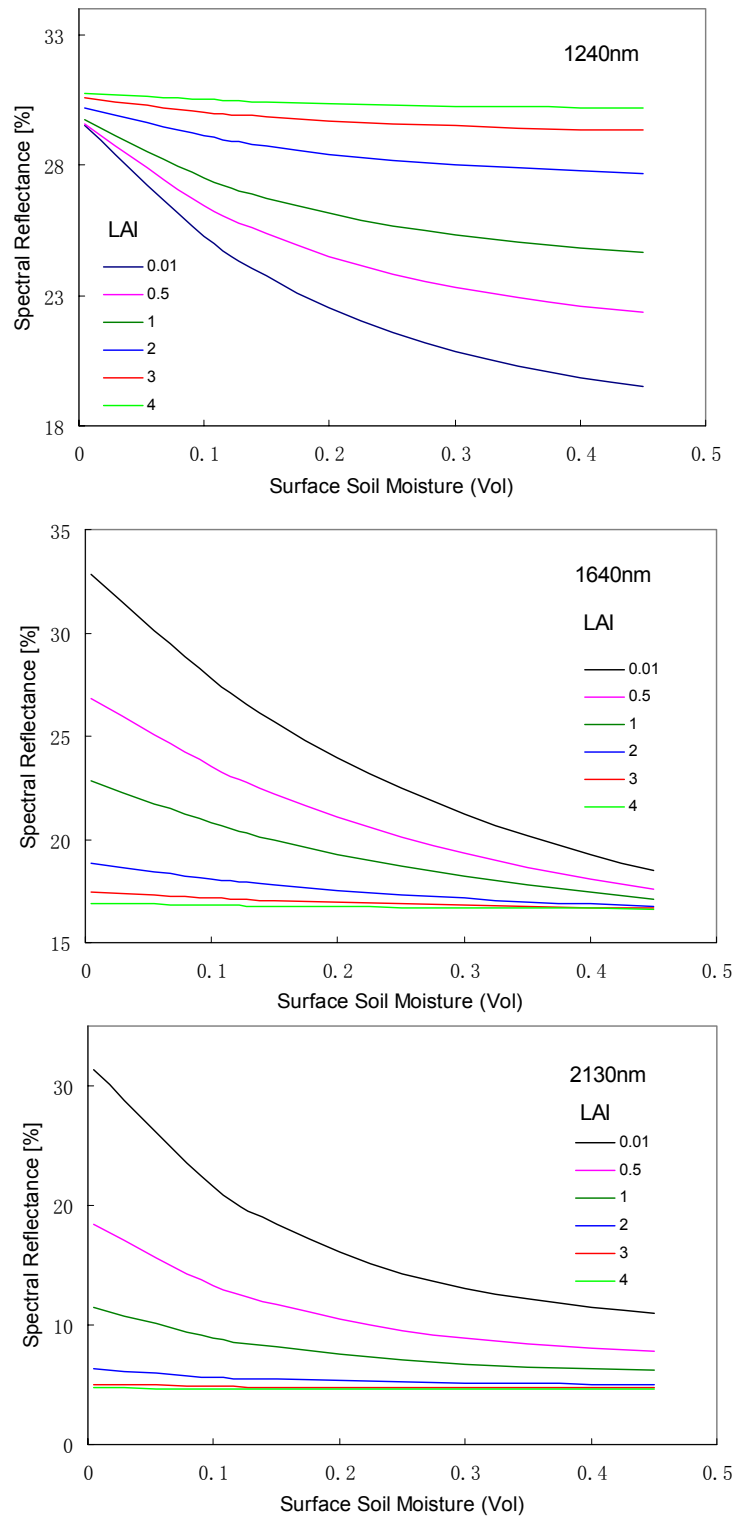


Figure 5.4. Sensitivity of MODIS SWIR reflectance to soil moisture

Not only does soil water affect the canopy reflectance, but also the water in the plants is an actor itself. The plots in Figure 5.5 show such simulations obtained for canopies with an LAI range of 0.5-6 assuming different leaf water contents. The increase of leaf water content provides similar reduction results in the signatures. This reduction is stronger for higher LAI values. MODIS bands 6 and 5 are better suited to measure leaf water content changes than band 7 since they both obtain higher variations near 15% when they are modelled with LAI value of 6 and C_w changes from 0.004 to 0.04. Regarding LAI effects, band 5 is less easy to saturate with high LAI values up to 5, while bands 6 and 7 saturate with an LAI of 3.

In general, an increase of soil moisture or leaf water content is connected with a reduction of the reflectance, while an increase of LAI generates reflectance increment for MODIS band 5, and reflectance reduction for bands 6 and 7. MODIS band 5 is more sensitive than bands 6 and 7 to both soil moisture and leaf water change: the reflectance of band 5 continues to respond to moisture at higher LAI values while the other two saturate at lower LAI values. In addition, the comparison of all plots of Figures 5.4 and 5.5 shows that the reflectance reduction induced by the increase of soil moisture or leaf water content has different characteristics. For a range of LAI, the reflectance of MODIS band 5 presents divergence with an increase of soil moisture, while convergence with leaf water content; both reflectances of MODIS bands 6 and 7 present convergence with soil moisture, while band 6 presents divergence and the latter has parallel shape. These differences may be useful to extract information about soil and vegetation water status.

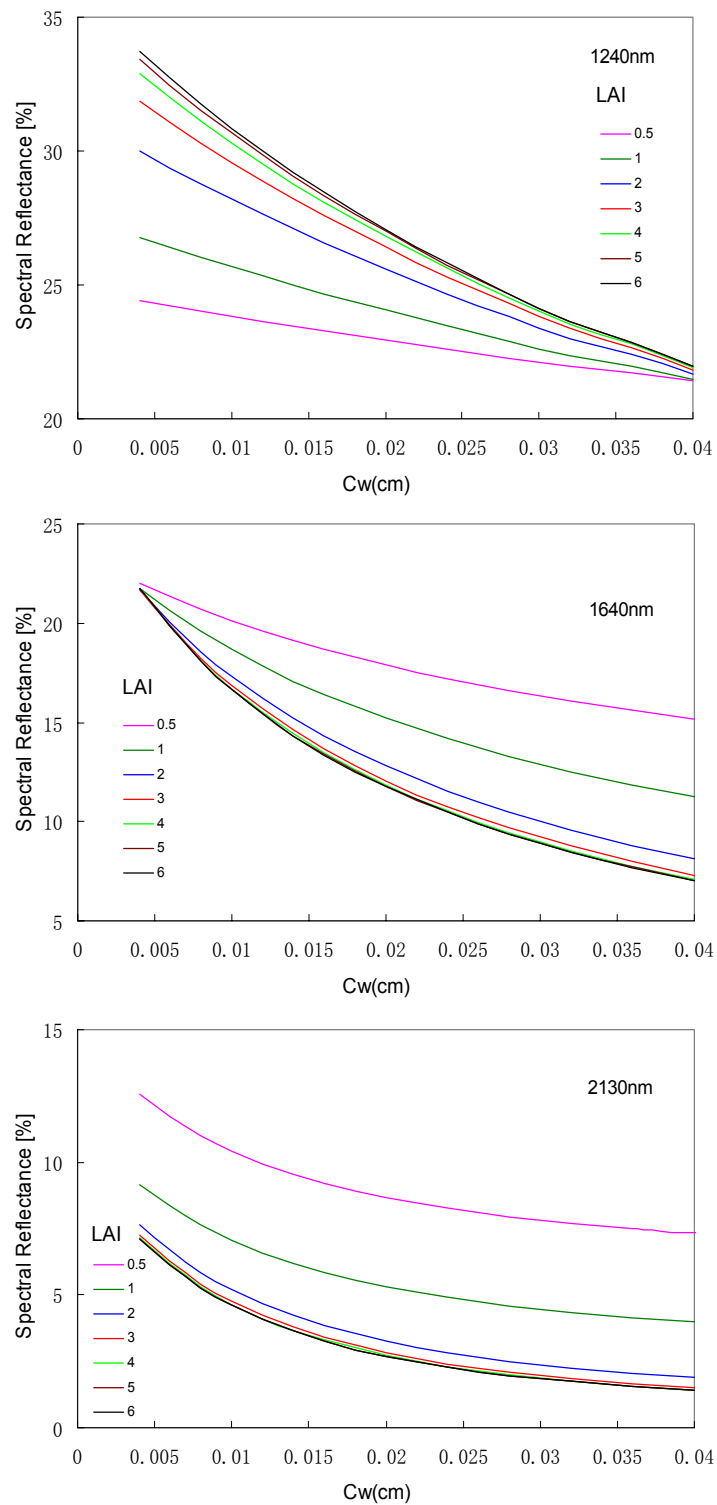


Figure 5.5. Sensitivity of MODIS SWIR reflectance to leaf water content

5.1.3.2 Modeling the moisture effects on water indices

The most popular NIR-SWIR vegetation water indices are NDWI and NDII. The NDWI calculated as $\frac{R_{860nm} - R_{1240nm}}{R_{860nm} + R_{1240nm}}$, where R represents the reflectance, was suggested by Gao (1996) based on the fact that the SWIR centred at 1240 nm is on the edge of the vegetation liquid water absorption, while the NIR centred at 860 nm is insensitive to water content changes, which make NDWI sensitive to changes in liquid water content of vegetation canopies. The NDII calculated as $\frac{R_{860nm} - R_{1640nm}}{R_{860nm} + R_{1640nm}}$ is similar to NDWI except that it uses the relatively stronger liquid water absorption band centred at 1640 nm as the water sensitive band (Hardisky et al., 1983; Ceccato et al., 2001). Strong absorption of water around 1640 nm makes this band most suitable for the estimation of plant water content.

The effects of soil moisture and leaf water content are also analyzed for NDWI and NDII, which are constructed using the simulated reflectance of MODIS bands centred at 858, 1240 and 1640 nm.

When NDWI and NDII were modelled with soil moisture varying from low to high values and an LAI range of 0.1–6, it becomes obvious that the soil effect is reduced by the normalized calculations of these indices compared with the soil effect on SWIR reflectance. Both NDWI and NDII have slight variations responding to soil moisture change when LAI is less than 2, and remain almost constant starting after an LAI value of 2. The normalized calculation for index NDWI is more efficient in removing the soil

effect than NDII considering the following facts: (1) the reflectance of band 5 which NDWI uses is more sensitive to soil moisture than band 6 which NDII operates on: the soil moisture effect on band 5 is visible up to an LAI of 3; (2) the NDWI is less sensitive than NDII to soil moisture effect after the normalized calculation: soil moisture effect on NDWI is nearly negligible starting after LAI of 0.5. NDII is more sensitive to LAI than NDWI with varying soil moisture. NDII changes from -0.35 to 0.25 while NDWI changes from -0.25 to 0 responding to LAI values from 0.01 to 2. Also shown in the plots of Figure 5.6 is that both NDWI and NDII have slight increments with increasing soil moisture except when LAI=0.01 which means bare soil.

The simulation obtained by varying C_w values and changing LAI from 0.5 to 7 shows that both NDWI and NDII increase with leaf water content for each LAI category (Figure 5.7). The increment is stronger with higher LAI values, obtaining the maximum variation near 40% when they are modelled with LAI value of 6 and C_w changes from 0.004 to 0.04. Compared with the maximum SWIR reflectance variation of 15% due to the same leaf water content change, the sensitivity of the indices to leaf water content has been enhanced significantly.

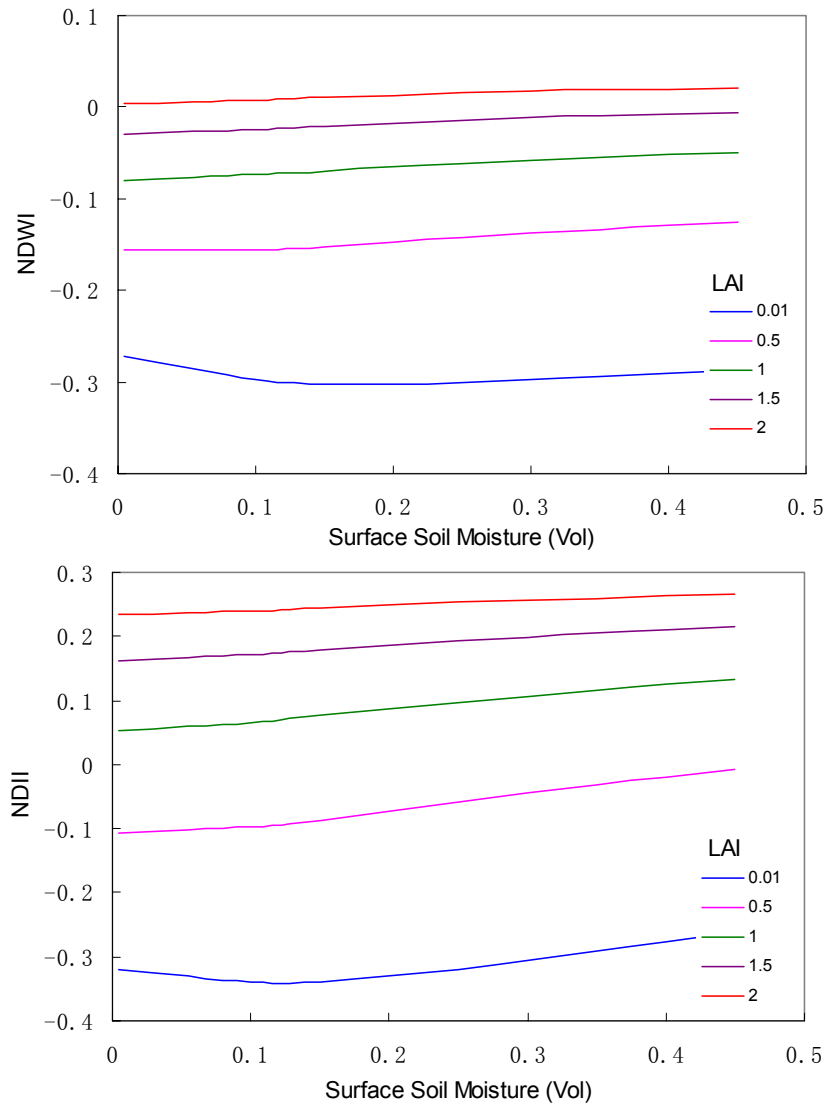


Figure 5.6. Sensitivity of NDWI and NDII to soil moisture

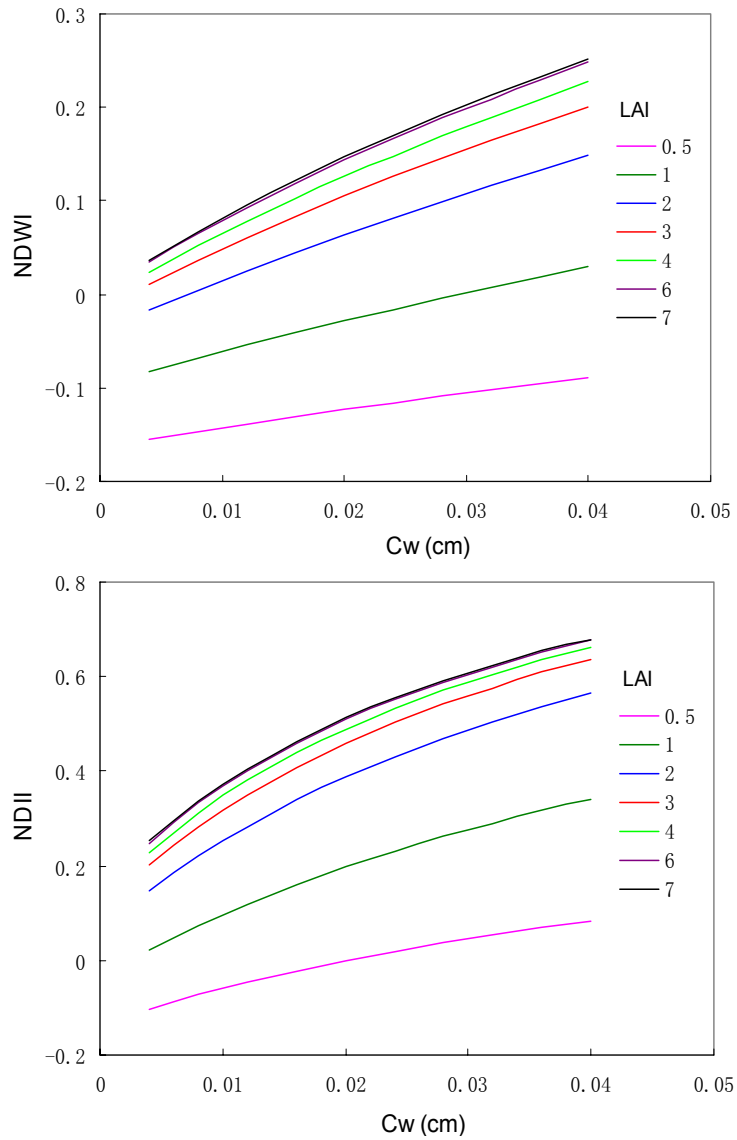


Figure 5.7. Sensitivity of NDWI and NDII to leaf water content

NDWI and NDII are highly sensitive to the canopy structural parameter LAI, obtaining a maximum variation about 45% when they are modelled with extreme C_w value of 0.04 and LAI changes from 1 to 7, demonstrating the large dependency of water-related indices on LAI. Both NDWI and NDII increase as LAI increases, while

NDWI is more sensitive to LAI with varying leaf water content, contrary to its easier saturation to LAI with varying soil moisture. LAI effects on NDII and NDWI become minimal with LAI approaching 4, and 6 respectively. Further, comparing the variations of NDWI with NDII, it is clear that the NDII has a larger range of variations with the highest value approaching 0.7, while the NDWI approaches 0.5.

Considering that MODIS has three SWIR bands at 500 m resolution, two of which have been used in NDWI and NDII respectively, we apply the last SWIR band 7 to generate the similar calculation: $\frac{R_{860nm} - R_{2130nm}}{R_{860nm} + R_{2130nm}}$. Using the same simulation, results

show that the soil effect on the new generated formula is obviously stronger compared with NDWI and NDII (Figure 5.8): it has a rapid increment with increasing soil moisture at LAI values less than 1, unlike the almost flat slopes of NDWI and NDII. Similar to NDWI and NDII, it increases with leaf water, while the increment is curved, becoming smoother at high C_w values. LAI has the strongest effect on this index with varying soil moisture: it changes from -0.3 to 0.7 responding to LAI values from 0.01 to 2, and weakest impact with varying leaf water content: LAI effect becomes minimal with LAI approaching 3.

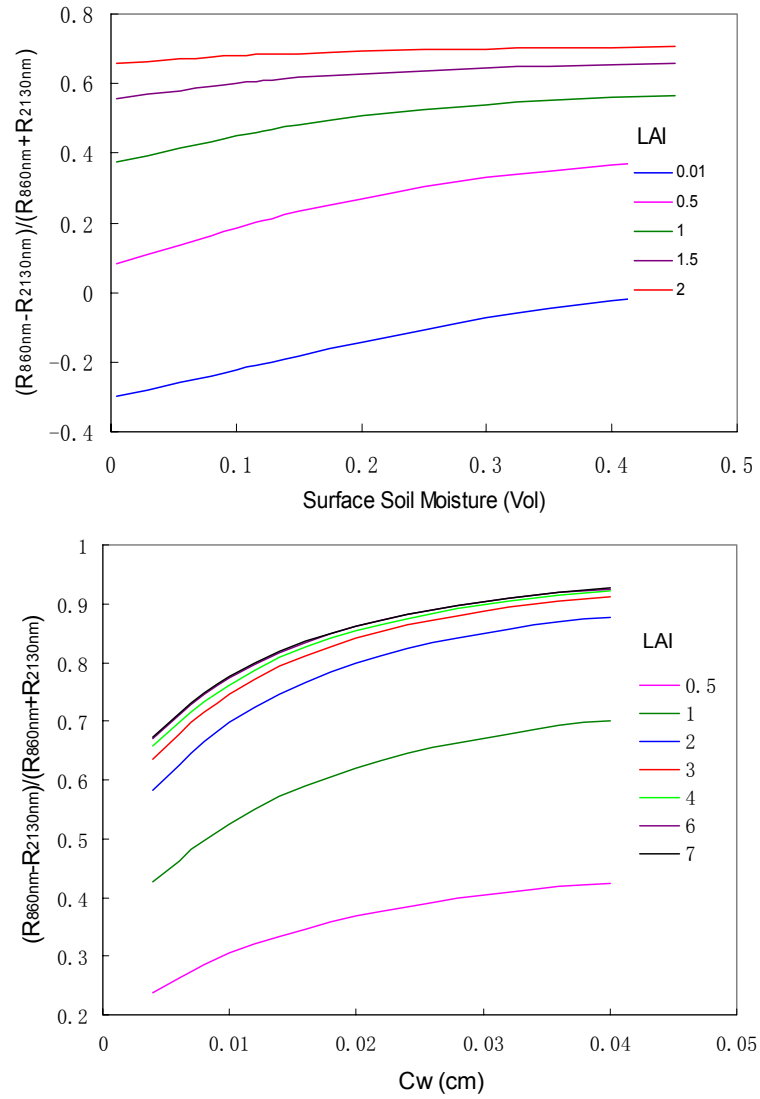


Figure 5.8. Sensitivity of $[(R_{860nm} - R_{2130nm}) / (R_{860nm} + R_{2130nm})]$ to soil moisture and leaf water content

5.1.4 Conclusion

Simulations have been performed by using the coupled soil-leaf-canopy reflectance model to study the effects of soil and leaf water content on MODIS SWIR bands and

related vegetation water indices. The results of this study can be summarized by the following:

1. Soil moisture has a large effect on the SWIR reflectance at low LAI values, and the effect continues up to an LAI of 3. This result is consistent with what has been reported in the earlier study by Bach and Verhoef (2003).

2. Among three MODIS SWIR bands, reflectance of band 5 is most sensitive to soil moisture content spanning from low values to high values, while reflectance of band 7 responds strongest to dry soil conditions.

3. The reflectance of band 5 is better suited to measure leaf water content change than bands 6 and 7, since it obtains a higher variation when C_w changes from dry to wet and it is less easy to saturate with high LAI values. This advantage has been enhanced by the normalized calculation of NDWI.

4. Reflectance of each SWIR band responds differently to the change of soil moisture and leaf water content. The MODIS band 5 presents divergence with the increase of soil moisture, while convergence with leaf water content; both MODIS bands 6 and 7 present convergence with soil moisture, while band 6 presents divergence and the latter has a parallel shape.

5. By using the normalized calculation between the water absorption sensitive band and insensitive band, NDWI shows the most capability to remove the soil background effect and enhance the sensitivity to leaf water content, while the soil moisture effect has been amplified for the new index generated using band 7 as the sensitive band.

Simple spectral indices similar to NDWI and NDII always use only two bands including one sensitive and one insensitive band to interpret changes in leaf water content. These simple spectral indices were suggested as suitable for traditional sensors that have only a few optical bands. With more optical bands, MODIS measurements provide a good opportunity to estimate leaf water and soil moisture more accurately and robustly. Combining multiple, rather than one MODIS SWIR band with a NIR band may provide a solution to separate two moisture variables by amplifying one signal and minimizing the other considering the fact that each SWIR band has a different characteristic response to soil moisture and leaf water.

5.2 Soil moisture estimation using MODIS SRB measurements

5.2.1 MODIS SRB measurements

MODIS has a total of 20 Solar Reflectance Bands (SRB) (1-19 and 26) covering the VNIR region, providing a good opportunity for land parameters retrieval. Table 5.3 shows the MODIS 250 m and 500 m SRB specifications (Salomonson et al., 2005). Each SRB has been used in one or more indices using empirical relations based on statistical analysis of ground measurements and spectral characteristics. MODIS bands 1 and 2 are mainly used for retrieval of the NDVI, since vegetation has low reflectance in the VIS (0.4 to 0.7 μ m) part of the spectrum due to the absorption of chlorophyll in the plants and high reflectance in the NIR range (0.7 to 1.3 μ m). Bands 4 and 6 are used to calculate the Normalized Difference Snow Index (NDSI) for snow detection based on the fact that snow has high reflectance in the VIS and low reflectance in the SWIR at about 1.6 μ m.

The NDWI and NDII have also been proposed as a ratio between band 2 and band 5/6 to monitor vegetation water content. Like most other normalized indices, the Normalized Difference Dust Index (NDDI) calculated as a ration between sand dust sensitive band 7 and insensitive band 3 was suggested by Qu et al. (2006).

Table 5.3 MODIS 250 m and 500 m SRB Specifications

Band	Bandwidth (μm)	Central Wavelength (μm)	Spatial resolution (m)	Primary Use
1	0.620-0.670	0.648	250	Land/Cloud/Aerosols Boundaries
2	0.841-0.876	0.858	250	
3	0.459-0.479	0.470	500	Land/Cloud/Aerosols Properties
4	0.545-0.565	0.555	500	
5	1.230-1.250	1.240	500	
6	1.628-1.652	1.640	500	
7	2.105-2.155	2.130	500	

However, simple spectral indices mentioned above which always use two bands including one sensitive and one insensitive band were suggested for traditional sensors such as Advanced Very High Resolution Radiometer (AVHRR), Landsat Thematics Mapper (TM) and Enhanced Thematic Mapper (ETM), which have only a few optical bands. With more optical bands, MODIS measurements might provide a good opportunity to estimate vegetation water content and soil moisture more accurately and robustly.

5.2.2 Formation of NMDI

By using simulations with the coupled soil-leaf-canopy reflectance models, sensitivity analyses have been performed to quantify the impact of soil and leaf water

content on the SWIR reflectance and water related indices. The study has illustrated that the reflectance of each MODIS SWIR band responds differently to the soil moisture and leaf water content variations (Wang et al., 2007).

The soil reflectances with varying moisture content for mollisol, representative of a typical soil type in the temperate savanna have been demonstrated in the left plot of Figure 5.9. The effect of leaf water content on canopy reflectance has also been illustrated by using the leaf radiative transfer model-PROSPECT (Jacquemoud and Baret, 1990) and the canopy reflectance model-SAIL (Verhoef, 1984) with an LAI range of 0.5-6 assuming different leaf water contents (right plot of Figure 5.9).

For both soil moisture and leaf water content, an increase of each is connected with a reflectance reduction. The sensitivity of MODIS bands 6 (1640 nm) and 7 (2130 nm) responding to the moisture change, however, is definitely different. It is evident from Figure 5.9 that the slope between bands 6 and 7 becomes steeper with the increase of soil moisture, while flatter with the increase of leaf water content. This characteristic ‘slope variation’ in response to different kinds of moisture changes might be useful to extract information about soil and vegetation water status.

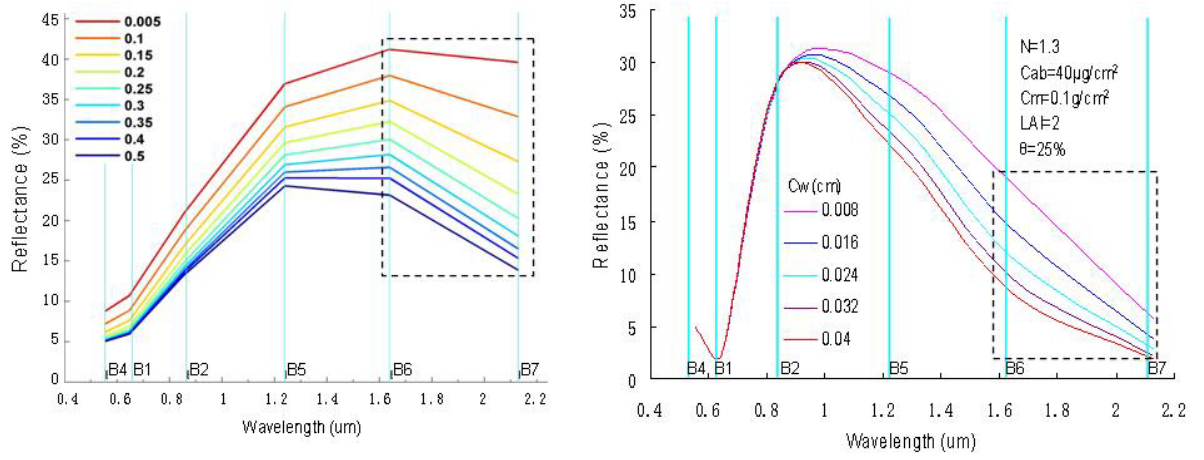


Figure 5.9. Simulated soil spectra at various soil moisture (left plot)and canopy spectra at different leaf water content (right plot)

Based on the soil and vegetation spectral signatures, the Normalized Multi-band Drought Index (NMDI) is proposed by using three wavelengths, one in the NIR centered approximately at 860 nm, and two in the SWIR centered at 1640 nm and 2130 nm, respectively. Following the simplicity of NDWI and NDII, NMDI is defined as:

$$NMDI = \frac{R_{860nm} - (R_{1640nm} - R_{2130nm})}{R_{860nm} + (R_{1640nm} - R_{2130nm})}, \quad (5.2)$$

where R_{860nm} , R_{1640nm} and R_{2130nm} are the apparent reflectances observed by a satellite sensor in the 860 nm, 1640 nm and 2130 nm bands, respectively. Similar to NDWI and NDII, this new designed index uses the channel centered at 860 nm, which is insensitive to leaf water content changes as the reference; however, instead of using a single liquid water absorption band like NDWI or NDII, it uses the difference (slope) between two liquid water absorption bands (1640 nm and 2130 nm), as the soil and vegetation water

sensitive band. Strong differences between two water absorption bands in response to soil and leaf water content give this combination potential to estimate water content for both soil and vegetations.

In order to show that the NMDI can be useful for remotely sensing both soil moisture and vegetation water status from space, its sensitivities to bare soil or weak vegetation, heavy vegetation, and mixture of soil and vegetation are investigated.

For the dry bare soil, the difference between MODIS bands 6 and 7 is relatively small, which gives high NMDI values, while for the wet bare soil the difference becomes large, giving low NMDI values. Simulations are obtained by the coupled soil-leaf-canopy reflectance models with varying soil moisture from low to high values and an LAI range of 0.01–2. The results show that when LAI equals 0.01 which means bare soil or weakly vegetated areas, the NMDI is a function of soil moisture content: an increase of soil moisture is connected with a reduction of NMDI. NMDI decreases from high values around 0.85 for extremely dry soil to low values around 0.15 for wet soil with soil moisture content higher than 0.3 (upper plot of Figure 5.10). NMDI is well suited to monitor dry soil status: it decreases rapidly from 0.85 to 0.4 responding to the soil moisture change from 0.005 to 0.1, and continues to gain 20% variation when soil moisture changes from 0.1 to 0.2. NMDI saturates when soil moisture content approaches 0.3, which means relatively wet soils.

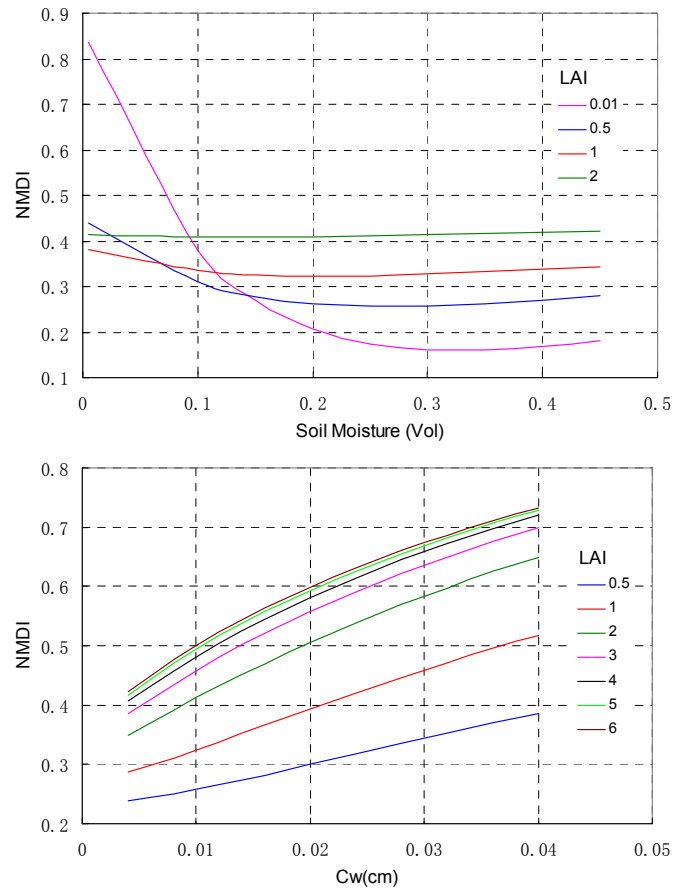


Figure 5.10. Sensitivity of NMDI to soil moisture (upper) and leaf water content (lower)

NMDI stops responding to soil moisture change starting from LAI equal to 2, i.e., no soil background effects are found on NMDI for any soil moisture range. Therefore, for a vegetation canopy with an LAI equal to or higher than 2, which means heavily vegetated areas, NMDI turns to be a complete index for estimating plant water content, rather than an index for soil moisture. Similar to NDWI, NMDI increases almost linearly with leaf water content for each LAI category. The increment presents parallel trends for each LAI category range from 2 to 6, obtaining high variations above 40% when they are modeled

with leaf water content from 0.004 to 0.04. Compared with the maximum SWIR reflectance variation of 15% due to the same leaf water content change (right plot of Figure 5.9), the sensitivity of NMDI to leaf water content has been enhanced significantly. NMDI saturates with LAI values up to 5.

For areas with moderate vegetation coverage, i.e., LAI equals to 0.5 and 1 in this study, NMDI is still sensitive to soil moisture and leaf water content, decreasing with soil moisture and increasing with leaf water content.

5.2.3 Validation of NMDI

5.2.3.1 Soil drought monitoring

For simplicity the soil moisture condition falls into three classes according to the volumetric soil moisture range: dry: 0–0.1; intermediate: 0.1–0.2 or wet: >0.2 (Idso et al., 1975; Miller et al., 2004). The following examples are taken to validate the application of NMDI to interpret the soil moisture change.

In the absence of suitable field data, it was decided to demonstrate the usefulness of NMDI for remote sensing of soil moisture by using the bare soil spectra under various soil water contents reported in previous studies by B. Leblon (Soil and vegetation optical properties, Remote sensing core curriculum, vol. 4, module 9, 2000, <http://www.r-s-c-c.org/rscc/Volume4/Leblon/leblon.htm>, hereinafter referred to as Leblon, Module 9, 2000) and Bach and Verhoef (2003). Figure 5.11 a is the spectral reflectance curves for Newtonia silt loam at dry to intermediate moisture contents of 0.008, 0.047, 0.088, 0.129, 0.169 and 0.202 given by Leblon (Module 9, 2000). Figure

5.11 b is the GeoSAIL (Bach et al., 2000) model simulated spectra of bare soil with varying soil moisture from dry of 0.005 to extremely wet of 0.6 by Bach and Verhoef (2003).

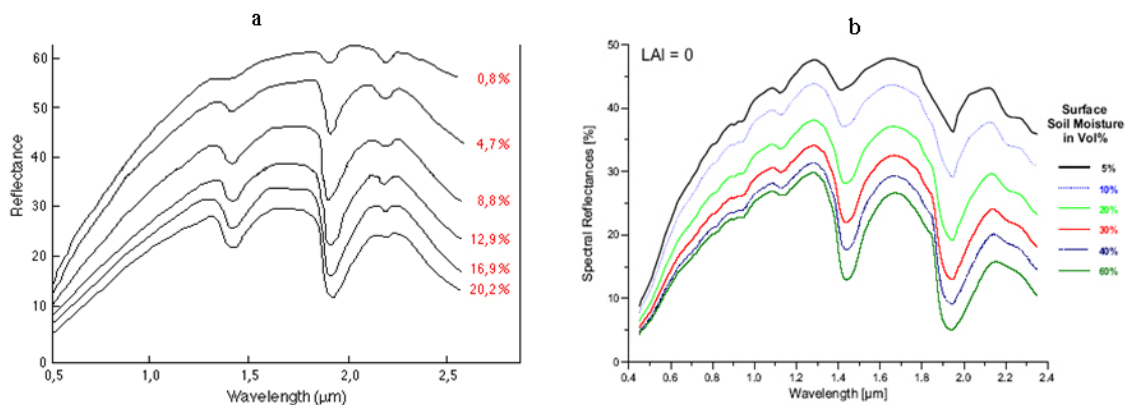


Figure 5.11. (a) Spectral reflectance curves for Newtonia silt loam at various moisture contents (after B. Leblon, Soil and vegetation optical properties, Remote sensing core curriculum, vol. 4, module 9, 2000, <http://www.r-s-c-c.org/rsc/Volume4/Leblon/leblon.htm>). (b) GeoSAIL model simulated spectra of bare soil with varying soil moisture [Bach and Verhoef, 2003] (copyright IEEE)

NMDI is constructed by using the reflectances corresponding to each MODIS band centered at 858 nm, 1640 nm and 2130 nm from Figure 5.11 with various soil moisture values. Figure 5.12 shows NMDIs calculated from the soil spectral reflectances are a function of soil moisture. Higher values of the NMDI indicate increasing severity of soil drought. The results reinforce that the NMDI is highly sensitive to soil moisture change, gaining rapid reduction responding to soil moisture change from extremely dry to intermediate and wet soil water status. Both cases show that NMDI values are within the range of 0.7 to 1 when soil moisture is less than 0.1, which means dry soil conditions. In other words, if NMDI is greater than 0.7, we can conclude that the soil is dry. NMDI

values are around 0.6 when soil moisture is about 0.2, which means intermediate moisture conditions. When NMDI is less than 0.6, the soil is under wet conditions.

Therefore, NMDI has demonstrated its ability to monitor soil moisture conditions including dry, intermediate and wet. Additional experiments are needed to identify NMDI threshold values for each soil moisture condition in the near future.

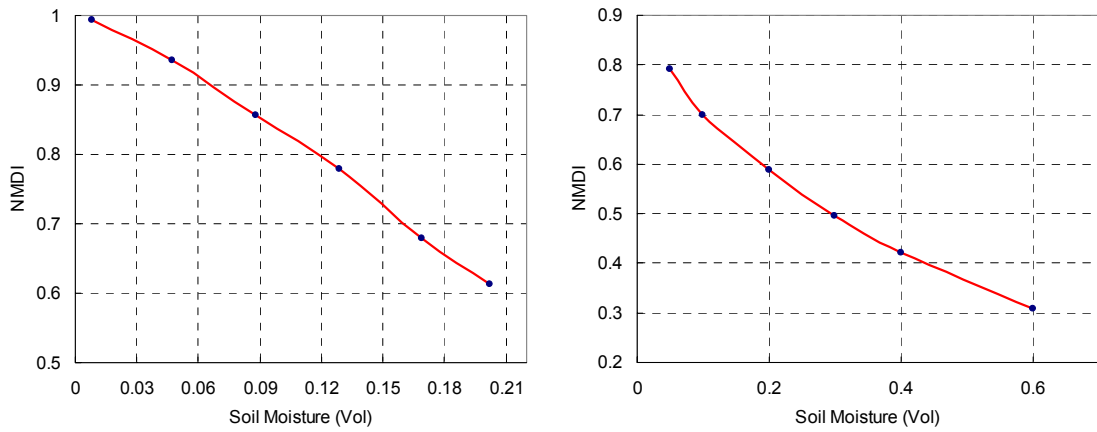


Figure 5.12. Sensitivity of NMDI to soil moisture values corresponding to Figures 5.11 a, and 5.11 b

Although both plots of Figure 5.12 as well as the upper plot of Figure 5.10 show that the increase of soil moisture leads to the decrease of NMDI, in regards to the decreasing pattern, the shapes of all plots appear to be somewhat different from each other. This difference may be a result of the soil spectral reflectances obtained for different soil types: Figure 5.10 is for mollisol soil type, while Figure 5.12 a is for silt loam; or from different soil reflectance models: Figure 5.10 is based on the exponential model proposed by Lobell and Asner (2002), while Figure 5.12 b is based on GeoSAIL model.

5.2.3.2 Vegetation drought monitoring

To test the performance of NMDI for remote sensing of vegetation drought, we use examples similar to those reported in a study by Gu et al. (2007). These authors analyzed five-year (2001–2005) sets of MODIS NDVI and NDWI data for grassland drought assessment for the Flint Hills of Kansas and Oklahoma. Flint Hills is the largest remaining area of native tallgrass prairie in North America. The relatively homogeneous land cover type allowed the influence of drought on the grasslands to be isolated from other factors and therefore more effectively studied. The drought conditions of the study area in 2003 and 2004 have been identified by the U.S. Drought Monitor as severe and non-drought category droughts, respectively. Figure 5.13 is the true color image of the study area centered at 35.25° N latitude and 91.81° W longitude on September 6, 2004.

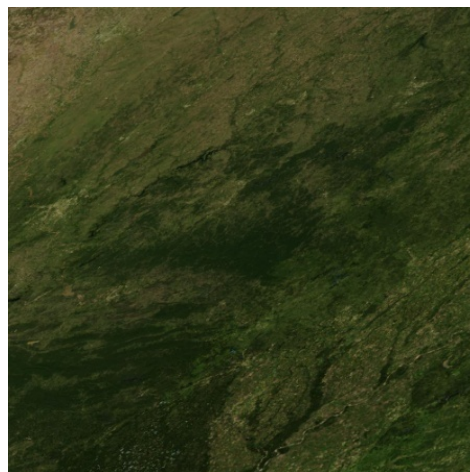


Figure 5.13. True color image of the study area on September 6, 2004

Eight granules of MODIS 8-day 500 m surface reflectance data (MOD09A1, Collection 4) (<http://deleann.gsfc.nasa.gov/~imswww/pub/imswelcome/>) during the

summer months from July to September were used to derive NMDI according to equation (5.2). To illustrate the relationship between NMDI and vegetation drought conditions, four NMDI images for the most severe drought periods in August and September at the Flint Hills are shown in Figure 5.14 in the severe drought year 2003 and non-drought year 2004. Lower NMDI values indicate increasing severity of vegetation drought. The drought development from August to September can be detected clearly from NMDI images. NMDI values were much lower for the severe drought year (2003) than for the non-drought year (2004). Also lower NMDIs cover much broader areas in 2003 than in 2004. Good agreements are shown between above and Gu et al. (2007) results. It demonstrates the potential of the NMDI for monitoring vegetation drought.

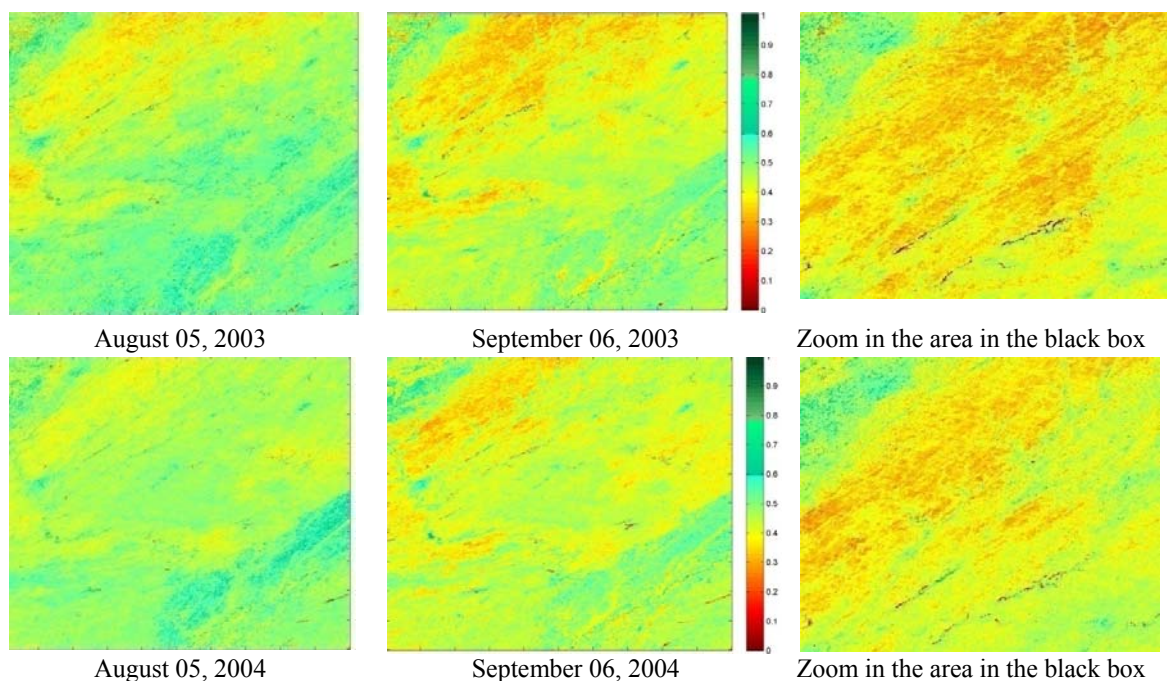


Figure 5.14. Spatial distribution of NMDI over the Flint Hills

5.2.3.3 Discussion

Despite the positive results, the application of NMDI is limited to bare soils or weakly vegetated areas, and heavy vegetation areas with $LAI \geq 2$ right now. For areas with moderate vegetation coverage, i.e., LAI equals to 0.5 and 1 in this study, the distinction between NMDI's roles as a soil drought indicator and a vegetation drought indicator blurs. Its application to directly interpret soil and vegetation moisture conditions could yield inaccurate results and therefore, remains challenge.

5.2.4 Uncertainty analysis

Accurate assessment of interannual, interseasonal, and spatial changes in soil and vegetation drought with NMDI data requires accurate knowledge of sensor calibration changes (Goward et al., 1991; Miura, et al., 2000). The uncertainty in the knowledge of the absolute calibration should be in the range 1– 5% (Slater, 1984, 1985), while 2% is the requirement for the reflectance calibration uncertainty for MODIS SRB bands 1-7 (Barbieri et al., 1997). This section evaluated the impact of MODIS calibration uncertainties on the accuracy of NMDI, specifically limited to the combined uncertainties of 2%, which includes different sources of uncertainties, such as uncertainties in the bias corrections for derivations of the effective digital counts and the uncertainties due to electrical noise.

The bare soil spectra under various soil water contents reported in previous study by Bach and Verhoef (2003), and the coupled soil-leaf-canopy model simulated canopy reflectances with an LAI value of 4 were used to investigate the impact of reflectance

calibration uncertainties on the accuracies of NMDI for soil and vegetation drought monitoring, respectively. Reflectance uncertainties of 2% were examined with no correlations between any pair of bands for all possible combination of MODIS bands 2, 6 and 7, which NMDI operates on.

5.2.4.1 NMDI for soil drought (hereinafter referred to as $\text{NMDI}_{\text{soil}}$)

$\text{NMDI}_{\text{soil}}$ was generated from the bare soil spectral under various soil moisture contents. Table 5.4 summarized $\text{NMDI}_{\text{soil}}$ uncertainties induced by a total of 24 kinds of possible combinations due to 2% reflectance uncertainty. The $\text{NMDI}_{\text{soil}}$ uncertainties decreased with increasing $\text{NMDI}_{\text{soil}}$ values due to calibration uncertainty of single band 2 or 6, while increased for band 7. For combinations of any pair of bands 2, 6 and 7, $\text{NMDI}_{\text{soil}}$ uncertainties decreased except the reflectance uncertainties of bands 2 and 6 are in the same direction, and those of bands 2 and 7 are in the opposite directions. When three bands change together, $\text{NMDI}_{\text{soil}}$ uncertainties decrease except when bands 2 and 6 change in the same direction. The $\text{NMDI}_{\text{soil}}$ derived from any combination with band 6 and 7 changing in the opposite directions resulted in larger uncertainties around 10%, while less uncertainties around 2% if bands 6 and 7 change in the same direction. One can notice that the main source of uncertainty is in the band 6. The mean $\text{NMDI}_{\text{soil}}$ uncertainty due to a 2% reflectance calibration uncertainty is 5.78%.

Table 5.4 Results of NMDI_{soil} uncertainties

No.	Calibration Uncertainty (2%)			NMDI _{soil} Uncertainty (%)		
	Band 2	Band 6	Band 7	Minimum	Maximum	Average
1	+			0.46	2.90	1.43
2	-			0.29	-13.68	5.16
3		+		-5.23	-6.81	-5.76
4		-		5.49	7.04	5.99
5			+	4.01	5.00	4.49
6			-	-3.94	-4.79	-4.35
7	+	+		-3.86	-4.69	-4.27
8	+	-		5.86	9.90	7.36
9	-	+		-5.80	-9.84	-7.30
10	-	-		4.10	5.10	4.58
11	+		+	5.38	6.90	5.87
12	+		-	-1.01	-4.25	-2.87
13	-		+	1.06	4.60	3.07
14	-		-	-5.34	-6.95	-5.87
15		+	+	-0.47	-2.92	-1.44
16		+	-	-9.80	-10.64	-9.94
17		-	+	10.74	11.19	10.67
18		-	-	0.47	2.96	1.46
19	+	+	-	-7.67	-9.20	-8.41
20	+	-	+	11.02	14.03	11.99
21	+	-	-	0.93	5.86	2.88
22	-	+	+	-0.96	-5.91	-2.93
23	-	+	-	-10.43	-13.68	-11.52
24	-	-	+	8.28	10.43	9.32

Figure 5.15 shows the NMDI_{soil} uncertainty trends for combinations of three bands. The resultant uncertainties are shown separated into three groups, i.e., the larger decreasing uncertainties induced by combinations with bands 6 and 7 changing in the opposite directions, the increasing induced by bands 2, and 6 change in the same direction, and smaller decreasing by bands 6 and 7 change in the same direction.

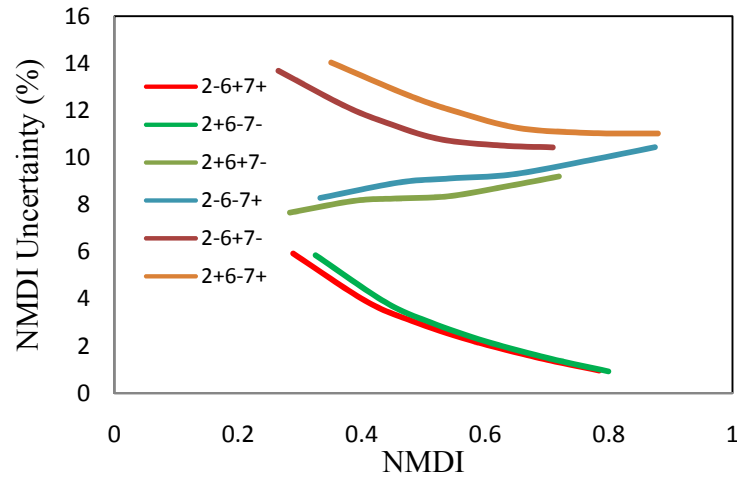


Figure 5.15. Uncertainties of NMDI_{soil} due to a 2% reflectance calibration uncertainty

5.2.4.2 NMDI for vegetation drought (hereinafter referred to as NMDI_{veg}):

The same analysis was conducted with the model simulated canopy reflectances to investigate the uncertainties trends in NMDI for vegetation drought. Different from NMDI_{soil}, decreasing trends of NMDI_{veg} uncertainties can be observed with increasing NMDI_{veg} values for all cases. The NMDI_{veg} derived from bands 2 and 6 changing in the same direction, or bands 2 and 7 in the opposite directions, however resulted in smaller uncertainties (less than 1%) than those from bands 2 and 6 changing in the opposite directions, or bands 2 and 7 in the same direction (table 5.5). Figure 5.16 shows how NMDI_{veg} uncertainties decreased with increasing NMDI_{veg} values for 6 kinds of typical combinations with bands 2, 6 and 7. Regardless of the same decreasing trend, the combinations of the same uncertainty direction of bands 2 and 6, and the opposite directions of bands 2 and 7 make uncertainties the lowest, compared with the larger uncertainties induced by combinations with bands 2 and 6 changing in the opposite

directions and bands 2 and 7 in the same direction. Once again, band 6 is the primary source of uncertainties. The mean NMDI_{veg} uncertainty is 1.68%.

Table 5.5 Results of NMDI_{veg} uncertainties

No.	Calibration Uncertainty (2%)			NMDI_{veg} Uncertainty (%)		
	Band 2	Band 6	Band 7	Minimum	Maximum	Average
1	+			0.66	2.03	1.16
2	-			-0.68	-2.08	-1.20
3		+		-0.83	-3.03	-1.58
4		-		0.84	3.09	1.60
5			+	0.17	1.01	0.41
6			-	-0.16	-1.00	-0.41
7	+	+		-0.16	-0.99	-0.40
8	+	-		1.49	5.09	2.75
9	-	+		-1.53	-5.15	-2.80
10	-	-		0.17	1.03	0.42
11	+		+	0.82	3.03	1.57
12	+		-	0.49	1.03	0.76
13	-		+	-0.50	-1.06	-0.78
14	-		-	-0.85	-3.09	-1.61
15		+	+	-1.91	-5.29	-3.07
16		+	-	-2.24	-4.02	-3.87
17		-	+	1.01	4.12	2.02
18		-	-	0.67	2.07	1.19
19	+	+	-	-0.33	-1.97	-0.80
20	+	-	+	1.654	6.11	3.16
21	+	-	-	1.32	4.08	2.34
22	-	+	+	-1.36	-4.14	-2.39
23	-	+	-	-1.70	-6.14	-3.21
24	-	-	+	0.34	2.07	0.84

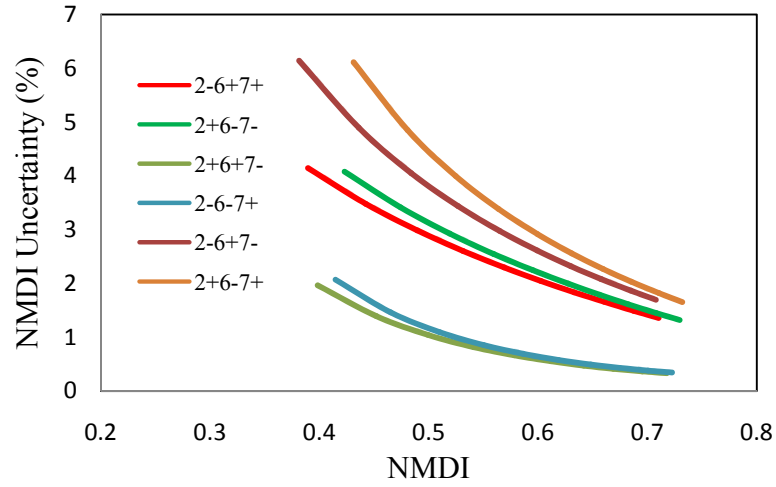


Figure 5.16. Uncertainties of $NMDI_{veg}$ due to a 2% reflectance calibration uncertainty

The results show that $NMDI_{soil}$ and $NMDI_{veg}$ respond to the reflectance uncertainties differently. $NMDI_{soil}$ is more sensitive to calibration uncertainties, resulting over 5% mean uncertainties due to 2% calibration uncertainty, while the mean uncertainties is less than 2% for $NMDI_{veg}$. Regardless of the difference, the uncertainties from MODIS band 6 are the primary contributor to both $NMDI_{soil}$ and $NMDI_{veg}$ uncertainties. The most severe combination for each NMDI occurred when bands 2 and 6 change in the opposite directions and bands 2 and 7 in the same direction.

5.2.5 Conclusion

A new moisture index, the Normalized Multi-band Drought Index (NMDI), is proposed for remote sensing of both soil and vegetation water content from space by using three channels centered near 860 nm, 1640 nm and 2130 nm.

The preliminary results suggest that for bare soil or weakly vegetated areas, a pixel

will be mapped as dry soil condition if the NMDI is ≥ 0.7 , intermediate if NMDI is within the range of 0.6 to 0.7, and wet if NMDI is < 0.6 . While for heavily vegetated areas with $LAI \geq 2$, the performance of NMDI is similar to NDWI and NDII. Therefore, by combining information from multiple NIR and SWIR channels, NMDI has enhanced the sensitivity to drought severity, and is well suited to estimate water content for both soil and vegetations.

Additional analyses of NMDI with respect to the mixture of soil and vegetation should be conducted with new experiments. If more broadly applicable, this index may provide an opportunity to estimate both soil and vegetation moisture on an operational basis.

5.3 Application of NMDI in fire detection

Forest fires have drawn a lot of attention in recent years due to their effects on climate change and ecosystems. It is necessary to locate active fire spots since they are important for a number of ongoing studies, like landuse and landcover change. Fire detection contributes in assessing the area and quantity of forests that are destroyed and further helps in wildlife management (Philip, 2007). Drought plays an important role in making the conditions favorable for forest fires to occur. Experience over the years has helped establish a close relationship between cumulative dryness, or drought, and extremely destructive fires (<http://www.wrh.noaa.gov/sew/fire/olm/KEETCH.htm>). The occurrence of fires is highly dependent upon the availability of moisture during the growing season, with more severe fires occurring during the drier, warmer years (Dyrness et al., 1986;

Kasischke et al., 1993). Soil moisture and vegetation water content are important factors that can and will influence the occurrence and behavior of both small and large wildland fires (<http://www.wrh.noaa.gov/sew/fire/olm/KEETCH.htm>).

Vegetation water indices derived from satellite data have recently been used to detect and monitor the moisture conditions of vegetation canopies for fire detection (Maki et al., 2004). The specific objective of this work is to investigate and compare the ability of the selected indices, NMDI, NDWI, and NBR (Normalized Burn Ratio), related to vegetation water status, to detect forest fires in southern Georgia, USA and southern Greece in 2007. Index performance is evaluated using MODIS fire products. Satellite images generated from each index are compared with the active fire map provided by the MODIS Rapid Response Team. Performance measures (overall accuracy, commission error, and fire detection rate) extracted from the statistical analyses using the confusion matrices are used to verify the capacity of the indices for active fire detection.

5.3.1 Study area and data

5.3.1.1 Study area

A severe drought in the southeastern United States created record-breaking fire events along the Georgia/Florida border in 2007 (<http://landsat.gsfc.nasa.gov/images/archive/e0009.html>). The Sweat Farm Road Fire/ Big Turnaround fire complex began to burn in southeastern Georgia during the afternoon hours of 16 April 2007, when a tree fell on a power line and, fanned by strong winds, quickly exploded into a major fire and became the largest wildfire in Georgia history

(http://eobadmin.gsfc.nasa.gov/NaturalHazards/natural_hazards_v2.php3?img_id=14241).

The study area was located at latitudes 30.8° N to 31.5° N and longitudes 82.0° W to 83.1° W.

Throughout the summer of 2007, a series of massive forest fires broke out in several areas across Greece (http://en.wikipedia.org/wiki/2007_Greek_forest_fires). The most destructive and deadly fires raged from August 23 to August 27 mainly in western and southern Peloponnese as well as in southern Euboea (Athens News Agency, 2007). This study will mainly focus on the Peloponnese Peninsula (36.4° N to 38.4° N, 21.0° E to 23.5° E).

5.3.1.2 Satellite Data

The dataset is composed of MODIS L1B calibrated radiance (MOD02, 1 km, version 5), L1A geolocation data (MOD03, 1 km, version 5), and thermal anomalies, fires, and biomass burning product (MOD14, 1 km, version 5) acquired over the study areas for the fire periods. Reflectance from MODIS solar reflective bands 1 (620-670 nm), 2 (840-876 nm), 6 (1628-1652 nm) and 7 (2105-2155 nm), are used to derive NDVI, NMDI, NDWI and NBR. The reflectance from MODIS bands 1 and 2, along with the brightness temperatures derived from MODIS thermal infrared band 32 (11770-12270 nm) are employed to flag cloud pixels based on the method developed by Giglio et al. (2003). The Land/sea mask obtained from the MODIS L1B geolocation data is applied to identify water pixels. MODIS active fire images with 250 m spatial resolution provided by the MODIS Rapid Response Team (<http://rapidfire.sci.gsfc.nasa.gov/>) and MODIS fire products are used to evaluate the performances of the selected indices for forest fire

detection. Only Terra MODIS data are used in this study given that Aqua MODIS band 6 has a striping problem (Wang et al., 2006).

5.3.2 Methodology for fire detection

The NDWI is calculated as the ratio of a NIR channel and a SWIR channel as

$$\frac{R_{860nm} - R_{1640nm}}{R_{860nm} + R_{1640nm}}$$
. Since NDWI is influenced by both desiccation and wilting in the vegetation canopy, it may be a sensitive indicator for drought monitoring (Gu et al., 2007).

The NBR is calculated as a normalized composite of NIR channel centered at approximately 860 nm and a SWIR channel centered at approximately 2130 nm:

$$\frac{R_{860nm} - R_{2130nm}}{R_{860nm} + R_{2130nm}}$$
. NBR has been widely used to map burned areas and burn severity (Key and Benson, 1999; Miller and Yool, 2002; Cocke et al., 2005; Key and Benson, 2005). Since the NIR and SWIR spectral bands have the greatest change among reflective spectral bands (White et al., 1996; van Wagendonk et al., 2004), with NIR decreasing and SWIR increasing through the fire, the NBR would be most discriminating for burn effects.

By combining information from multiple NIR and SWIR channels, NMDI has proven to be a good indicator for both soil and vegetation drought. For bare soil or sparsely vegetated areas, higher values of the NMDI indicate an increasing severity of soil drought. While for heavily vegetated areas with $LAI \geq 2$, lower NMDI values indicate an increasing severity of vegetation drought, similar to NDWI and NBR (Wang and Qu, 2007). Since NMDI can monitor both vegetation and soil water content at the same time, it is expected to provide more accurate and valuable information about drought and fire conditions,

considering that the bare soil in the area will become exposed if vegetation burns.

Figure 5.17 describes the flowchart of the application of NMDI to monitor soil and vegetation drought. First the Land/sea mask obtained from the MODIS L1B geolocation data, and cloud mask derived based on the method developed by Giglio et al. (2003) are applied to identify water- and cloud-free pixels for the study area. The vegetation index, NDVI, derived from MODIS bands 1 and 2 is employed to separate bare soil and vegetation pixels, given that NDVI is one of the most extensively applied vegetation indices related to LAI: a theoretical interpretation for the relationships between vegetation indices and LAI has been provided by Myneni et al. (1995). In general, the higher NDVI value, the denser the vegetation, and if the NDVI value exceeds 0.4, the area is thought to be covered entirely by forest, greenery, or other vegetation (Suzuki et al., 2001; Nihei et al., 2002). The fixed NDVI threshold of 0.4, instead of LAI value of 2, is employed to flag soil and vegetation pixels. A water- and cloud-free pixel will be mapped as vegetation if the NDVI is ≥ 0.4 , otherwise the pixel will be classified as soil.

NMDI generated directly using equation (5.2) as
$$\text{NMDI}_{\text{veg}} = \frac{R_{860\text{nm}} - (R_{1640\text{nm}} - R_{2130\text{nm}})}{R_{860\text{nm}} + (R_{1640\text{nm}} - R_{2130\text{nm}})}$$
 can be used to interpret vegetation moisture conditions for vegetation pixels, with lower values corresponding to vegetation drought. Since NMDI responds oppositely to soil moisture than to vegetation water content, equation (5.2) should be adjusted for soil pixels in order to keep consistency between these two moisture statuses. The previous study suggests that the possible range of NMDI values for soil is between 0 and 1 with higher values indicating increasing soil drought, but the typical range is from 0.7 to 0.9 for very dry bare soil (Wang and Qu, 2007). The

following format of NMDI is adopted to monitor soil moisture conditions:

$$\text{NMDI}_{\text{soil}} = 0.9 - \frac{R_{860\text{nm}} - (R_{1640\text{nm}} - R_{2130\text{nm}})}{R_{860\text{nm}} + (R_{1640\text{nm}} - R_{2130\text{nm}})} \quad (5.3).$$

By applying this modification, NMDI can be used to interpret both soil and vegetation moisture status in the same direction, ranging from 0 to 0.9 with higher values indicating wet conditions and values lower than 0.2 indicating extreme severity of soil and vegetation drought, which may be induced by burning fires.

Several fires burning in southern Georgia, USA and southern Greece in 2007 were selected to test the usefulness of the abovementioned water related indices for fire detection.

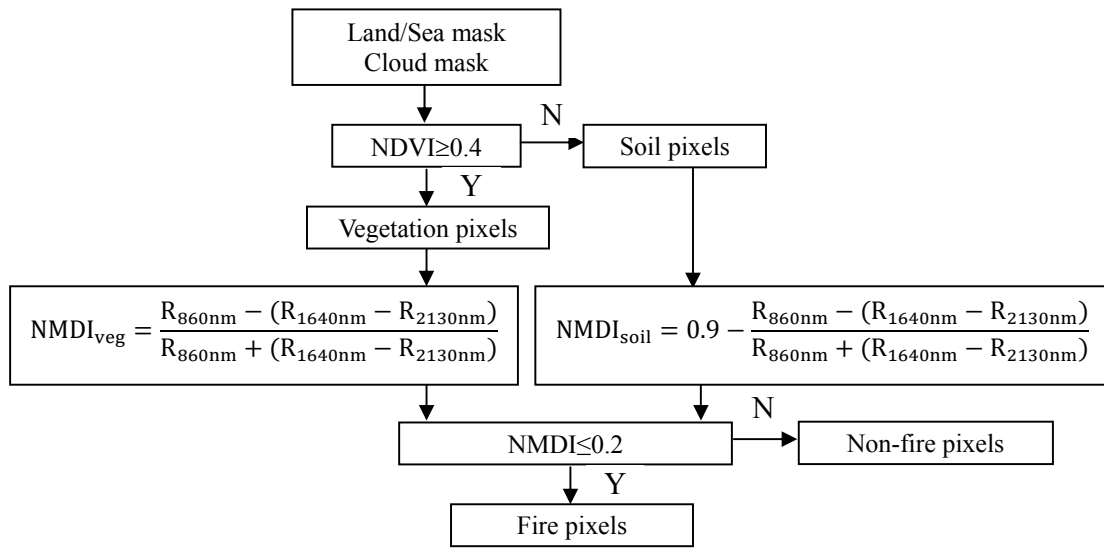


Figure 5.17. Flowchart of the multi-threshold method for fire detection

5.3.3 Indices testing and discussion

5.3.3.1 Georgia Fires

We selected satellite data of forest fires in southern Georgia obtained on April 17, 25 and 29, relatively clear days and intense fire periods.

Test case 1: fire on April 17th

The Sweat Farm Road Fire in southern Georgia exploded rapidly in less than 24 hours between April 16 and 17. The image of the fire (upper left of Figure 5.18) was captured by the Terra MODIS at 15:40 UTC on April 17. The locations where MODIS detected actively burning fires are outlined in red.

The NMDI image (upper right of Figure 5.18) derived by combining equations (5.2) and (5.3) revealed the obvious red-colored “hot spots” associated with the fire areas in the active fire map. NMDI values are much lower ($NMDI \leq 0.2$) for the active fire pixels than non-burning pixels ($NMDI > 0.5$) identified by the MODIS active fire map. The much lower NMDI values separate the burning spots from the neighboring area. It illustrates that there are strong relationships between NMDIs and fire activities. Compared to the 250 m resolution MODIS active fire image, the 1 km resolution NMDI image offered almost the same accurate depiction of the active fire shape, coverage, and location.

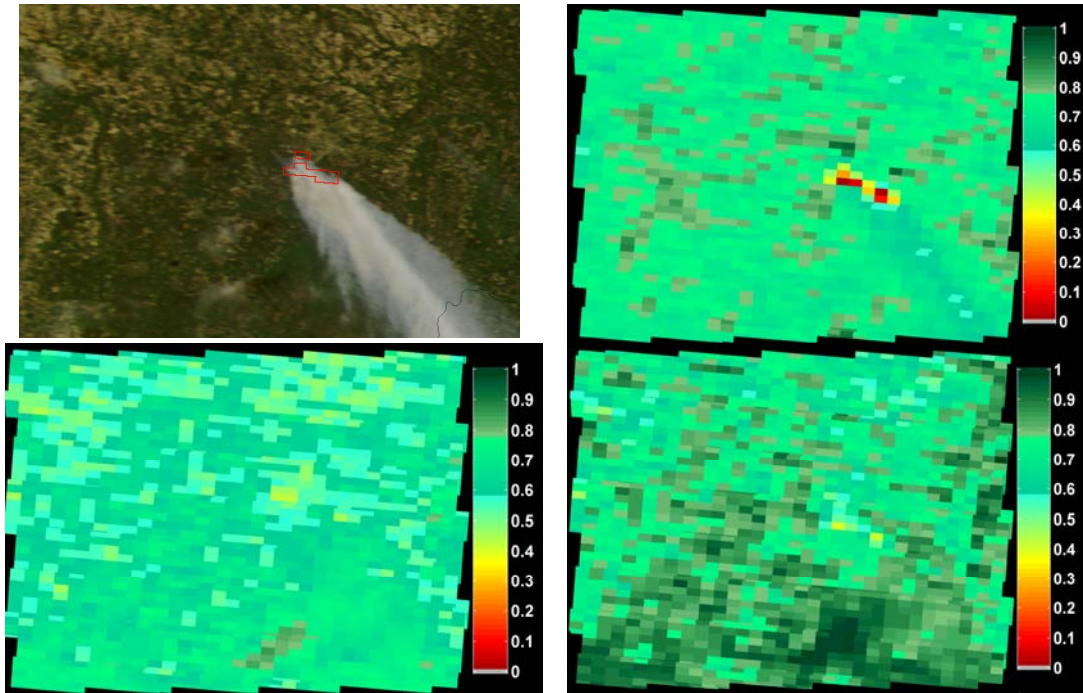


Figure 5.18. Images of active fire (upper left), NMDI (upper right), NDWI (lower left) and NBR (lower right) on 17 April, 2007

It was not possible to locate the active fire pixels within the cluster of green and sparse yellow pixels on the NDWI and NBR images (lower left and right of Figure 5.18). Neither NDWI nor NBR demonstrated any visible response to the fire activities.

Test case 2: fire on April 25th

The Sweat Farm Road Fire continued to burn on April 25, 2007, when the Terra MODIS passed overhead and captured the active fire image (upper left of Figure 5.19) at 16:30 UTC time. The brown burn scar can be seen next to the burning fire (shown in the red dashed triangle).

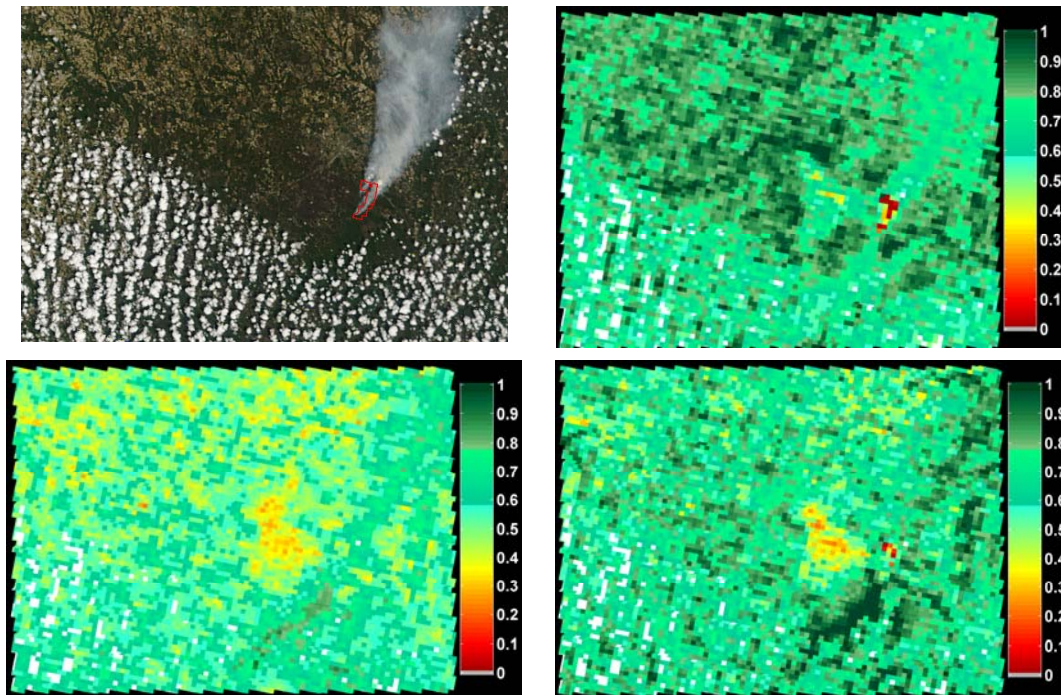


Figure 5.19. Images of active fire (upper left), NMDI (upper right), NDWI (lower left) and NBR (lower right) on 25 April, 2007

As expected, the NMDI values are substantially lower for the pixels experiencing the active fire, which make them stand out from the surrounding areas. The burn scar is also obvious as the lightgreen-colored areas in NMDI image. These details revealed by the NMDI image are consistent with the MODIS active fire map.

The large size of the resulting burn scar can be identified in the NBR image. With the lower NBR values around 0.3, the NBR image shows the yellow-colored scar covering a significant portion along the southeastern edge of the burning fires. Several pixels experiencing active fire have been detected by NBR, which are denoted by the sparse red-colored spots; however, most of the burning pixels have been missed and cannot be located in the NBR image. The NDWI image also shows the yellow-colored

area for the burn scar, but it is difficult to separate the scar from the similar yellow-colored surrounding pixels.

Test case 3: fire on April 29th

The image at the upper left of Figure 5.20, taken at 16:05 UTC on 29 April, 2007 by Terra MODIS, shows the Sweat Farm Road and Big Turnaround Fires in southern Georgia and the Roundabout Fire burning in northwestern Georgia

Two large blazes burning in the northwestern and southeastern part of the study area were evident by the significant red-colored “hot spots” in the NMDI image. Compared with the former two NMDI images, it is clear that the Sweat Farm Road Fire had moved to the southeastern perimeter at the end of April. NMDI is in good agreement with the MODIS active fire image, demonstrating once again that NMDI is a sensitive indicator for active fire monitoring. In addition, the fires appeared to intensify somewhat on 29 April indicated by the much deeper red-colored fire spots in the NMDI image.

As mentioned above, some burn pixels can be captured by the NBR image, while most of them have been omitted. Moreover, NBR revealed saturation to the smoke plumes, which caused the smoke pixels to be mis-displayed in deep green as “heavy vegetation” pixels. There are almost no clear fire signals in the NDWI image, which suggests that NDWI is not sensitive to active fires.

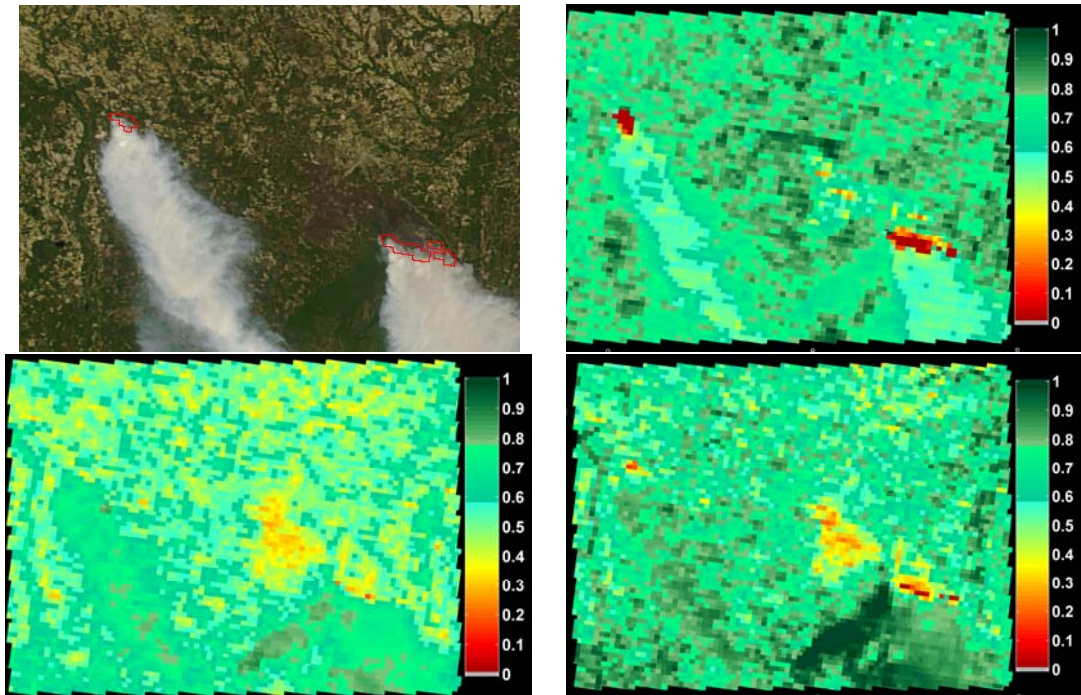


Figure 5.20. Images of active fire (upper left), NMDI (upper right), NDWI (lower left) and NBR (lower right) on 29 April, 2007

Since neither NBR nor NDWI has an obvious response to active fires, statistical analyses using confusion matrices (Kohavi and Provost, 1998) have only been conducted for the NMDI to further evaluate the accuracy of the active fire detection by comparing it with the corresponding MODIS fire product. If any fire is identified by the MODIS fire products, this fire spot will be marked as a fire pixel. When fire detection results using NMDI agrees with the MODIS products, a correct hit will be counted. Table 5.6 shows the confusion matrices used to compare NMDI fire detection results against MODIS products. The total numbers of correct fire hits and non-fire hit are represented by a , and d , respectively. In the case that NMDI indicates a non-fire event at a certain location which disagrees with the MODIS products, the event is labeled as “fire missing”. The

total number of fires missing is summed up as b . When NMDI data indicates fire but the MODIS product is fire free, the event is labeled as “false alarm”. The total number of false alarms is denoted by c .

In general, the overall accuracy of the fire detection rate can be evaluated as the proportion of the total number of correct hits:

$$\text{Overall accuracy} = (a+d)/(a+b+c+d).$$

The fire detection rate is defined as the ratio of fire cases that were detected correctly by NMDI to the total number of fire events:

$$\text{Fire detection rate} = a/(a+b).$$

The false alarm rate is the proportion of non-fire cases that were incorrectly classified as fire, as calculated using the equation:

$$\text{False alarm rate (commission error)} = c/(c+d).$$

Table 5.6 Confusion matrices for fire detection by NMDI against MODIS products

MODIS \ NMDI	Fire	Non-fire
Fire	a	b
Non-fire	c	d

Table 5.7 summarizes the fire detection results including the total pixel amounts, fire pixels detected by MODIS products and NMDI, overall accuracy, false alarm rate and fire detection rate. The results show that the overall accuracy of active fire detection by using NMDI is approaching 100%. False alarm rate is almost zero percent except for 0.11%

for the fire event on 29th April. The average NMDI fire detection rate is about 80% with the highest value above 90%.

Table 5.7 Comparison of active fire detection results by MODIS products and NMDI (Georgia fire)

MM/DD	Total pixels	Fire pixels		a	b	c	d	Overall accuracy (%)	False alarm rate (%)	Fire detection rate (%)
		MOD14	NMDI							
04/17	2611	13	12	12	1	0	2598	99.96	0.00	92.31
04/25	7004	16	11	11	5	0	6988	99.93	0.00	68.75
04/29	6467	40	35	28	12	7	6420	99.71	0.11	70.00

Both, performance evaluations by image interpretation and statistical analyses, indicate that the active fire detection using NMDI is quite accurate for Georgia fires.

In order to show that NMDI is not site-specific and can be applicable to different sites with different canopy characteristics, the wildfires that broke out in southern Greece are used to validate the application of NMDI for fire detection.

5.3.3.2 Greek Fires

The most destructive fires that raged from August 23 to August 25 in western and southern Peloponnese are selected for this case study.

Test case 1: fire on August 23rd

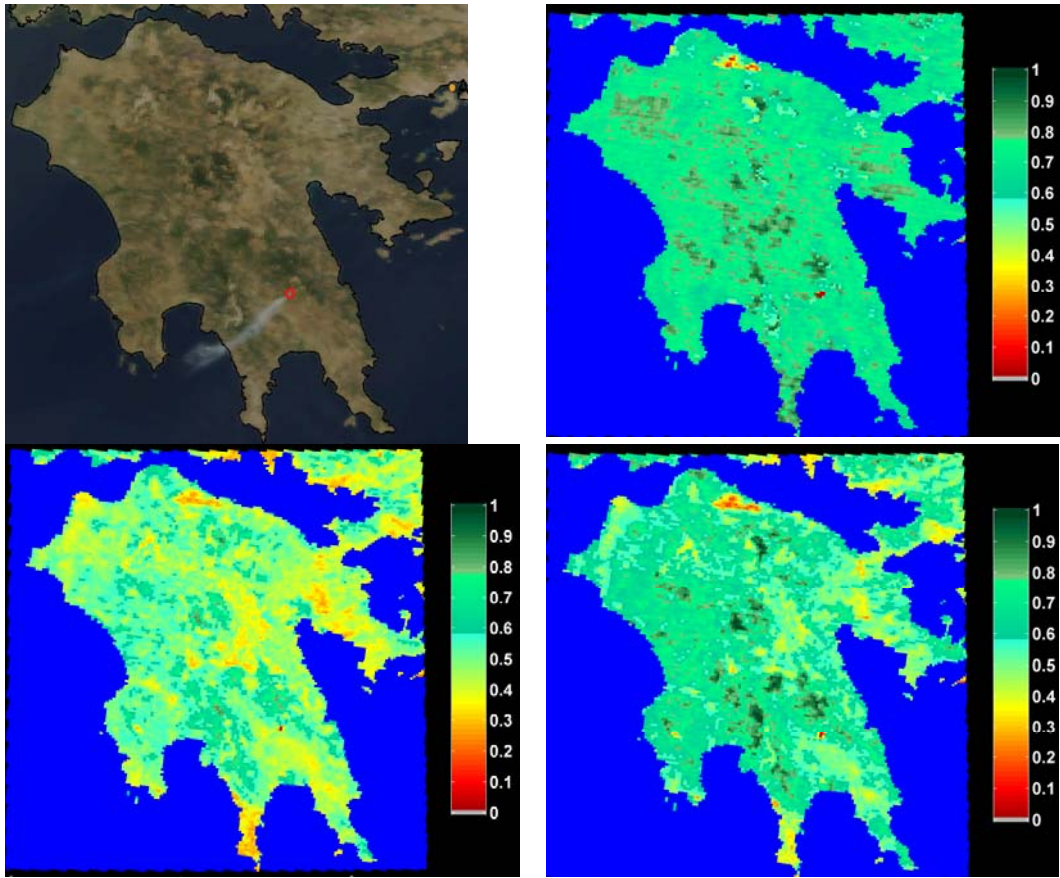


Figure. 5.21. Images of active fire (upper left), NMDI (upper right), NDWI (lower left) and NBR (lower right) on 23 August, 2007

Fires started in Greece on 23 August 2007. The active fire location represented by the red circle in the MODIS active fire image can also be identified in NMDI, NDWI and NBR images by the red-colored dots (Figure 5.21). While considering the scope of the burning fire, the NMDI image offers the best fire area mapping which agrees well with the active fire image. Only a very small part of the burning area can be detected in the other two images. The yellow- and red-colored areas in the top part of the NMDI image are visible in the NDWI and NBR images, which may suggest dry soil conditions. A large part of the yellow-colored areas in the NDWI image corresponds to bare soil

coverage, since NDWI values are expected to be relatively lower for most bare soils than for vegetation (Gao, 1996).

Test case 2: fire on August 24th

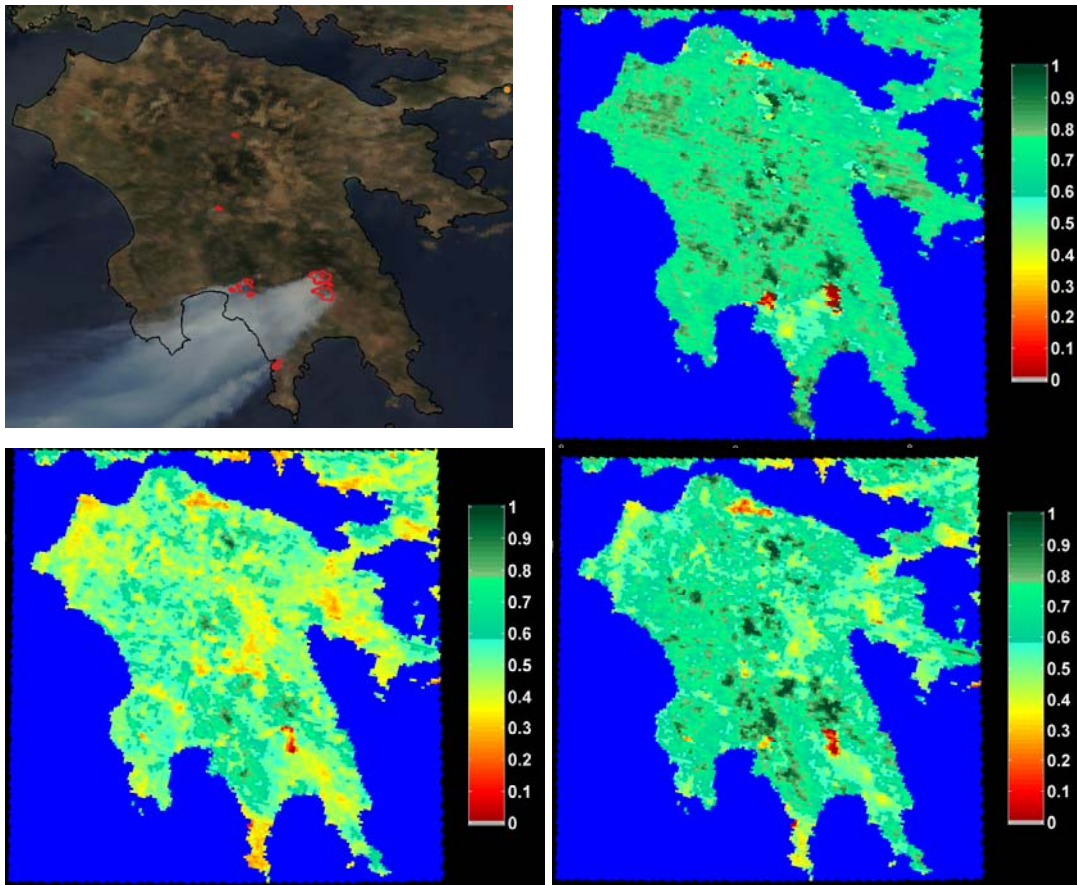


Figure. 5.22. Images of active fire (upper left), NMDI (upper right), NDWI (lower left) and NBR (lower right) on 24 August, 2007

On 24 August 2007, the MODIS active fire map captured five clusters of blazing fires as well as the billowing smoke from fires raging across Greece's southern Peloponnese Peninsula (Figure 5.22). The NMDI image provides exactly the same

information about fire location, fire coverage, and fire shape as the active fire map, without omitting the two relatively small fires in the top and middle part of the Peloponnese peninsula. Only two fire spots can be seen with weak signals in the NDWI image. The NBR image provides the rough locations of five fires, but it has obvious limitations with respect to the fire shape and coverage, especially for the two larger fires.

Test case 3: fire on August 25th

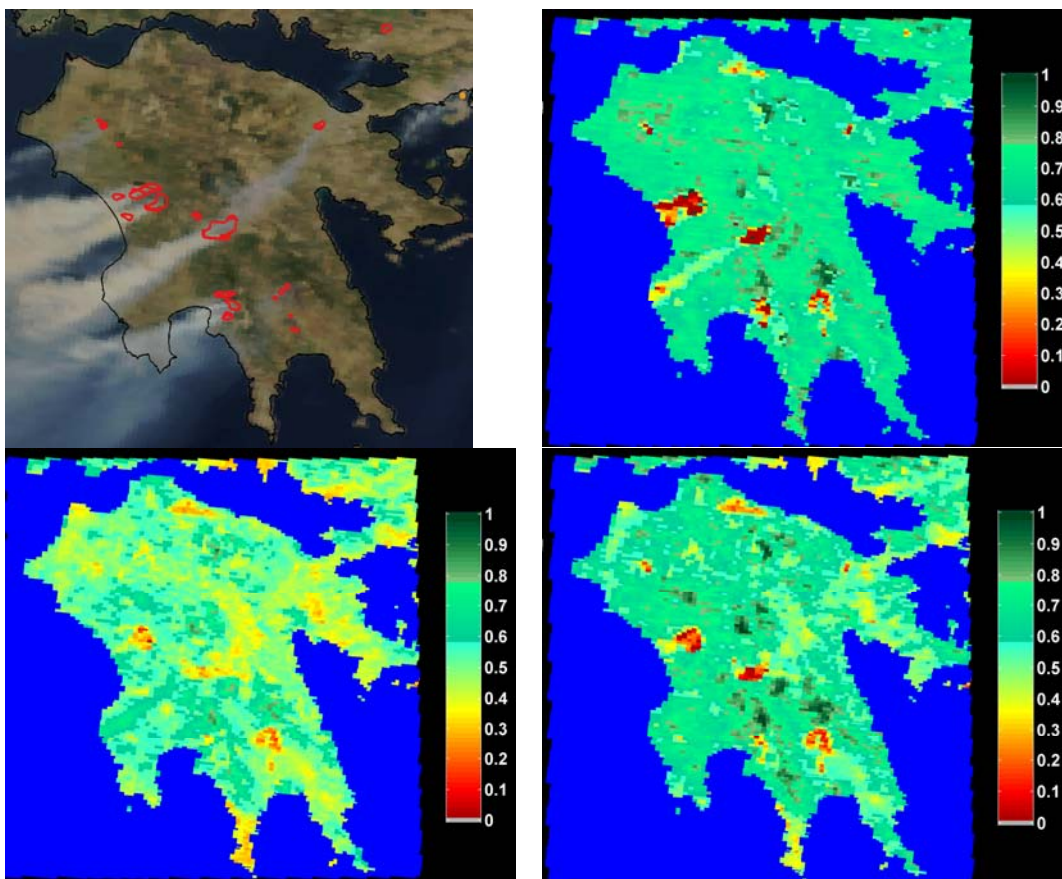


Figure. 5.23. Images of active fire (upper left), NMDI (upper right), NDWI (lower left) and NBR (lower right) on 25 August, 2007

The active fire image captured by Terra MODIS on 25 August shows a line of fires stretching along the western coast of Greece's Peloponnesus Peninsula (Figure 5.23). Once again, NMDI shows the highest performance and discrimination power in active fire detection compared to NDWI and NBR. The deeper red color in the NMDI image compared with the former NMDI images reveals that forest fires are raging unabated on the Peloponnesus Peninsula. To the northeast, a fire is casting a plume of smoke in the active fire map, which can only be detected in the NMDI image (outlined by the red circle).

The statistical analysis of the Greek active fire detection by NMDI is summarized in Table 5.8. With almost a 100% overall accuracy, less than 1% false alarm rate, and around 75% average fire detection rate, fire detection using NMDI matches well with MODIS fire products. It thus demonstrates that NMDI is a consistent regional-to-global-scale indicator for active fire detection. Such a capacity can help monitor large-scale fire hazards and is therefore useful to carry out regional and global studies.

Table 5.8 Comparison of active fire detection results by MODIS products and NMDI (Greek fire)

MM/DD	Total pixels	Fire pixels		a	b	c	d	Overall accuracy (%)	False alarm rate (%)	Fire detection rate (%)
		MOD14	NMDI							
08/23	32047	11	10	7	4	3	32033	99.98	0.01	63.64
08/24	32080	72	68	54	18	14	31994	99.90	0.04	75.00
08/25	20856	125	119	100	25	19	20712	99.79	0.09	80.00

5.3.4 Conclusion

The ability of satellite-derived indices for detecting the forest fires in southern Georgia, USA and southern Greece of 2007 was investigated. MODIS fire products were applied to evaluate the performance of NMDI, NDWI, and NBR for fire detection.

Taking advantage of information contained in multiple NIR and SWIR channels, NMDI demonstrated the highest overall performance and discrimination power when compared to NDWI and NBR. For each test case, NMDI has strong signals corresponding to active fires and pinpoints the active hot spots accurately. The substantially lower NMDI values make the burning pixels stand out from the neighboring areas. Compared to the 250 m resolution MODIS active fire image, the 1 km resolution NMDI image offered almost the same accurate depiction of the active fire shape, coverage, and location. Moreover, NMDI provides quantitative hints about fire intensity, complementary to the burning locations outlined in the MODIS active fire map. Performance evaluations by using the statistical analyses reinforce that the active fire detection using NMDI is quite accurate. The successful application of NMDI for detecting fires in Georgia, USA and Greece demonstrate that NMDI is not site-specific and can be applicable to different sites with different canopy characteristics. The NMDI therefore proves that it is a promising indicator for monitoring active fire in regional-to-global scales.

NBR is sensitive to resultant burn scars, which can be detected with lower NBR values around 0.3. A few pixels experiencing active fire can be identified by NBR, while

most of the burning pixels will be omitted. NDWI, however, does not show a clear response to active fires for any cases presented in this study.

A more thorough evaluation of the NMDI as an active fire monitoring tool for other vegetation types and different geographic areas will be conducted in the near future.

5.4 Chapter summary

In order to quantify the impact of soil and leaf water content on canopy reflectance, sensitivity study has been conducted by using the coupled soil-leaf-canopy reflectance model. The study has illustrated that soil moisture has a different effect than leaf water content, and each MODIS SWIR band responds to these two moisture variables differently.

Based on the findings of the sensitivity study, this chapter has developed a new drought index, the Normalized Multi-band Drought Index (NMDI) for monitoring soil and vegetation moisture from space. Instead of using a single liquid water absorption channel, it uses the slope between two liquid water absorption channels centered at 1640 nm and 2130 nm as the soil and vegetation moisture sensitive band. Typical soil reflectance spectra and satellite-acquired reflectances are used to demonstrate the usefulness of NMDI. By combining information from multiple near infrared and short wave infrared channels, this index has been shown to be a promising indicator for both soil and vegetation drought monitoring.

Forest fires in southern Georgia, USA and Greece in 2007 are used to investigate and compare the ability of NMDI, NDWI, and NBR for active fire detection. NMDI

demonstrated the highest overall performance and discrimination power when compared to NDWI and NBR. NMDI image offered accurate depiction of the active fire shape, coverage, and location, smoke plume, burn scar as well as quantitative information about fire intensity.

The next generation of MODIS sensor - the Visible/Infrared Imager/Radiometer Suite (VIIRS) will have channels centered at 865 nm, 1610 nm and 2250 nm (Ou et al., 2003). This newly designed index can be applied to data that will be acquired by the VIIRS to extract information about soil and vegetation moisture.

CHAPTER SIX

6. SOIL MOISTURE PROFILE ESTIMATION

Given the current technology, satellite remote sensing can only provide soil moisture measurements for the top few centimetres of the soil profile. Since these upper few centimetres of the soil are the most exposed to the atmosphere, their moisture varies rapidly in response to rainfall and evaporation (Jackson, 1993). These observations of near-surface soil moisture must be related to the complete soil moisture profile in the unsaturated zone (Walker, 1999), in order to be more useful for agricultural, hydrologic and climatic studies. The ability to retrieve the soil moisture profile by assimilating near-surface soil moisture measurements in a soil model has received increasing attention over the past decade. However, the incomplete knowledge of soil model physics and the limitation of assimilation technique itself restrict the use of data assimilation approach.

Different from previous studies which use the conceptual model to assimilate near-surface soil moisture observations with the objective of improving runoff predictions, or have only investigated the estimation of soil moisture profiles using synthetic data, this research proposes to solve the governing differential equation for water transport in unsaturated soil by applying a new numerical scheme with which to discretize the equation on the space-time plane. The solution was compared with the measurements of the observed events reported by Menziani et al. (2003).

6.1 Richards Equation

Great efforts have been done to simulate water transport in soil, in which the Richards Equation introduced in 1931 is the primary tool for this purpose. Vertical water infiltration in layered soil profiles is usually modeled using the Richards Equation (Parlange et al., 1972, 1980; Sanders et al., 1988).

The flow of water in homogeneous, nonhysteretic, nonswelling soils can be described by the continuity equation,

$$\frac{\partial \theta}{\partial t} = -\frac{\partial q}{\partial z} \quad (6.1.1)$$

and Darcy's Law:

$$q(\theta, t) = -D(\theta) \frac{\partial \theta}{\partial z} - k(\theta) \quad (6.1.2)$$

where t is time, z is the vertical distance from the soil surface, θ is the volume water content, q is the volumetric flux of water, $D(\theta)$ is the water content dependent soil-water diffusivity, and $k(\theta)$ is the hydraulic conductivity.

Substituting equation (6.1.2) into equation (6.1.1) yields the nonlinear Richards Equation used to describe one-dimensional water transport in unsaturated soils:

$$\frac{\partial \theta}{\partial t} = \frac{\partial}{\partial z} \left[D(\theta) \frac{\partial \theta}{\partial z} \right] - \frac{\partial k(\theta)}{\partial \theta} \frac{\partial \theta}{\partial z} \quad (6.1.3)$$

Equation (6.1.3) is a nonlinear partial differential equation describing the changes of moisture content θ in space and time due to vertical flows. It is nonlinear because the

soil-water diffusivity and the hydraulic conductivity vary with θ . As two parameters of the Richards Equation, the soil-water diffusivity D and the soil-water conductivity k govern the different behaviours in the moisture dynamic. The nonlinearity, however, usually can be solved in a linear mode by considering the soil-water diffusivity D , and K expressed as $\partial k / \partial \theta$ to be constant. Thus the Richards Equation reduces to a linear diffusion wave equation.

The linearized Richards Equation satisfied by soil water content ranging from 0 to 1 can be written as:

$$\frac{\partial \theta}{\partial t} = D \frac{\partial^2 \theta}{\partial z^2} - K \frac{\partial \theta}{\partial z} \quad (6.1.4)$$

The initial and boundary conditions for equation (6.1.4) can be expressed as following arbitrary conditions:

$$\begin{cases} \theta(z, 0) = \theta_i(z) & (z \geq 0) \\ \theta(0, t) = \theta_0(t) & (t \geq 0) \\ \lim_{z \rightarrow \infty} \theta(z, t) = 0 & (t \geq 0) \end{cases} \quad (6.1.5).$$

We now turn to the methods employed to solve the governing equations. Procedures for solving these partial differential equations are either analytical or numerical. Analytical solutions provide answers for a simplified class of problems, while problems of a more general type are handled with numerical solutions through attendant discretization of the solution domain. Numerical simulation of the Richards Equation has been the focus of considerable research (Hills et al., 1989; Celia et al., 1990; Pan and Wierenga, 1995).

6.2 Numerical solution to Richards Equation

The numerical solutions to the governing differential equations for water transport in unsaturated soil are normally obtained by using Finite Difference (FD) or Finite Element (FE) calculation schemes (Van Genuchten, 1982). Often, explicit FD models become numerically unstable and give large numerical errors because of the strong nonlinearity inherent in the equation. The numerically more involved FE and implicit FD models are numerically stable and accurate if appropriate values of the time and depth increments are chosen. However, criteria for avoiding different types of numerical errors, and consequently for selecting the correct values of the time and depth increments, are poorly understood and often not available. Moreover, the FE and implicit FD models are relatively complicated to program and to solve (Moldrup et al., 1992). Moldrup et al. (1989) presented an easily programmed alternative labeled the moving mean slope (MMS) model to the FE and the implicit FD models. The MMS model, an integrated version of the Darcy equation is used together with a simple, explicit forward time discretization of the continuity equation to calculate water transport.

Instead of directly solving the diffusion wave equation as others did, we proposed to approximate the Richards Equation by applying a new numerical scheme with which to discretize the kinematic wave equation on the space-time plane. Numerical diffusions are known to be introduced by a non-central discretization of the differential equation (Vestergaard, 1989). This artificially introduced dispersion is usually required to be removed to improve the simulation accuracy since it results in an erroneously large or small degree of spreading of the calculated concentration profiles (Moldrup et al., 1994).

However, this numerically induced dispersion has been used in this work to simulate the physical diffusion, other than being removed and therefore, the second order accurate approximation of the diffusion wave equation has been achieved.

6.2.1 Introduction

Neglecting the diffusion term in Richards Equation (6.1.4) and introducing the differential operator L yields the kinematic wave equation in the following form:

$$L\theta \equiv \frac{\partial \theta}{\partial t} + K \frac{\partial \theta}{\partial z} = 0, \quad (6.2.1)$$

which describes the movement of water waves which are kinematic in nature. It is a first-order partial differential equation, therefore, kinematic waves travel with wave celerity of K and do not attenuate. Wave attenuation can only be described by a second order partial differential equation.

By expressing the values in terms of discrete adjacent values in space and time, numerical diffusions are known to be introduced in numerical solutions of partial differential equation by the finite grid size. This numerically induced dispersion is an important source of calculation errors in transport simulations. Moldrup et al. (1994) had derived the correction terms for removing numerical dispersion from four commonly used FD calculation schemes on the general transport equation using Taylor Series. On the other side, Cunge (1969) first proposed to use the numerical diffusion generated in the difference solution to the kinematic wave equation to simulate the physical diffusion of the diffusive wave under certain conditions and achieved the known

Muskingum-Cunge flood routing method (Rui, 1995). However, few similar studies focus on water transport in unsaturated soil.

Based on Cunge's idea and aimed to control the amount of numerical diffusion in such a way that it matches the diffusion of the physical problem, a new numerical method is presented. By using a new numerical scheme with which to discrete the kinematic wave equation on the space-time plane, this method not only shows the capability to simulate the physical diffusion of the diffusive wave, but also enhances the solution precision from the first to the second order.

6.2.2 Discretization of kinematic wave equation

The kinematic wave equation is discretized on the Z - t plane. Figure 6.1 shows the computational scheme. This computational grid is defined by equal space and time steps, ΔZ and Δt , respectively. The spatial positions of the grid points are denoted by index i and the time moments by index k .

t_{k+1}		θ_{i+l}^{k+l}
t_k	θ_i^k	θ_{i+l}^k
t_{k-1}	θ_i^{k-1}	
	Z_i	Z_{i+l}

Figure 6.1. Space-time discretization of kinematic wave equation

In Figure 6.1, Z is the vertical coordinate (positive downward) , t is the time coordinate, i and k are space and time steps, respectively, θ means the sequence of the

discrete values θ_i^k , which should approximate the values $\theta(t_k, Z_i)$ ($k=1, 2, 3, \dots; i=0, 1, 2, \dots$).

The differential θ with respect to space is approximated by applying the first-order finite differences at point (t_k, Z_i) with forward in space,

$$\frac{\partial \theta}{\partial Z} \approx \frac{\theta_{i+1}^k - \theta_i^k}{\Delta Z} \quad (6.2.2)$$

Introducing weighting factor x in discretizing θ with off-centering the temporal derivative by means of backward for going toward point, and forward for leaving point (Hoos et al., 1989; Rui and Wang, 2000; Wang, 1999), we get,

$$\frac{\partial \theta}{\partial t} \approx \frac{x(\theta_i^k - \theta_i^{k-1}) + (1-x)(\theta_{i+1}^{k+1} - \theta_{i+1}^k)}{\Delta t} \quad (6.2.3)$$

where x is the weighting factor between 0 and 1, as it is shown: $0 \leq x \leq 1$.

Substituting equations (6.2.2) and (6.2.3) into equation (6.2.1), the differential operator L is approximated by the following finite difference operator:

$$L_{\Delta t, \Delta z} \equiv K \frac{\theta_{i+1}^k - \theta_i^k}{\Delta Z} + \frac{x(\theta_i^k - \theta_i^{k-1}) + (1-x)(\theta_{i+1}^{k+1} - \theta_{i+1}^k)}{\Delta t} = 0 \quad (6.2.4).$$

Manipulating equation (6.2.4) by grouping the terms, the deeper layer soil moisture θ_{i+1}^{k+1} can be expressed as a linear function of the soil moistures θ_i^k , θ_i^{k-1} and θ_{i+1}^k as follows:

$$\theta_{i+1}^{k+1} = C_1 \theta_i^k + C_2 \theta_i^{k-1} + C_3 \theta_{i+1}^k \quad (6.2.5)$$

The coefficients C_1 , C_2 , and C_3 in equation (6.2.5) have the following expressions:

$$C_1 = \frac{C - x}{1 - x} \quad (6.2.6)$$

$$C_2 = \frac{x}{1 - x} \quad (6.2.7)$$

$$C_3 = 1 - \frac{C}{1 - x} \quad (6.2.8)$$

where C is the Courant number, defined as follows:

$$C = K\Delta t / \Delta Z \quad (6.2.9).$$

Notice that Courant number is the ratio of physical wave celerity to grid celerity $\Delta Z / \Delta t$. The sum of the coefficients is equal to the unity: $C_1 + C_2 + C_3 = 1$, which expresses the storage conservation, meaning that the storage entered at the up layer of the profile leaves the down end layer.

Since θ_{i+1}^k , θ_i^{k-1} and θ_i^k are known for a given time increment, θ_{i+1}^{k+1} is computed using equation (6.2.5) and then the computation sequentially proceeds from upper layers towards deeper layer grid points, in a successive time step. By this means, a forecast lead time equaling time interval can be obtained for soil moisture profile estimation. With valuable increases in lead time, this method therefore permits more effective drought management and drought warning.

It should be emphasized that equation (6.2.5) is numerical solution to kinematic wave equation and, therefore the feasibility and condition of its use in diffusion wave equation need to be investigated and analyzed.

6.2.3 Conditions for simulating the physical diffusion

Truncation error is known to be introduced if equation (6.2.4), the first-order finite difference is used to approximate the kinematic wave equation (6.2.1). By applying the Taylor series expansion to variable θ at the point of (t_k, Z_i) , and neglecting the terms of third and higher order, we obtain:

$$\begin{aligned}\theta_i^k &= \mathcal{G} \\ \theta_i^{k-1} &= \mathcal{G} - \frac{\partial \mathcal{G}}{\partial t} \Delta t + \frac{\partial^2 \mathcal{G}}{\partial t^2} \Delta t^2 / 2 \\ \theta_{i+1}^k &= \mathcal{G} + \frac{\partial \mathcal{G}}{\partial z} \Delta z + \frac{\partial^2 \mathcal{G}}{\partial z^2} \Delta z^2 / 2 \\ \theta_{i+1}^{k+1} &= \mathcal{G} + \frac{\partial \mathcal{G}}{\partial z} \Delta z + \frac{\partial^2 \mathcal{G}}{\partial z^2} \Delta z^2 / 2 + \frac{\partial \mathcal{G}}{\partial t} \Delta t + \frac{\partial^2 \mathcal{G}}{\partial t^2} \Delta t^2 / 2\end{aligned}\tag{6.2.10}$$

Substituting equation (6.2.10) into equation (6.2.4) and arranging yields:

$$\frac{\partial \theta}{\partial t} + K \frac{\partial \theta}{\partial Z} = \left[-\frac{K \Delta Z}{2(1-x)} + \frac{K^2 x \Delta t}{2(1-x)} - \frac{K^2 \Delta t}{2} + K \Delta Z \right] \frac{\partial^2 \theta}{\partial Z^2}\tag{6.2.11}$$

Then the truncation error τ can be expressed as follows:

$$\tau = L \theta - L_{\Delta t, \Delta z} = \left[-\frac{K \Delta Z}{2(1-x)} + \frac{K^2 x \Delta t}{2(1-x)} - \frac{K^2 \Delta t}{2} + K \Delta Z \right] \frac{\partial^2 \theta}{\partial Z^2} + \varepsilon_2 + \dots\tag{6.2.12}$$

where ε_2 is the second-order precision truncation error.

For simplicity, equation (6.2.12) may be written as:

$$\frac{\partial \theta}{\partial t} + K \frac{\partial \theta}{\partial Z} = L_{\Delta t, \Delta x} + \varepsilon_1 + \varepsilon_2 + \dots \quad (6.2.13)$$

where ε_1 in equation (6.2.13) is the first-order precision truncation error, and it can be obtained by equation (6.2.14)

$$\varepsilon_1 = \left[-\frac{K\Delta Z}{2(1-x)} + \frac{K^2 x \Delta t}{2(1-x)} - \frac{K^2 \Delta t}{2} + K\Delta Z \right] \frac{\partial^2 \theta}{\partial Z^2} \quad (6.2.14).$$

For convenience, the terms in the square brackets of right-hand side in equation (6.2.14) may be expressed as D , i.e.

$$D = -\frac{K\Delta Z}{2(1-x)} + \frac{K^2 x \Delta t}{2(1-x)} - \frac{K^2 \Delta t}{2} + K\Delta Z \quad (6.2.15)$$

which is considered as the numerical dispersion coefficient. To ensure that wave amplification does not occur (i.e., the numerical diffusion is damped), D should be greater than zero: $D > 0$.

Substituting equation (6.2.15) into equation (6.2.13) leads to:

$$\frac{\partial \theta}{\partial t} + K \frac{\partial \theta}{\partial Z} - D \frac{\partial^2 \theta}{\partial Z^2} = L_{\Delta t, \Delta x} + \varepsilon_2 + \dots \quad (6.2.16)$$

Equation (6.2.16) shows that, although equation (6.2.4) is a first-order approximation of the kinematic wave equation, it becomes a second order accurate numerical solution to the diffusion equation if the amount of numerically induced diffusion is in such a way that it matches the physical diffusion.

Rearranging equation (6.2.15) yields:

$$x = \frac{2 / P + C - 1}{2 / P + 2C - 2} \quad (6.2.17)$$

where P is the well-known Péclet number, defined as follows:

$$P = K \Delta Z / D \quad (6.2.18).$$

Generally speaking, equation (6.2.4) constitutes a second order accurate approximation of the diffusion wave equation if the weighting coefficient x is evaluated as equation (6.2.17) and chosen in such a way that the false (numerical) diffusion generated by the scheme exactly coincides with the physical diffusion. The numerical solution resembles a diffusion wave with higher order accuracy rather than a kinematic wave. In other words, the new numerical scheme used can not only simulate the physical diffusion, but also improve the solution precision to the second order.

6.2.4 Stability considerations

Replacing the continuous original problem with an integration over a discrete computational grid introduces numerical errors into the results. A finite-difference scheme is stable if such errors are not amplified during computation from one time level to the next. The numerical stability depends on the size of the time and space steps and on some flow characteristics. Therefore, any explicit scheme is conditionally stable.

The method presented in this study uses an explicit scheme and one must be careful to satisfy constraints for numerical stability.

6.2.4.1 Courant condition

Notice that Courant number C expressed as $K\Delta t / \Delta Z$ is the ratio of the movement

distance during the time interval Δt to the space interval ΔZ . The time step Δt must be small enough that the wave propagating at the velocity K will not outrun the spatial grid sampling ΔZ . If the wave can travel through the length ΔZ in a time less than the computational interval Δt , then computational instabilities may evolve. Therefore, C is restricted to values less than 1 for numerical stability reasons. For values of C greater than 1, the amount of diffusion introduced in the numerical problem is unrelated to the true diffusion, if any of the physical problem. The condition to satisfy here is known as the Courant condition and is expressed as $0 < C < 1$.

6.2.4.2 Stability condition of numerical diffusion

The Courant condition is a necessary but insufficient condition for stability of an explicit scheme. Other concerns are also required for stability.

Dividing the right-hand side terms of equation (6.2.15) by $\Delta t / (\Delta x)^2$ and taking into account constraints of $\Delta Z > 0$, $\Delta t > 0$, $C > 0$, and $D > 0$, it follows that:

$$\frac{-C}{2(1-x)} + \frac{xC^2}{2(1-x)} - \frac{C^2}{2} + C > 0 \quad (6.2.19)$$

Equation (6.2.19) then reduces to:

$$\frac{1+C-C \times 2x}{1-x} < 2 \quad (6.2.20)$$

When $C = 1$ or $x = 0.5$, relation (6.2.20) will be violated.

When $0.5 < x < 1$, the denominator is positive, and therefore:

$$1 + C - 2xC < 2 - 2x$$

or

$$C(1 - 2x) < 1 - 2x \quad (6.2.21)$$

Since $1-2x < 0$, it follows that $C > 1$, the Courant constraint is violated, and the numerical stability is compromised.

When $x > 1$, the denominator is negative, and therefore:

$$1 + C - C \times 2x > 2 - 2x$$

or

$$C(1 - 2x) > 1 - 2x \quad (6.2.22)$$

Since $1-2x < 0$, it follows that $C < 1$, satisfying the Courant condition.

In a similar way, when $x < 0.5$, the computation is conditionally stable and convergent to the analytical solution as the Courant number less than 1.

Considering that x is a weighting factor in temporal direction between 0 and 1, we can achieve that for numerical stability, the parameter x must satisfy the constraint $0 \leq x < 0.5$.

As implied by equation (6.2.5), the non-negativity constraint must be verified by every coefficient:

$$0 \leq C_3 \leq 1 \quad (6.2.23)$$

or
$$0 \leq C_2 \leq 1 \quad (6.2.24)$$

or
$$0 \leq C_1 \leq 1 \quad (6.2.25)$$

If these constraints are violated, when either two terms in the right hand side of equation (6.2.5) are made to equal zero due to soil moisture or coefficient of zero, negative values for down layer soil moisture can be obtained and the numerical stability will be compromised.

Equation (6.2.23) requires that

$$0 \leq C \leq 1 - x \quad (6.2.26)$$

Equation (6.2.24) is satisfied if $0 \leq x < 0.5$.

Equation (6.2.25) requires that

$$x \leq C \leq 1 \quad (6.2.27)$$

Assembling above restrictions as well as Courant condition achieves the following form:

$$\begin{cases} 0 \leq x < 0.5 \\ 0 \leq C < 1 \end{cases} \quad (6.2.28)$$

In general, this numerical method is stable as long as the constraint (6.2.28) is met. After the x parameter has been determined, the routing space and time steps ΔZ and Δt can be adjusted using the relationship with C to satisfy stability conditions.

6.2.5 Application example

The following example is taken to illustrate the application of this new numerical method. By solving equation (6.2.5), the soil water content at all points in the soil profile for all time can be determined. The parameters in the model mainly include the hydraulic

conductivity K and the soil-water diffusivity D .

It is well known that numerical solutions are suitable and powerful in solving nonlinear equations starting from the experimental initial and boundary conditions. This appears to be quite appropriate when solving specific problems such as evolution of the vertical profile of the soil water content starting from initially dry soil. In the absence of suitable field data, it was decided to evaluate the model performance assuming flow conditions similar to those reported in a study by Menziani et al. (2003). Those authors analyzed the soil water content trend during the driest period based on the data collected at Pallanzeno. On 19 July 1999, the distribution of the experimental soil volumetric water content in the first 40 cm soil layer was quite uniform at 31%, representative of a simple initial condition for solving the partial differential equation. The soil layer below 40 cm remained at practically the same soil water content during the period 19-27 July. The uniform initial condition and the upper and lower boundary conditions were obtained from the experimental data.

For simplicity and clarity, the soil layer from the surface down to 40 cm is considered as having the mean soil physical characteristics and a mean K equal to $8 \cdot 10^{-7}(\text{m/s})$, D equal to $1.6 \cdot 10^{-8}(\text{m}^2/\text{s})$. The K and D values used are between the measured values of the hydraulic conductivity and close to the laboratory estimation (Menziani et al., 2003). The finite-difference grid and time steps used in solving the Richards equation were fixed at 5 cm and 1, and 2 hour, respectively. The corresponding values for numerical solution are shown in Table 6.1.

Table 6.1 Values for numerical solution

$\Delta Z(\text{m})$	$\Delta t \text{ (h)}$	C	x	$C1$	$C2$	$C3$	Stability condition
0.05	1	0.0576	0.142	-0.0984	0.1655	0.9329	satisfied
0.05	2	0.1152	0.1	0.0168	0.1112	0.8720	satisfied

Figure 6.2 shows the evolution of the daily vertical profile of the soil water content in the first 40 cm layer from 19 to 27 July 1999 (driest period), which were compared to the characteristics of the observed events reported by Menziani et al. (2003). It is obvious that these two evolutions of the soil water content match well with each other, which indicates that this numerical approach ensures easily satisfied solution convergence while providing relatively accurate solutions of the equation at reasonable CPU times.

It is important to point out that the parameter values used in this study should be considered typical values that may show a high degree of variability in application (Chow et al., 1988). Hydraulic conductivity and soil-water diffusivity values are far less consistent, varying by one to two orders of magnitude (James et al., 1992). More reliable soil moisture profile predictions can be expected if model parameters are obtained from field measurements since these measurements tend to lump the effect of soil heterogeneities (Leconte and Brissette, 2001).

Consequently, the example case presented in this paper can only serve as a means to evaluate the validity of the numerical solution to the Richards Equation. They are not indicative of actual field conditions. Additional research is required to extend and test the usefulness of the approach presented here. Comparison with already available FE and FD calculation schemes should be conducted with new experiments.

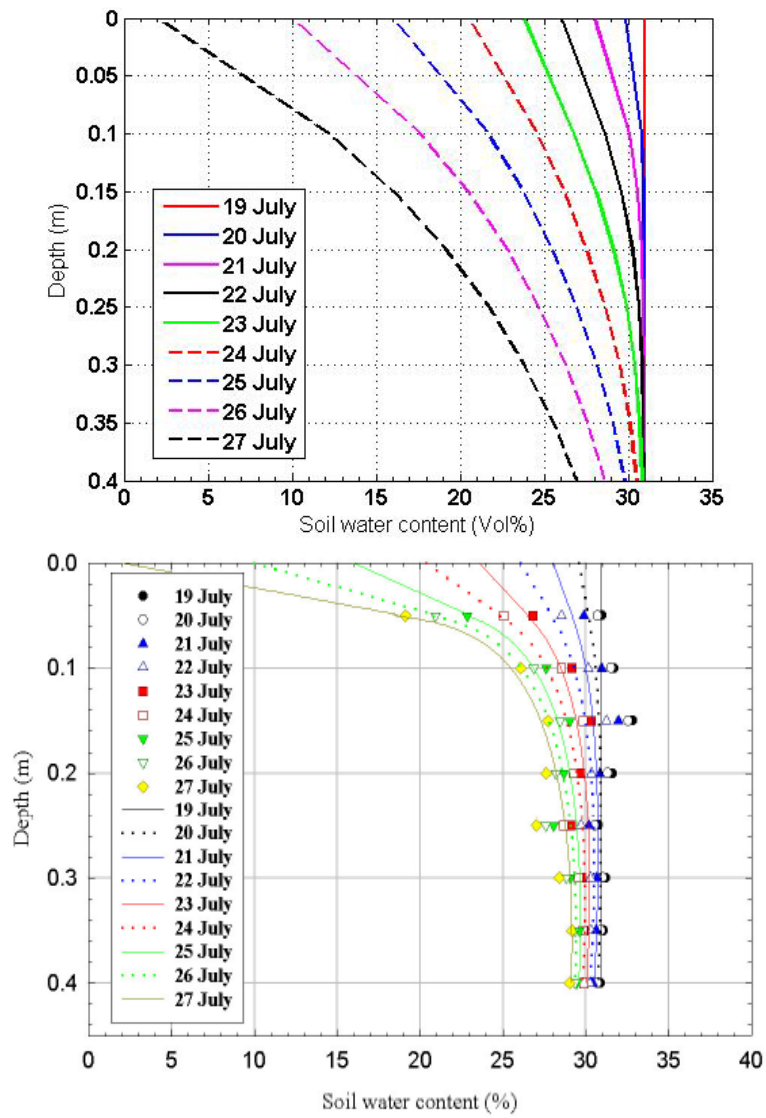


Figure 6.2. Evolution of the daily vertical profile of the soil water content from 19 to 27 July 1999 (driest period). Upper: obtained by numerical solution; Lower: adopted from Menziani et al. (2003)

6.3 Chapter summary

A new numerical method for solving Richards Equation is presented by matching physical and numerical diffusion. Following conclusion can be drawn from the numerical

analysis and application:

1. By applying a new numerical scheme with which to discrete the kinematic wave equation on the space-time plane, this method shows the capability to simulate the physical diffusion of the diffusive wave with the numerical diffusion generated in the difference solution under certain conditions.

2. The algebraic formulae of the new method for soil water content routing are explicit, and the formulae are simple to use and program. The model parameters can be determined either by literature values or the laboratory estimation.

3. Although any explicit scheme is conditionally stable, analysis suggests that the stability conditions of the new scheme used in this study are simple and can be easily achieved. The numerical stability depends on the satisfaction of Courant condition and the optimal selection of the temporal weighting factor.

4. Compared with other numerical method with the first-order finite differences scheme, this method has enhanced the solution precision to the second order.

5. The example application shows that this method has good convergence properties. The diffusion wave scheme is formulated by matching physical and numerical diffusion, which results in an effective control of numerical diffusion.

6. The merit of this method includes it provides a forecast lead-time equal to one time step. This advantage will be significant for drought control if the time step is large.

CHAPTER SEVEN

7. CONCLUSIONS AND FUTURE DIRECTION

The dissertation has explored the use of remote sensing science and technologies towards the monitoring of soil moisture and drought. By using approaches that utilize remote sensing measurements, ground observations, and a vertical water transport model, the ability to estimate the spatial distribution and temporal variation of soil moisture has been investigated. The near-surface soil moisture observations have been combined with remote sensing measurements for soil moisture estimation to achieve higher accuracy and spatial resolution. Remote sensing measurements from multiple optical channels are used to monitor soil and vegetation drought based on the spectral reflectance change responding to vegetation and soil moisture variations. The water transport model is the kernel of the soil moisture profile estimation algorithm, as it forecasts the spatial distribution and temporal variation of soil moisture profiles from the near surface soil moisture which gained by ground observations or remote sensing measurements. Combining these means, daily soil moisture profile at high resolution can be gained.

7.1 Conclusions

The main achievements of this dissertation fall into three categories, namely: (i) estimation of soil moisture by combining the strengths of multi-sensor and ground

measurements to achieve higher accuracy and spatial resolution; (ii) development of a new drought index for both soil and vegetation drought monitoring by using multiple NIR-SWIR spectral signatures; (iii) one-dimensional soil moisture profile estimation algorithm to relate the near-surface soil moisture observations to different soil layers. Finally, the applications of the research presented in this thesis and their impact on further studies are summarized.

7.1.1 Soil moisture estimation using multi-sensor and ground measurements

A soil moisture estimation algorithm at moderate resolution was developed based on the well known ‘Universal Triangle’ relation among soil moisture, vegetation cover and land surface temperature. Two years of Terra MODIS measurements and ground observations at 137 stations in Shandong province, P. R. China were used to investigate the regression relationships. Analysis shows that MODIS NDVI and LST are strongly correlated with the ground soil moisture measurements, and regression relationships are soil type and vegetation type dependent. The land cover and soil types based regression relations, in conjunction with MODIS NDVI and LST data, are then regressed backward to obtain soil moisture at MODIS resolution. The validation by using a new set of one year ground observations and MODIS data shows a good agreement between ground observed and algorithm derived soil moisture. It suggests this approach has good potential to retrieve soil moisture at high spatial resolution for regional applications. The 1 km soil moisture maps can provides regional soil moisture details and soil moisture spatial pattern, which are valuable for many applications, such as drought monitoring and fire danger detecting.

AMSR-E onboard Aqua provides daily global soil moisture of the top 2 cm soil layer with spatial resolution of 25 km. Though lower in spatial resolution than MODIS optical bands, AMSR-E microwave measurements are typically less affected by clouds, making them complementary to MODIS measurements over regions of clouds.

7.1.2 Soil moisture estimation using multiple MODIS SRB measurements

By using simulations with the coupled soil-leaf-canopy reflectance models, sensitivity analyses have been performed to quantify the impact of soil and leaf water content on the SWIR reflectances and water related indices. The results demonstrate that soil moisture has to be considered in realistic simulations of land surface reflectances and vegetation water indices since it has a large effect on the canopy reflectance when vegetation density is low. The study has also illustrated that soil moisture has a different effect than leaf water content, and each MODIS SWIR band responds to these two moisture variables differently.

Based on the findings of the sensitivity study, a new drought index, the Normalized Multi-band Drought Index (NMDI) was designed for monitoring soil and vegetation moisture from space by using three wavelengths, one in the NIR centered approximately at 860 nm, and two in the SWIR centered at 1640 nm and 2130 nm, respectively. Multiple bands, rather than two bands with the normalized calculations, have not been used previously in the formation of vegetation moisture indices. Instead of using a single liquid water absorption channel like NDII and NDWI, it uses the slope between two liquid water absorption channels centered at 1640 nm and 2130 nm as the soil and vegetation moisture sensitive band. Strong differences of soil water and leaf water effects

between two water absorption bands make this combination most appropriate for the estimation of water content for both soil and vegetations.

Typical soil reflectance spectra and satellite acquired canopy reflectances, are used to validate the usefulness of NMDI for remotely sensing soil and vegetation moisture. NMDI has strong responses to both severe soil and vegetation drought conditions in opposite directions: higher values with increasing soil drought and lower values with increasing vegetation drought, suggesting a promising indicator for monitoring both soil and vegetation drought from space.

2007 forest fires in southern Georgia, USA and southern Greece are used to investigate and compare the ability of NMDI, NDWI, and NBR for active fire detection. Taking the advantage of information contained in multiple NIR and SWIR channels, NMDI demonstrated highest overall performance and discrimination power when compared to NDWI and NBR. Compared to the 250 m resolution MODIS active fire image, the 1 km resolution NMDI image offered almost the same accurate depiction of the active fire shape, coverage, and location, as well as smoke plume and burn scar. Moreover, NMDI provides quantitative analysis about fire intensity, complementary to the burning locations outlined in the MODIS active fire map. NMDI therefore proves it a potential indicator for monitoring active forest fire.

7.1.3 Soil moisture profile estimation

A new numerical method for solving Richards equation presented in this thesis provides a convenient alternative to existing models and approaches to estimate the soil moisture profile from the surface moisture data. By applying a new numerical scheme

with which to discrete the kinematic wave equation on the space-time plane, this method shows the capability to simulate the physical diffusion of the diffusive wave with the numerical diffusion generated in the difference solution under certain conditions. The algebraic formulae of the new method for soil water content routing are explicit, and the formulae are simple to use and program. Although any explicit scheme is conditionally stable, analysis suggests that the stability conditions of the new scheme used in this study are simple and can be easily achieved. The numerical stability depends on the satisfaction of Courant condition and the optimal selection of the temporal weighting factor. Compared with other numerical method with the first-order finite differences scheme, this method has enhanced the solution precision to the second order. The example application shows that this method has good convergence properties. The diffusion wave scheme is formulated by matching physical and numerical diffusion, which results in an effective control of numerical diffusion. In addition, the merit of this method also includes it provides a forecast lead time equal o one time step. This advantage will be significant for drought control if the size of time step is large.

7.2 Applications of this research

The research conducted in this dissertation is expected to be useful for soil moisture estimation, drought monitoring, and active forest fire detecting.

The soil moisture products at 1 km resolution presented in Chapter 4 can provide decision makers detailed information on soil moisture spatial distribution and temporal variation, which are valuable for many applications, such as drought monitoring and fire

danger detecting. Although the study was conducted over Shandong province, P. R. China, the soil moisture estimation algorithms are expected to apply to other similar areas with same land cover and soil type.

The new drought index, NMDI, will provide a new foundation of physics based indices for monitoring both soil and vegetation moisture from space. Combining information from multiple channels makes NMDI response to both severe soil and vegetation drought conditions in opposite directions and therefore, a promising indicator for both soil and vegetation drought monitoring. Its highest overall performance and discrimination power compared to other vegetation water related indices in detecting Georgia and Greek fires demonstrated its ability for active fire detection. This index can be applied to the next generation of satellite instruments, such as VIIRS, to extract information about soil and vegetation moisture condition.

The new numerical solution of Richards Equation presented in Chapter 6 provides convenient an alternative to existing models and approaches to estimate the soil moisture profile from surface soil moisture data. Better retrievals of soil moisture profile are not only useful for drought monitoring, but also can aid in climate studies as well.

The research presented in this thesis explores a new direction in the use of remote sensing science and technologies towards soil moisture and drought estimation. It will provide a physics foundation for remote sensing-based approaches for assessing and monitoring soil moisture and drought at a finer spatial and temporal resolution.

7.3 Limitations of this work

This study was carried out in some limited condition due to data availability in time and space. In the absence of suitable laboratory and field data (such as the soil spectra with varying soil moisture, the vegetation spectra at various leaf water content, and the soil moisture profile under different initial and boundary conditions), some results are thus mainly based on the model simulation and limited available datasets. Simulation performed by soil, leaf and canopy reflectance models is a primary part in this research, which are used to achieve the desired objectives. Although these models have been well calibrated and widely used, and are known to perform reasonably well, models as always represent a reasonable simplification of the complex real processes. The availability of more relevant data in the future would entail more extensive evaluations and validations of the results (Dasgupta, 2007).

One of the significant achievements of this research is the proposed new index NMDI for monitoring both soil and vegetation water conditions. Currently the use of NMDI, however, is limited to bare soils or weakly vegetated areas, and heavy vegetation areas. For areas with moderate vegetation coverage, which are common conditions found in reality, the distinction between NMDI's roles as a soil drought indicator and a vegetation drought indicator blurs. Its application to directly interpret soil and vegetation moisture conditions could yield inaccurate results. New experiments are required to extend and test the proposed techniques.

7.4 Future works

Recommendations for future research fall into three categories, namely: (i) extensive applications of NMDI for drought monitoring and active fire detecting; (ii) improvements of soil moisture profile estimation; and (iii) development of an operational system for drought monitoring. Potential research in each of these three categories is addressed below.

7.4.1 Extensive applications of NMDI

More extensive validations of the new spectral index NMDI need to be performed as suitable data becomes available. Its applicability to areas with moderate vegetation coverage must be investigated and tested. Further studies on identifying LAI or NDVI thresholds to separate bare soil, moderate vegetation, and heavy vegetation areas, and NMDI thresholds to classify fire and non-fire pixels, need to be carried out to adapt NMDI to operational applications.

7.4.2 Improvements of soil moisture profile estimation

One objective of this dissertation has been investigating an appropriate methodology for estimating the spatial distribution and temporal variation of soil moisture profiles. Hence, the obvious progression from the work established in this thesis, is to test the soil moisture profile estimation algorithm with actual observations on soil moisture and evapotranspiration under natural hydrologic conditions. A series of numerical experiments with this soil moisture profile estimation algorithm should be carried out to

demonstrate the methodology, and to prove the effectiveness of the techniques used. Moreover, further validations and evaluation of this numerical approach need to be conducted by comparing with already available FE and FD calculation.

7.4.3 Development of an operational system for drought monitoring

Remote sensing plays a major role in applications of soil moisture and drought monitoring. In specific remote sensing based estimation of soil and vegetation moisture has shown a lot of promise for drought monitoring in this study. The cost effectiveness, and the easy availability of remote sensing data with higher spatial and temporal resolution possibly in near real time (Dasgupta, 2007) make remote sensing based operational system for drought monitoring very attractive. This has not been thoroughly investigated here, and would be a key direction for the future work.

REFERENCES

REFERENCES

- Akinremi, O. O., and McGinn, S. M., 1996. Evaluation of the palmer drought index on the Canadian Prairies. *Journal of Climate* 9(5): 897-905.
- Alley, W.M., 1984. The Palmer Drought Severity Index: Limitations and assumptions. *Journal of Climate and Applied Meteorology*, 23, 1100–1109.
- Ångström, A., 1925. The Albedo of Various Surfaces of Ground. *Geograf. Ann.*, 7, 323-342.
- Arya, L. M., Richter, J. C. and Paris, J. F., 1983. Estimating Profile Water Storage from Surface Zone Soil Moisture Measurements Under Bare Field Conditions. *Water Resour. Res.*, 19(2), 403-412.
- Asner, G.P., 1998. Biophysical and biochemical sources of variability. *Remote Sens. Environ*, 76, 173–180.
- Atzberger, c., Jarmer, T., Schlerf, M., Kotz, B. and Werner, W., 2003. Retrieval of wheat bio-physical attributes from hyperspectral data and SAILH+PROSPECT radiative transfer model. Presented at the 3rd EARSeL Workshop on Imaging Spectroscopy, Oberpfaffenhofen.
- Bach, H. and Verhoef, W., 2003. Sensitivity Studies on the Effect of Surface Soil Moisture on Canopy Reflectance Using the Radiative Transfer Model GeoSAIL. [J].*IGARSS*, 3, 1679~1681.
- Bach, H., Verhoef, W. and Schneider, K., 2000. Coupling remote sensing observation models and a growth model for improved retrieval of (geo)biophysical information from optical remote sensing data. *Remote Sens. for Agric., Ecosystems and Hydrology*, SPIE, 4171, 1-11.

- Barbieri, R., Montgomery, H., Qiu, S., Barnes, B., Knowles, D., Jr., Che, N. and Goldberg, I. L., 1997. The MODIS Level 1B Algorithm Theoretical Basis Document Version 2.0 (ATBMOD-01). Greenbelt, MD: NASA Goddard Space Flight Center, p. 68.
- Baret, F. and Guyot, G., 1991. Potentials and limits of vegetation indices for LAI and APAR assessment. *Remote Sens. Environ.*, 35, 161-173.
- Baret, F., Jacquemond, S. and Hanocq, J.F., 1993. The soil line concept in remote sensing. *Remote Sens. Rev.*, 7, 65–82.
- Barnes, W. L. and Salomonson, V.V., 1993. MODIS: A global image spectroradiometer for the Earth Observing System. *Critical Reviews of Optical Science and Technology*, CR47, 285-307.
- Barnes, W. L., Pagano, T. S. and Salomonson, V.V., 1998. Prelaunch characteristics of the Moderate Resolution Imaging Spectroradiometer (MODIS) on EOS-AM1. *IEEE Transactions on Geoscience and Remote Sensing*, 36(4), 1088-1100.
- Barnes, W. L., Xiong, X. and Salomonson, V.V., 2002. Status of Terra MODIS and Aqua MODIS. *Proceedings of IGARSS*.
- Barnes, W. L., Xiong, X. and Salomonson, V.V., 2003. Status of Terra MODIS and Aqua MODIS. *J. of Advances in Space Research*, 32/11, 2099-2106.
- Barton, I.J., 1978. A case study of microwave radiometer measurements over bare and vegetated surfaces. *J. Geophys. Res.*, 83, 3515-3517.
- Baumgardner, M.F., Silva, L.F., Biehl, L.L. and Stoner, E.R., 1985. Reflectance properties of soils. *Adv. Agron.*, 38, 1–44.
- Ben-Dor, E., Irons, J.R. and Epema, G.F., 1999. Soil reflectance. In A.N. Rencz (ed.) *Remote sensing for the Earth sciences: Manual of remote sensing*. Wiley & Sons, New York. 111–188.
- Betts, A. K., Ball, J. H., Beljaars, A. C. M., Miller, M. J. and Viterbo, P., 1996. The land-surface-atmosphere interaction: A review based on observational and global

modeling perspectives. *J. Geophys. Rev.*, 7209-7225.

Bryant, E. A., 1991. *Natural Hazards*. Cambridge: Cambridge University Press.

Carlson, T. N. and Ripley, D.A., 1997. On the relation between NDVI, fractional vegetation cover, and leaf area index. *Remote Sensing of Environment*, 62(3): 241-252.

Carlson, T., Gillies, R. and Perry, E., 1994. A method to make use of thermal infrared temperature and NDVI measurements to infer surface soil water content and fractional vegetation cover., *Remote Sensing Reviews*, 9, 161-173.

Ceccato, P., Flasse, S., Tarantola, S., Jacquemoud, S. and Gregoire, J. M., 2001. Detecting Vegetation Leaf Water Content Using Reflectance in the Optical Domain. *Remote Sensing of Environment*, 77, 22-33.

Celia, M. A., Bouloutas, E. T. and Zarba, R., 1990. A general mass conservative numerical solution for the unsaturated flow equation. *Water Resour. Res.*, 26(7), 1483–1496.

Changnon, S.A., 1999. Impacts of 1997-98. El Niño-generated weather in the United States. *Bulletin of the American Meteorological Society*, 80, 1,819-1,827.

Chauhan, N. S., 2003. Spaceborn soil moisture estimation at high resolution: a microwave-optical/IR synergistic approach. *INT. J. Remote Sensing*, 24(22), 4599-4622.

Chauhan, N., Le Vine, D. and Lang, R., 1999. Passive and active microwave remote sensing of soil moisture under a forest canopy. *Geoscience and Remote Sensing Symposium. IGARSS '99 Proceedings. IEEE 1999 International*, 4, 1914-1916.

Chow, V. T., Maidment, D. R. and Mays, L. W., 1988. *Applied hydrology*, McGraw-Hill, New York.

Clark, C. A. and Arritt, R. W., 1995. Numerical simulations of the effect of soil moisture and vegetation cover on the development of deep convection. *J. Appl. Meteorol.*, 34, 2029-2045.

- Clevers, J. G. P. W. and Verhoef, W., 1991. Modelling and synergetic use of optical and microwave remote sensing. Report 2: LAI estimation from canopy reflectance and WDVl: a sensitivity analysis with the SAIL model. BCRS Report 90-39, 70.
- Crosson, W.L., Limaye, A.S. and Laymon, C.A., 2005. Parameter sensitivity of soil moisture retrievals from airborne C- and X-band radiometer measurements in SMEX02. *Geoscience and Remote Sensing, IEEE Transactions*, 43(12), 2842 – 2853.
- Cunge, J.A., 1969. On the subject of a flood propagation computation method (Muskingum method). *Journal of Hydraulic Research*, 7(2).
- Dasgupta, S. and Qu, J. J., 2006. Combining MODIS and AMSR-E based vegetation moisture retrievals for improved fire risk monitoring. SPIE Optics and Photonics. August 13-17 2006, San Diego, CA, US.
- Dasgupta, S., 2007. Remote sensing techniques for vegetation moisture and fire risk estimation. Ph.D. dissertation, George Mason University, Virginia, United States.
- de Troch, F. P., Troch P. A., Su, Z. and Lin, D. S., 1996. Chapter 9: Application of Remote Sensing for Hydrological Modelling. In: Abbott, M. B., and Refsgaard, J. C. (Eds.), *Distributed Hydrological Modelling*, Kluwer Academic Publishers, Dordrecht.
- Dobson, M. C., Ulaby, F. T., Hallikainen, M. T. and El-Rayes, M. A., 1985. Microwave dielectric behavior of wet soil - part II: dielectric mixing models. *IEEE Trans. Geosci. Remote Sens.*, GE-23, 35-46.
- Dyrness, C. T., Viereck, L. A., and Van Cleve, K. (1986), Fire in taiga communities of interior Alaska, in *Forest Ecosystems in the Alaskan Taiga* (K. Van Cleve, F. S. Chapin III, P. W. Flanagan, L. A. Viereck, and C. T. Dyrness, Eds.), *Ecological Series Vol. 57*, Springer-Verlag, New York, 74-86.
- Eagleman, J. R. and Lin, W.C., 1976. Remote sensing of soil moisture by a 21-cm passive radiometer. *J. Geophys. Res.*, 81, 3660-3666.
- Edwards, D.C. and McKee, T. B., 1997. Characteristics of 20th century drought in the United States at multiple time scales. *Climatology Report Number 97-2*, Colorado

State University, Fort Collins, Colorado.

- Ek, M.B., Mitchell, K.E., Lin, Y., Rogers, E., Grunmann, P., Koren, V., Gayno, G. and Tarplay, J.D., 2003. Implementation of Noah land-surface model advances in the NCEP operational mesoscale Eta model. *J.Geophys. Res.*, 108(D22), 8851, doi:10.1029/2002JD003296.
- Engman, E. T. and Chauhan, N., 1995. Status of Microwave Soil Moisture Measurements with Remote Sensing. *Remote Sens. Environ.*, 51(1), 189-198.
- Engman, E. T., 1991. Application of Microwave Remote Sensing of Soil Moisture for Water Resources and Agriculture. *Rem. Sens. Environ.*, 35, 213-226.
- Engman, E.T., 1990. Progress in microwave remote sensing of soil moisture. *Canadian Journal of Remote Sensing*, 16(3), 6-14.
- Fennessey, M. J., and Shukla, J., 1999. Impact of initial soil wetness on seasonal atmospheric prediction. *J. Climate*, 12: 3167-3180.
- Gao, B.C., 1996. NDWI - a Normalized Difference Water Index for Remote Sensing of Vegetation Liquid Water from Space. *Remote Sensing of Environment*, 58, 257-266.
- Georgakakos, K. P. and Baumer, O. W., 1996. Measurement and Utilization of On-Site Soil Moisture Data. *J. Hydrol.*, 184, 131-152.
- Giglio, L., Descloitres, J., Justice, C.O. and Kaufman, Y.J., 2003. An enhanced contextual fire detection algorithm for MODIS. *Remote Sensing of Environment*, 87, 273-282.
- Gillies, R. R. and Carlson, T.N., 1995. Thermal remote sensing of surface soil water content with partial vegetation cover for incorporation into mesoscale prediction models. *J. Appl. Meteorol*, 34, 745-756.
- Gillies, R., Carlson, T., Kustas, W. and Humes, K., 1997. A verification of the “triangle” method for obtaining surface soil water content and energy fluxes from remote

- measurements of the Normalized Difference Vegetation Index (NDVI) and surface radiant temperature., *Int. J. Remote Sens.*, 18, 3145-3166.
- Goward, S. N., Markham, B. L., Dye, D. G., Dulaney, W. and Yang, J., 1991. Normalized difference vegetation index measurements from the advanced very high resolution radiometer. *Remote Sens. Environ.*, vol. 35, pp. 257–277, 1991.
- Gu, Y., Brown, J. F., Verdin, J. P. and Wardlow, B., 2007. A five-year analysis of MODIS NDVI and NDWI for grassland drought assessment over the central Great Plains of the United States, *Geophys. Res. Lett.*, 34, L06407, doi:10.1029/2006GL029127.
- Guttman, N. B., 1998. Comparing the Palmer Drought Index and the Standardized Precipitation Index. *Journal of the American Water Resources Association* 34(1): 113-121.
- Hallikainen, M., Ulaby, F., Dobson, M. and El-Rayes, M., 1985. Microwave dielectric behavior of wet soil—Part I: empirical models and experimental observations. *IEEE Transactions on Geoscience and Remote Sensing*, 23, 25–34.
- Hao, X., 2006. Estimation of Live Fuel Moisture and Soil Moisture Using Satellite Remote Sensing. Ph.D. dissertation, George Mason University, Virginia, United States.
- Hardisky, M.A., Klemas, V. and Smart, R.M., 1983. The influence of soilsalinity, growth form, and leaf moisture on the spectral radiance of *Spartina alterniflora* canopies. *Photogrammetric Engineering and Remote Sensing*, 49, 77-83.
- Hills, R. G., Porro, I., Hudson, D. B. and Wierenga, P. J., 1989. Modeling one-dimensional infiltration into very dry soils. 1. Model development and evaluation. *Water Resour. Res.*, 25(6), 1259–1269.
- Hoos, A.B., Koussis, A.D., Beale, G.O., 1989. A channel dynamics model for real-time flood forecasting. *Water Resources Research*, 25(4).
- Houser, P., Peters-Lidard, C., Kumar, S., Tian, Y., Geiger, J., Olden, S., Lighty, L., Sheffield, J., Wood, E., Mitchell, K., Dirmeyer, P., Doty, B., and Adams, J., 2005. The Land Information System. *Earth-Sun System Technology Conference*.

- Hunt, R.E., Rock, B.N. and Park, S.N., 1987. Measurement of leaf relative water content by infrared reflectance. *Remote Sensing of Environment*, 22, 429-435.
- Idso, S. B., Jackson, R. D., Reginato, R. J., Kimball, B. A. and Nakayama, F. S., 1975. The Dependence of Bare Soil Albedo on Soil Water Content. *Journal of Applied Meteorology*, 14, 109-113.
- Ishida, T., Ando, H. and Fukuhara, M., 1991. Estimation of complex refractive index of soil particles and its dependence on soil chemical properties. *Remote Sens. Environ.* 38, 173–182.
- Jackson T.J., 1980. Profile soil moisture from surface measurements. *J Irrigation Drainage Div, Proc ASCE*;106 (IR2):81–92.
- Jackson, T. J., 1986. Soil Water Modeling and Remote Sensing. *IEEE Trans. Geosci. Rem. Sens.*, GE-24(1), 37-46.
- Jackson, T. J., 1993. III Measuring Surface Soil Moisture Using Passive Microwave Remote Sensing. *Hydrol. Processes*, 7, 139-152.
- Jackson, T. J., 1997. Soil Moisture Estimation Using Special Satellite Microwave/Imager Satellite Data Over a Grassland Region. *Water Resour. Res.*, 33(6), 1475-1484.
- Jackson, T. J., Schmugge, T. J. and Engman, E. T., 1996. Remote Sensing Applications to Hydrology: Soil Moisture. *Hydrological Sciences Journal*, 41(4), 517-530.
- Jacquemoud, S. and Baret, F., 1990, PROSPECT: a model of leaf optical properties. *Remote Sens. Environ*, 34, 75-91.
- Jacquemoud, S., 1993. Inversion of the PROSPECT+SAIL canopy reflectance model from AVIRIS equivalent spectra: theoretical study. *Remote Sens. Environ.*, 44, 281-292.
- James, W. P., Warinner, J., and Reedy, M., 1992. Application of the Green-Ampt infiltration equation to watershed modeling. *Water Resour.Bull.*, 28(3), 623–635.
- Jensen, M. E., Burman, R. D. and Allen, R. G., 1990. Evapotranspiration and irrigation

water requirements. ASCE Manuals and Reports on Engineering Practice No. 70. New York, NY: American Society of Civil Engineers.

Justice, C.O., Vermote, E., Townshend, J., et al., 1998. The Moderate Resolution Imaging Spectroradiometer (MODIS): Land Remote Sensing for Global Change Research. *IEEE Transaction on Geoscience and Remote Sensing*, 36(4), 1228-1249.

Kasischke, E. S., French, N. H. F., Harrell, P., Christensen, N. L., Ustin, S. L. and Barry, D., 1993. Monitoring of wildfires in boreal forests using large-area AVHRR NDVI composite image data. *Remote Sens. Environ.*, 45, 61–71.

Kite, G. W. and Pietroniro, A., 1996. Remote Sensing Applications in Hydrological Modelling. *Hydrological Sciences Journal*, 41(4), 563-591.

Kohavi, R. and Provost, F., 1998. Glossary of terms. Editorial for the special issue on application of machine learning and the knowledge of discovery process. *Machine Learning*, 30, 271–274.

Koster, R. D. and Suarez, M. J., 1999. A simple framework for examining the interannual variability of land surface moisture fluxes. *J. Climate*, 12, 1911-1917.

Kostov, K. G. and Jackson, T. J., 1993. Estimating Profile Soil Moisture From Surface Layer Measurements – A Review. In: *Proc. The International Society for Optical Engineering*, 1941, Orlando, Florida, 125-136.

Leconte, R. and Brissette, F. P., 2001. Soil moisture profile model for two-layered soil based on sharp wetting front approach. *J. Hydrologic Eng.*, 6(2), 141–149.

Liu, W., Baret, F., Gu, X., Tong, Q., Zheng, L. and Zhang, B., 2002. Relating soil surface moisture to reflectance. *Remote sensing of environment*. 81, 238-246. (doi:10.1016/S0034-4257(01)00347-9).

Lobell, D.B. and Asner, G.P., 2002. Moisture Effects on Soil Reflectance. *Soil Sci Soc Am J*. 66, 722-727.

Maki, M., Ishiara, M. and Tamura, M., 2004. Estimation of leaf water status to monitor the

risk of forest fires by using remotely sensed data. *Remote Sens. Environ.*, 90, 441–450.

Mancini M., Vandersteene F., Troch P.A., Bolognani O., Terzaghi G., D'Urso G. and Wüthrich, M., 1995. Experimental setup at the EMSL for retrieval of soil moisture profiles using multifrequency polarimetric data. *International Geoscience and Remote Sensing Symposium*, Firenze, Italy, p. 2023-25.

McKee, T.B., Doesken, N.J. and Kleist, J., 1993. The relationship of drought frequency and duration to time scales. *Preprints, 8th Conference on Applied Climatology*, 179–184. January 17–22, Anaheim, California.

Menziani, M., Pugnaghi, S., Vincenzi, S. and Santangelo, R., 2003. Soil moisture monitoring in the Toce valley (Italy). *Hydrology and Earth System Sciences*, 7(6), 890-902.

Miller, D., Mohanty, B. P., Jacobs, J. M. and Hsu, E. C., 2004. SMEX02: field scale variability, time stability and similarity of soil moisture, *Remote Sensing of Environment*, 2004, 92,436-446.

Miura, T., Huete, A.R. and Yoshioka, H., 2000. Evaluation of sensor calibration uncertainties on vegetation indices for MODIS. *IEEE Transactions on Geoscience and Remote Sensing*, 38(3), 1399-1409.

Moldrup, P., Rolston, D.E. and Hansen, A.A., 1989. Rapid and numerically stable simulation of one dimensional, transient water flow in unsaturated, layered soils. *Soil Science*, 148, 219–226.

Moldrup, P., Yamaguchi, T., Hansen, J.AA. and Rolston, D. E., 1992. An accurate and numerically stable model for one-dimensional solute transport in soils. *Soil Sci.*, 153, 261-273.

Moldrup, P., Yamaguchi, T., Rolston, D. E., Vestergaard, K. and Hansen, J. AA., 1994b. Removing numerically induced dispersion from finite difference models for solute and water transport in unsaturated soils. *Soil Sci.*, 157, 153-161.

Moran, M.S., Clarke, T.R., Inoue, Y. and Vidal, A., 1994. Estimating crop water deficit

using the relation between surface-air temperature and spectral vegetation index. *Remote Sensing of Environment*, 49, 246-263.

Myneni, R. B., Hall, F. G., Sellers, P. J. and Marshak, A. L., 1995. The interpretation of spectral vegetation indexes. *IEEE Transactions on Geoscience and Remote Sensing*, 33, 481– 486.

Narasimhan, B. and Srinivasan, R., 2005. Development and evaluation of Soil Moisture Deficit Index (SMDI) and Evapotranspiration Deficit Index (ETDI) for agricultural drought monitoring. *Agricultural and Forest Meteorology*, 133, 69-88, doi:10.1016/j.agrformet.2005.07.012.

Narasimhan, B., 2004. Development of Indices for Agricultural Drought Monitoring Using Spatially Distributed Hydrologic Model. Ph.D. dissertation, Texas A&M University, Texas, United States.

Newton, R.W., Heilman, J.L. and van Bavel, C.H.M., 1983. Integrating passive microwave measurements with a soil moisture/heat flow model. *Agri Water Management* 7, pp. 379–389.

Nihei, N., Hashida, Y., Kobayashi, M., Ishii, A., 2002. Analysis of Malaria Endemic Areas on the Indochina Peninsula Using Remote Sensing. *Japanese Journal of Infectious Diseases*, 55(5), 160-166.

Njoku, E. G. and Entekhabi, D., 1996. Passive Microwave Remote Sensing of Soil Moisture. *J. Hydrol.*, 184, 101-129.

Njoku, E. G. and Kong, J. A., 1977. Theory for passive microwave remote sensing of near-surface soil moisture. *J. Geophys. Res.*, 82, 3108-3118.

Njoku, E. G., 1999. Retrieval of land surface parameters using passive microwave measurements at 6-18 GHz. *IEEE Transactions on Geoscience and Remote Sensing*, 37, 79-93.

Njoku, E.G., Wilson, W.J., Yueh, S.H., Dinardo, S.J., Li, F.K., Jackson, T.J., Lakshmi, V. and Bolten, J. , 2002. Observations of soil moisture using a passive and active low-frequency microwave airborne sensor during SGP99. *Geoscience and Remote*

- Sensing, IEEE Transactions, 40 (12), 2659 – 2673.
- Ottlé, C. and Vidal-Madjar, D., 1994. Assimilation of Soil Moisture Inferred from Infrared Remote Sensing in a Hydrological Model Over the HAPEX-MOBILHY Region. *J. Hydrol.*, 158, 241-264.
- Ou, S., Takano, Y., Liou, K. N., Higgins, G., George, A. and Slonaker, R., 2003. Remote sensing of cirrus cloud optical thickness and effective particle size for the National Polar-orbiting Operational Environmental Satellite System Visible_Infrared Imager Radiometer Suite: sensitivity to instrument noise and uncertainties in environmental parameters. *APPLIED OPTICS*, 42, 7202-7214.
- Palmer, W. C., 1965. Meteorological drought. Research Paper 45. Washington, D.C.: U.S. Department of Commerce, Weather Bureau.
- Pan, L. and Wierenga, P. J., 1995. A transformed pressure head-based approach to solve Richards' equation for variably saturated soils. *Water Resour. Res.*, 31(4), 925–932.
- Parlange, J.-Y. and Braddock, R. D., 1980. An application of Brutsaert's and optimization techniques to the non-linear diffusion equation: The influence of tailing. *Soil Sci.*, 129, 145–149.
- Parlange, J.-Y., 1972. Theory of water movement in soils, 8, One dimensional infiltration with constant flux at the surface. *Soil Sci.*, 114, 1–4.
- Peake, W., 1959. Interaction of electromagnetic waves with some natural surfaces. *IEEE TAP*, 7, S324-S329.
- Penuelas, J., Filella, I., Sav, R., Serrano, L., et al., 1996. Cell wall elasticity and water index (R970nm/R900nm) in wheat under different nitrogen availabilities. *International Journal of Remote Sensing*, 17(2), 373-382.
- Penuelas, J., Filella, I., Serrno, L., et al., 1993. The reflectance at the 950-970 nm region as an indicator of plant water status. *International Journal of Remote Sensing*, 14, 1887-1905.

- Penuelas, J., Pinol, J., Ogaya, R. and Filella, I., 1997. Estimation of plant water concentration by the reflectance water index WI (R900/R970). *International Journal of Remote Sensing*, 18(13), 2869-2872.
- Philip, S., 2007. Active fire detection using remote sensing based polar-orbiting and geostationary observations: an approach towards near real-time fire monitoring. M.S. thesis, International Institute for Geo-Information Science and Earth Observation, Enschede, The Netherlands.
- Qu, J. J., Hao, X., Kafatos, M. and Wang, L., 2006. Asian Dust Storm Monitoring Combining Terra and Aqua MODIS SRB Measurements. *IEEE Geoscience and Remote Sensing Letters*, 3(4), 484-486.
- Qu, J. J., Serafino, G., Kafatos, M., Lathrop, R. and Trimble, J., 2001. New application of Earth science remote sensing data at NASA/GDISC: Remote Sensing Information Partner (RSIP) with Rutgers University. In *Proceedings. International Geoscience and Remote Sensing Symposium (IGARSS) 2001*, July 9-13, at University New South Wales, Sydney.
- Ragab, R., 1995. Towards a Continuous Operational system to Estimate the Root-Zone Soil Moisture from Intermittent Remotely Sensed Surface Moisture. *J. Hydrol.*, 173, 1-25.
- Ramírez, J. A., 2000. Prediction and Modeling of Flood Hydrology and Hydraulics. Chapter 11 of *Inland Flood Hazards: Human, Riparian and Aquatic Communities*. Eds. Ellen Wohl; Cambridge University Press.
- Richard, R. and Heim, J. R., 2002. A review of twentieth-century drought index used in the United States[J]. *Bulletin American Meteorological society*, 83, 1149-1165.
- Riebsame, W.E., Changnon, S.A. and Karl, T.R., 1990. Drought and Natural Resource Management in the United States: Impacts and Implications of the 1987-1989 Drought. Westview Press, Boulder, Colorado.
- Rui, X. and Wang, L., 2000. A study of flood routing method with forecast period. [J]. *Advances in Water Science*, 11(3), 291-295, in Chinese.

- Rui, X., 1995. Theory of Runoff Generation, China WaterPower Press, in Chinese.
- Sadeghi, A. M., Hancock, G. D., Waite, W. P., Scott, H. D. and Rand, J. A., 1984. Microwave Measurements of Moisture Distributions in the Upper Soil Profile. *Water Resour. Res.*, 20(7), 927-934.
- Salomonson, V.V., Barnes, W.L. and Masuoka, E. J., 2005. Introduction to MODIS and An Overview of Associated Activities, Qu, J. J. et al eds, *Earth Science Satellite Remote Sensing, Volume I: Science and Instruments*. Springer-Verlag and Tsinghua University Press.
- Salomonson, V.V., Barnes, W.L., Xiong, X., Kempner, S. and Masuoka, E., 2002. An Overview of the Earth Observing System MODIS Instrument and Associated Data Systems Performance. *Proceedings of IGARSS*.
- Sanders, G. C., Parlange, J.Y., Kuehn, V., Hogarth, W.L., Lockington, D., O'Kane, J.P.J., 1988. Exact nonlinear solution for constant flux infiltration. *J. Hydrol.*, 97,341-346.
- Schmugge, T. J., Jackson, T. J. and McKim, H. L., 1980. Survey of Methods for Soil Moisture Determination. *Water Resour. Res.*, 16(6), 961-979.
- Schmugge, T., 1985. Chapter 5: Remote Sensing of Soil Moisture, In: Anderson, M. G., and Burt, T. P., (Eds.), *Hydrological Forecasting*, John Wiley and Sons, New York, 101-124.
- Schmugge, T.J., Menennly, J.M., Rango, A., and Neff, R., 1977. Satellite microwave observations of soil moisture variations, *Water Resources Bull.*, 13, 265-281.
- Si, B.C. and Kachanoski, R.G., 2000. Estimating Soil Hydraulic Properties During Constant Flux Infiltration: Inverse Procedures. *Soil Sci. Soc. Am. J.*, 64(2), 439-449.
- Slater, P. N., 1984. The importance and attainment of absolute radiometric calibration. in *Proc. SPIE Critical Rev. Remote Sensing*, vol. 475, 34-40.
- Slater, P. N., 1985. Radiometric considerations in remote sensing. *Proc. IEEE*, vol. 73, no.

6, 997–1011.

Suzuki, R., Nomaki, T. and Yasunari, T., 2001. Spatial distribution and its seasonality of satellite-derived vegetation index (NDVI) and climate in Siberia, *International Journal of Climatology*, 21(11), 1321 – 1335.

Tannehill, I. R., 1947. *Drought: Its Causes and Effects*. Princeton, NJ: Princeton University Press.

Thornthwaite, C. W. and Mather, J. R., 1955. The water budget and its use in irrigation. *Water—Yearbook of Agriculture 1955*, A. Stefferud, Ed., U.S. Dept. of Agriculture, 346–358.

Thornthwaite, C. W., 1948. An approach toward a rational classification of climate. *Geographical Review* 38(January):55-94.

Twomey, S.A., Bohren, C.F. and Mergenthaler, J.L., 1986. Reflectances and albedo differences between wet and dry surfaces. *Appl. Optics.*, 25, 431–437.

Van Genuchten, M. Th., 1982. A comparison of numerical solutions of the one-dimensional unsaturated-saturated flow and mass transport equations. *Adv. Water Resour.*, 5, 47-55.

Verbesselt, J., Lhermitte, S., Coppin, P., Eklundh, L. and Jonsson, P., 2004. Biophysical drought metrics extraction by time series analysis of SPOT Vegetation data. *Geoscience and Remote Sensing Symposium. IGARSS apos; 04. Proceedings. IEEE International*, 3, 2062 – 2065.

Verhoef, W., 1984. Light scattering by leaf layers with application to canopy reflectance modeling : the SAIL model. *Remote sensing of environment*, 16, 125-141.

Vestergaard, K., 1989. Numerical modeling of streams: Hydrodynamic models and models for transport and spreading of pollutants. Ph.D. dissertation, Aalborg University, Denmark.

Walker, J. P., Willgoose, G. R., Kalma, J. D., 2001. One dimensional soil moisture profile

retrieval by assimilation of near surface measurements: a simplified soil moisture model and field application. *J. Hydromet.*, 2, 356-373.

Walker, J., 1999. Estimating Soil Moisture Profile Dynamics from Near-Surface Soil Moisture Measurements and Standard Meteorological Data. Ph.D. dissertation, The University of Newcastle, Australia.

Wang L., 1999. A study of Flood Forecasting Models on Xijiang River, Pearl Basin. Thesis. Hohai University, Nanjing, P. R. China, , in Chinese.

Wang, L. and Qu, J.J., 2007. NMDI: A Normalized Multi-band Drought Index for Monitoring Soil and Vegetation Moisture with Satellite Remote Sensing. *Geophysical Research Letters*, 34 (2007), L20405. (DOI:10.1029/2007GL031021).

Wang, L., Qu, J. J., Xiong, J., Hao, X., Xie, Y. and Che, N., 2006. A New Method for Retrieving Band 6 of Aqua MODIS. *IEEE Geoscience and Remote Sensing Letters*, 3(2), 267-270.

Wang, L., Qu, J.J., Hao, X. and Zhu, Q., 2007. Sensitivity studies of the moisture effects on MODIS SWIR reflectance and vegetation water indices. *Int. J. Remote Sens.*, in press.

Wang, L., Qu, J.J., Zhang, S., Hao, X. and Dasgupta, S., 2007a. Soil Moisture Estimation Using EOS MODIS and Ground Measurements in the Eastern China. *International Journal of Remote Sensing*, 28, 1413-1418.

Wilhite, D. A. and Glantz, M. H., 1985. Understanding the drought phenomenon: the role of definitions. *Water International*, 10(3), 111-120.

Wilhite, D. A., 2000. Drought as a natural hazard: concepts and definitions. In *Drought: A Global Assessment* (Vol. I), ed. Donald A. Wilhite, ch.1, 3-18, New York: Routledge.

Wilhite, D.A., (ed.), 2000a: *Drought: A Global Assessment* (2 volumes, 51 chapters, 700 pages). *Hazards and Disasters: A Series of Definitive Major Works* (7 volume series), edited by A.Z. Keller. Routledge Publishers.

- Wood, E. F., Lettenmaier, D. P. and Zartarian, V. G., 1992. A Land-Surface Hydrology Parameterization With Subgrid Variability for General Circulation Models. *J. Geophys. Res.*, 97(D3), 2717-2728.
- Zarco-Tejada P.J. and Ustin, S.L., 2001. Modeling canopy water content for carbon estimates from MODIS data at land EOS validation sites. *Proceedings, IEEE 2001 International Geoscience and Remote Sensing Symposium*, 342–344.
- Zarco-Tejada, P.J., Rueda, C.A. and Ustin, S.L., 2003. Water content estimation in vegetation with MODIS reflectance data and model inversion methods. *Remote Sensing of Environment*, 85, 109–124.
- Zhan, X., Miller, S., Chauhan, N., Di, L., Ardanuy, P. and Running, S., 2002. Soil Moisture Visible/Infrared Imager/Radiometer Suite Algorithm Theoretical Basis Document., Version 5.

CURRICULUM VITAE

Lingli Wang was born on December 7, 1974, in Hubei, P. R. China. She received her Bachelor and Master of Science in Hydrology and Water Resources from Hohai University, P. R. China in 1997 and 2000. She was employed as a hydrologist at Ministry of Water Resources, P. R. China for five years before joining George Mason University as a research assistant and Ph.D. student in 2005. Her research area at the time of this dissertation included remote sensing based estimations of soil moisture and agricultural drought, as well satellite instrument calibration and characterization effects on satellite products.